LOW FREQUENCY RADIO ASTRONOMY

Proceedings of a Workshop held at the National Radio Astronomy Observatory Green Bank, West Virginia on November 16-17, 1984

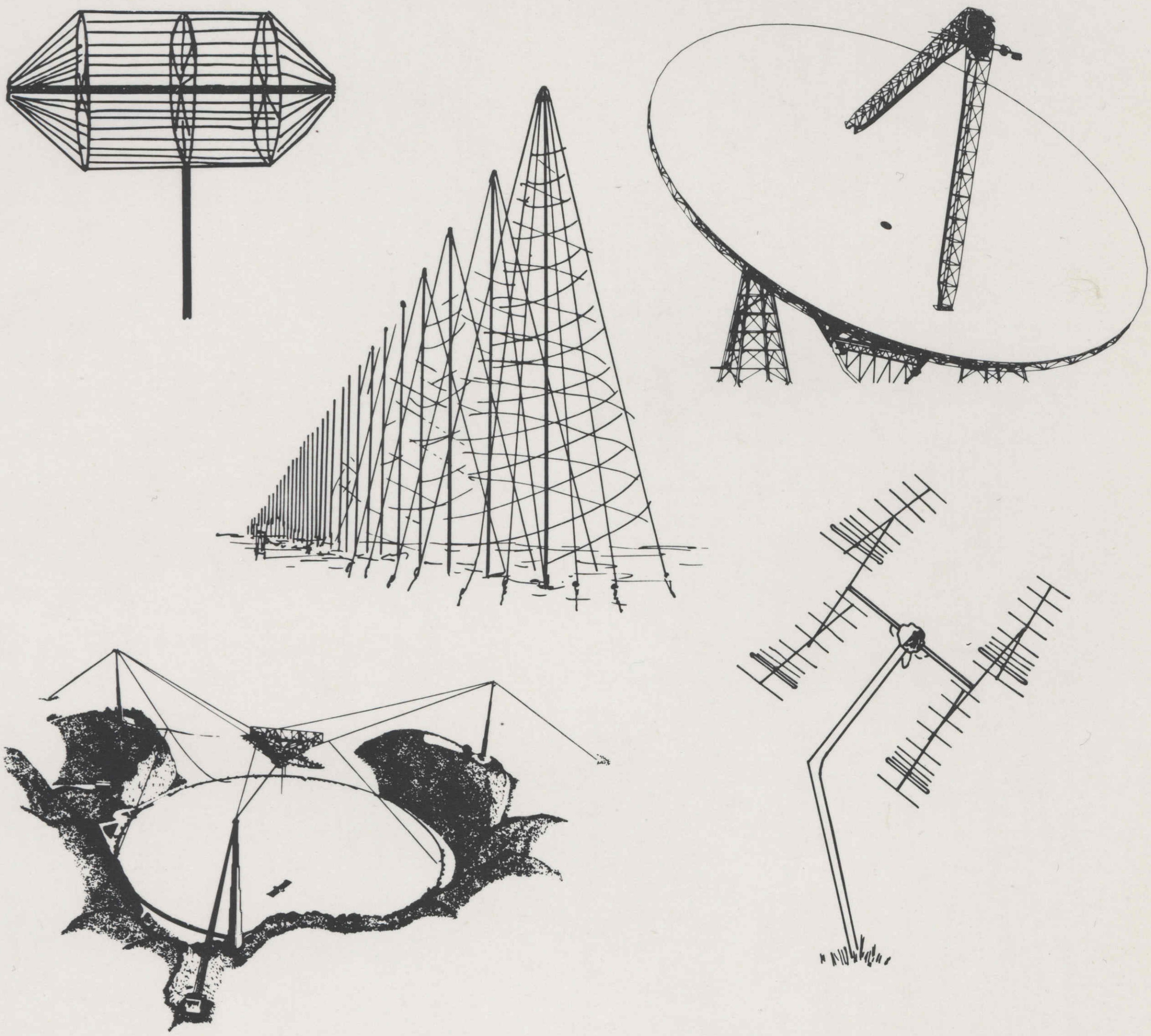

Edited by W.C. Erickson and H.V. Cane

NRAO

LOW FREQUENCY RADIO ASTRONOMY

Proceedings of a Workshop held at the
National Radio Astronomy Observatory
Green Bank, West Virginia on
November 16-17, 1984

Edited by W.C. Erickson and H.V. Cane

Workshop No. 10

Distributed by:
National Radio Astronomy Observatory
P.O. Box 2
Green Bank, WV 24944-0002 USA

The National Radio Astronomy Observatory
Associated Universities, Inc., under contract with the National Science Foundation

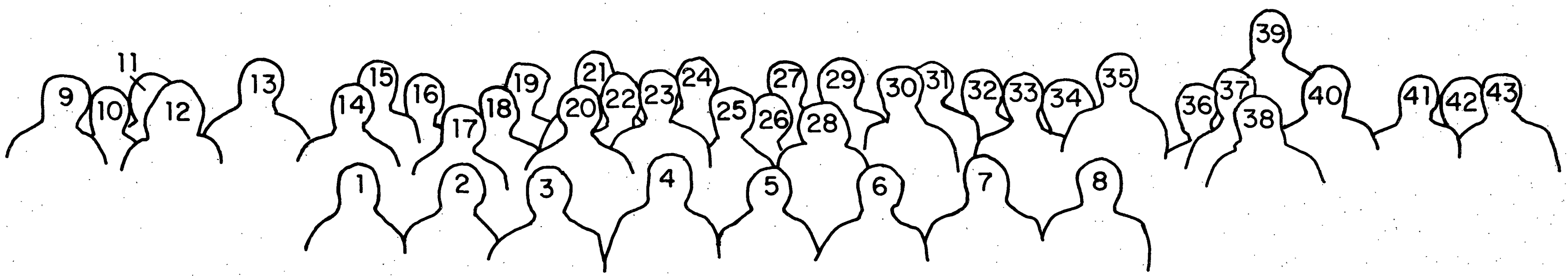

1. Hanisch
2. Fisher
3. Perley
4. Davis
5. Kellermann
6. Condon
7. Harris
8. Rickett
9. Gergely
10. Lillie
11. Bignell
12. Cane
13. Mahoney
14. Baldwin
15. Duffett-Smith
16. Rees
17. Grueff
18. Carr
19. Broderick
20. Montebignoli
21. Crane
22. Gottesman
23. Shevgaonkar
24. Dulk
25. Barvainis
26. Hunt
27. Erickson
28. Baum
29. Cotton
30. Payne
31. Romney
32. Hjellming
33. O'Dea
34. Warner
35. Bridle
36. Ekers
37. Odegard
38. Anantharamaiah
39. Simon
40. Schwab
41. Killeen
42. Jackson
43. Bagri

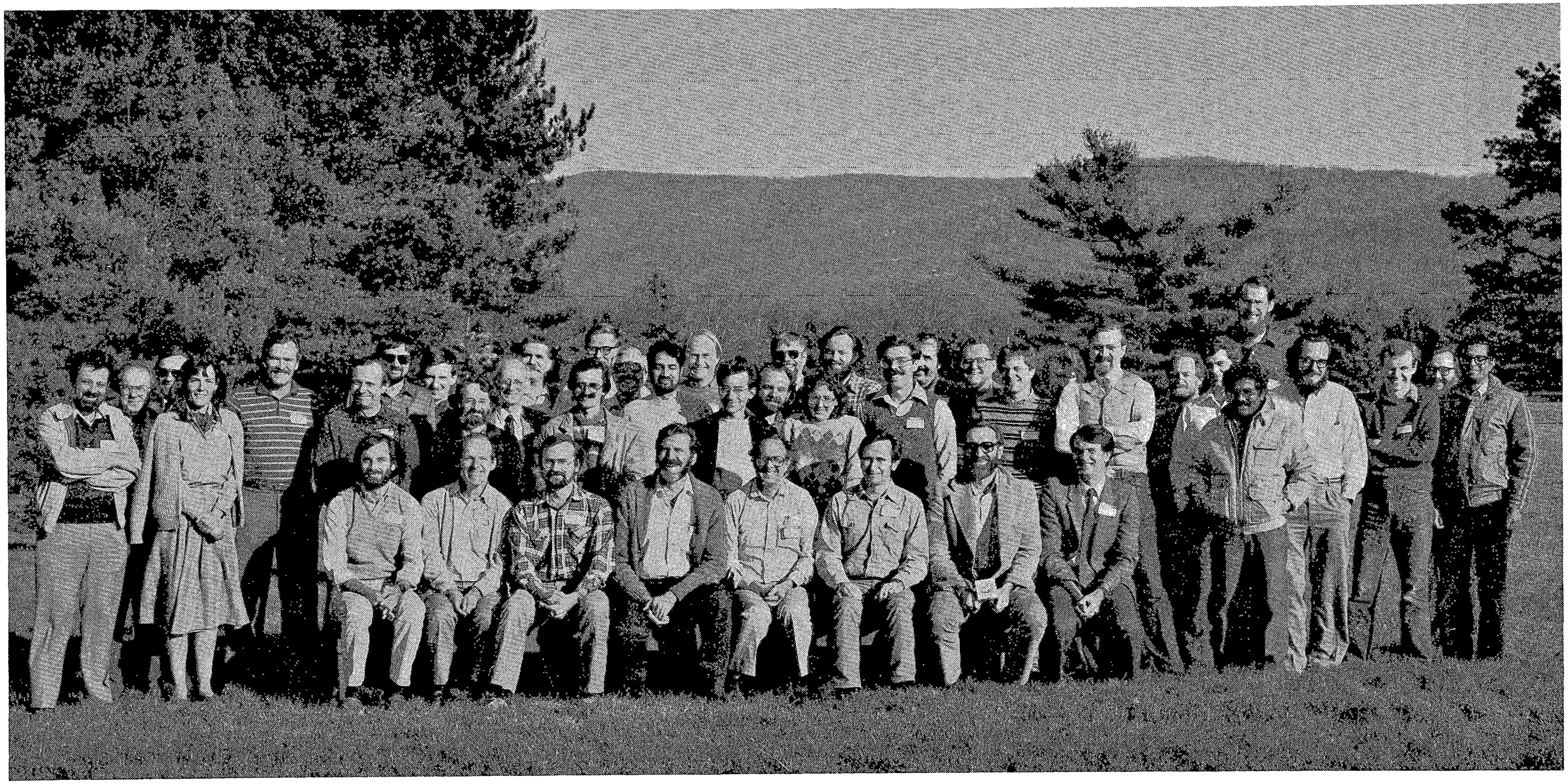

NRAO GREEN BANK WORKSHOP ON METER-WAVELENGTH RADIO ASTRONOMY
16-17 NOVEMBER 1984

TABLE OF CONTENTS

(Titles of the papers presented at the workshop are given in the order in which they were presented. Page numbers are given for the papers reproduced here. For papers that have been published elsewhere, references are given in brackets [ ]. Papers which are not reproduced here and which do not appear to have been published elsewhere are listed in this table by title and author only.)

REFERENCES

[1] B. J. Rickett, W. A. Coles, and G. Bourgois, 1984, Astr. Ap. 134, 390.

[2] K. R. Anantharamaiah, W. C. Erickson, and V. Radhakrishnan, 1985, Nature 315, 647

[3] G. A. Dulk, 1985, Ann. Rev. Astron. Astrophys. 23, 169

INTRODUCTION

The NRAO-Greenbank Workshop on Meter-Wavelength Radio Astronomy was held on November 16-17, 1984. The principal impetus behind this workshop was the proposal (VLA Scientific Memorandum No. 162) for a 75-MHz system at the VLA. It was felt that it would be timely to assemble a group of radio astronomers who are active in meter-wavelength research to discuss the science that is and should be done, to discuss the merits of the 75-MHz proposal, and to discuss the implementation of this proposal.

Research at 327 MHz is actively pursued in the Netherlands, India, and the United States. This frequency is not technically within the "meter-wavelength" band and this work was not specifically included, nor was ground-based decameter-wavelength work or hectometer-wavelength work from space.

Meter-wavelength radio astronomy is practiced by a rather small subset of radio astronomers. The institution with the longest and most sustained tradition in the field is the Cavendish Laboratory. The Cavendish group have led the field since the earliest days of radio astronomy and was well-represented at the Workshop. From the United States, the Clark Lake, UCSD, Florida, Colorado, and NRAO groups participated. There were reports from the meter-wavelength projects in India but, unfortunately, no members of the Australian or Soviet Union groups were able to attend.

Sessions were held concerning Meter-Wavelength Science and concerning Meter-Wavelength Instrumentation and Techniques. In order to accommodate the travel plans of some of the key participants, the sessions were somewhat mixed in their order. Sessions 1, 2 and 5 were on Science while Sessions 3 and 4 concerned Instrumentation and Techniques.

INTERPLANETARY SCINTILLATION AS A PROBE OF THE UNIVERSE

W.G. Rees, P.J. Duffett-Smith, S.J. Tappin & A. Hewish.
Mullard Radio Astronomy Observatory
Cambridge, UK.

This paper is principally a brief review of the technique of interplanetary scintillation (IPS); with a short discussion of two pieces of work recently performed at Cambridge.

Interplanetary scintillation is the fluctuation produced in the apparent brightness of a radio source, owing to refractive effects in the turbulent solar wind. Turbulent fluctuations in the electron density cause the solar wind to act as a random phase-changing medium. If this medium is illuminated coherently (by a point radiation source), analysis of the spatial and temporal properties of the radiation reaching the earth's surface allows the stochastic properties of the medium to be inferred; such inferences may also be drawn from observations on signals exchanged through the medium between the earth and a spacecraft, or between two spacecraft. Conversely, once the refractive properties of the medium are known, observations of the radiation field at the earth's surface allow deductions to be made concerning the coherence of the radiation which illuminates the medium, thus permitting inferences to be drawn concerning the structure of the radio source. Since the phase deviation due to a plasma is proportional to wavelength, IPS is predominantly a low-frequency phenomenon. Although it has been observed at several GHz, most useful data have been obtained between 50 and 200 MHz. Table 1 summarizes a few properties of the solar wind.

Table 1

Some relevant properties of the solar wind

	0.1 a.u.	1.0 a.u.
N_e/cm^{-3}	1000	10
$\Delta N_e/cm^{-3}$	40	0.1
V/kms^{-1}	400	400
V_{alfven}/kms^{-1}	500	50
B/gauss	10^{-2}	10^{-4}
T_e/K	10^5	10^5
ν_{plas}/MHz	0.1	0.01
ν_{scint}/Hz	~10	0.5

1) Observation of the medium.

Figure 1 (adapted from Rickett) illustrates the geometry of IPS. The density irregularities (turbulent blobs) introduce a phase modulation, which develops into an amplitude modulation when the wave has propagated a distance roughly equal to the Fresnel distance $Z_F = a^2/\lambda$. For this reason, very large irregularities produce no IPS (just phase variations). The intensity pattern on the ground propagates at the velocity v of the solar wind, and so observations at a single antenna show the flux density fluctuating with an amplitude ΔS on a timescale of roughly a/v. The scintillation index m is defined as $\Delta S/S$.

Observations at a single antenna have established that, in weak

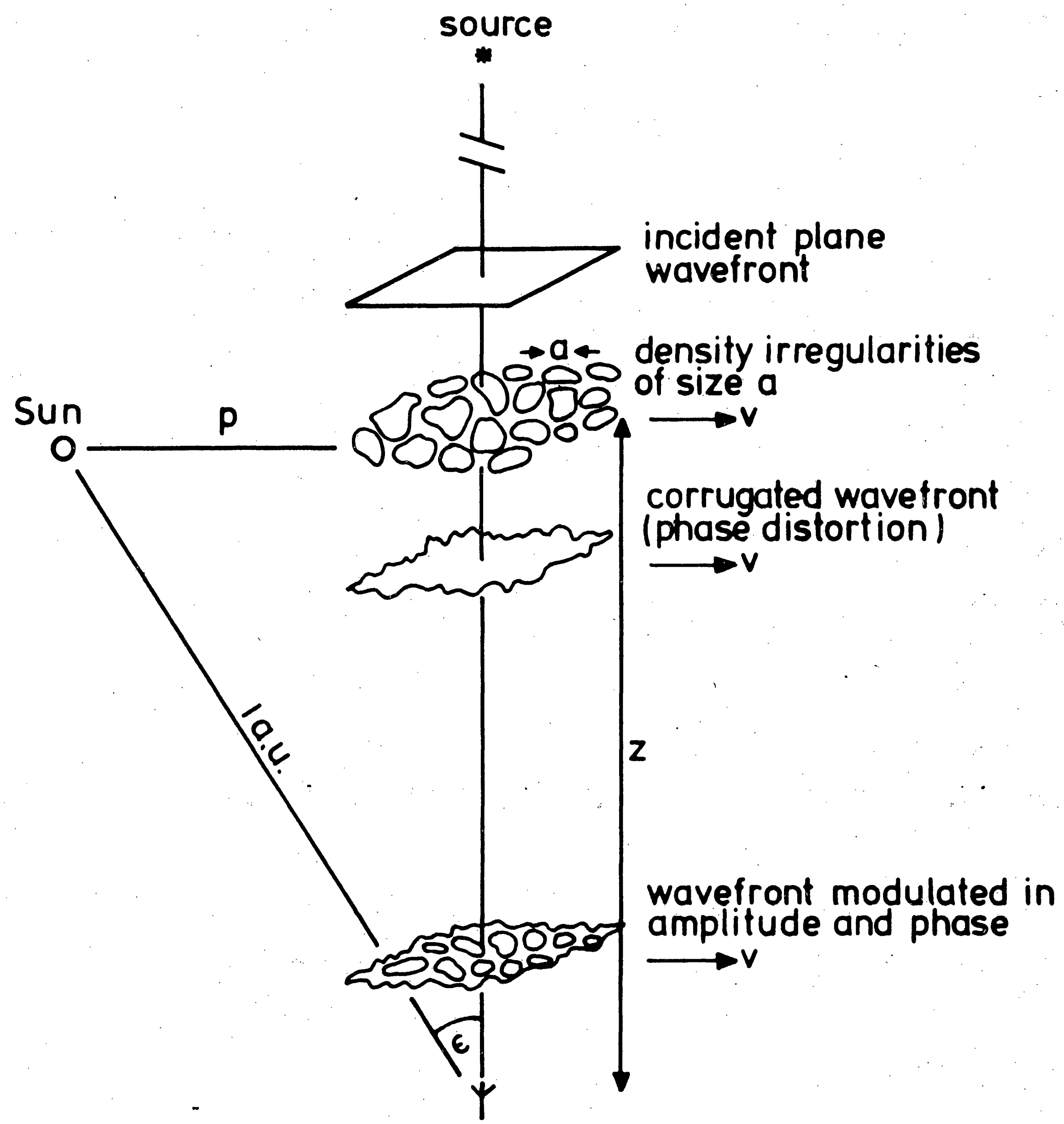

Figure 1

scattering, the scintillation index is well described by $m = 0.08\ \lambda p^{-1.5}$, where λ is the wavelength in metres and p is the closest distance of approach of the line of sight to the sun, measured in au. It can easily be seen that $p = \sin \varepsilon$. The condition of weak scattering means, in essence, that the formula should give $m < 1$. This tells us three things about the solar wind:

i. $m \propto p^{-1.5}$ implies that the scattering power $\beta(r)$ of the solar wind varies as r^{-4}, where r is the distance from the sun. This is roughly consistent with $\Delta N \propto N$. (N is the electron density, ΔN is its rms variation.)
ii. $m \propto \lambda$ implies that, within the range of scale sizes which can contribute to IPS (i.e. $a <$ Fresnel scale $a_F = \sqrt{\lambda z} = 700$ km when $\lambda = 3.68$ m

and z = 1 au), the dominant feature of the turbulence spectrum is a characteristic scale size a.
iii. The normalization implies that $\Delta N \simeq 0.1\ cm^{-3}$ at 1 au

By making 2- or preferably 3-station simultaneous observations, the size and velocity of the intensity pattern on the ground may be deduced, and hence the velocity of the solar wind itself. There are permanent multi-station IPS networks in the U.S.A., India and Japan.

The common assumptions have been that the pattern is 'frozen', i.e. that the turbulent blobs do not rearrange themselves as they blow along, and that the autocorrelation function of the density variations is Gaussian, i.e. characterized by a single scale-size a. With these assumptions, the velocity of the solar wind has been found to be about 400 km/s, directed radially from the sun to within 10°, and the scale size is roughly 200 $(r/au)^{0.9}$ km. IPS observations of the solar wind have also demonstrated the existence of an acceleration region in the first 0.05 au from the sun.

The pattern is slightly anisotropic (axial ratio $\simeq$ 1.3), and it seems from 4-station observations that it does in fact rearrange as it drifts, although the rearrangement velocity is less than 40 percent of the bulk velocity. The scale size observations assume that the source which illuminates the medium is effectively a point source. This can be checked by dual-frequency IPS, by observing pulsar broadening, or by interferometry.

Observations of the particle flux detected by artificial satellites have found fluctuations on timescales from 1 to 10^5 seconds, implying variations on length scales from 10^5 to 10^{10} m. (Structures larger than 10^{10} m occur, but they are due to stream structure in the solar wind and are not part of the turbulence spectrum). These variations appear to fit the Kolmogorov theory of turbulence rather well, in which the spectral density of the irregularities varies as an inverse power of the spatial frequency. At first sight this seems flatly to contradict the IPS observations, although satellite data now suggest that there is a marked flattening of the spectrum at spatial frequencies corresponding to scale lengths of about 200 km. When this is combined with the fact that IPS, because of the action of the Fresnel filter, is insensitive to large-scale structures, it seems that the single-scale-size Gaussian model is in fact a better approximation to the true spectrum, for IPS purposes, than is a pure power-law. There is not however, universal agreement about this.

2) Observations of interplanetary weather.

In this section we decscribe observations of large-scale transient phenomena in the solar wind, made at Cambridge during the period 1978 - 1981. These observations were made with the 36 000 m^2 array, operating at 81.5 MHz over two continuous periods of about 400 days. For the first period, we observed a grid of about 900 sources, and for the second this was increased to about 2500 sources covering most of the sky visible at Cambridge. This is a far larger number than has been used in any previous work.

Rather than simply mapping the scintillation index m, we found the long-term trends in the average scintillation indices <m> of all the sources in the grid, and then observed for each source the scintillation <u>enhancement</u> g = m/<m>. This makes the transient disturbances much easier to see: They appear as large regions, with well-defined boundaries, in which g differs significantly from unity. Careful comparison of our values of g with solar wind parameters measured by spacecraft near the Earth have shown beyond reasonable doubt that the scintillation observations measure density, or more accurately √density, at 1 au. Because the transient disturbances are three-dimensional and we see only the projection of these onto the sky, it is necessary to fit models to the observations. For this purpose, computer models to calculate the appearance of idealized disturbances have been developed.

This method has proved very successful in elucidating the large-scale structure of the transient disturbances that were seen during the observations. One example is that of a disturbance which caused a geomagnetic storm on 28 August 1978. This disturbance, which caused severe disruption to communications and power transmissions, was easily detectible on the IPS observations of the day before it arrived. Thus, a day's warning of the likelihood of geomagnetic activity could have been given, had the observations been analyzed in real time. Conventional techniques failed entirely to predict the storm.

The information obtained from large numbers of disturbances, both by direct observation and by statistical means, have enabled us to construct a standard picture of an interplanetary disturbance at solar maximum. This is a compression region formed by a fast flow in the solar wind which sweeps up the 'quiet' wind in front of it. The high density region usually travels from the Sun to the Earth at 400 to 450 km/s. This is followed by a fast low-density stream with a speed of about 500 km/s and a density of about half the ambient value.

The information obtained by IPS and from spacecraft are largely complementary, insofar as IPS measures large-scale structure while spacecraft make high-precision local measurements. For constraining dynamical models of the solar wind it is clear that the large-scale structure is the more important, and IPS is the <u>only</u> observational method of determining this structure.

3) Observations of radio source structure.

IPS observations are an important means of obtaining high resolution structural data on individual radio sources. The resolution obtainable is about 0.1 arcsec, with a maximum of about 2 arcsec. At 81.5 MHz, such data could be obtained interferometrically only with baselines between 500 and 10 000 km. The other advantages of IPS are that it is fast, and cheap. The principal disadvantage is that it gives only limited information about the structure of the observed source. IPS has been used in this way to obtain structural information which would otherwise have been difficult to obtain on many sources, including the compilation of catalogues of thousands of sources. The technique is also well suited to the identification of possible pulsars.

The determination of source structure by IPS relies on the fact that an extended source blurs the random diffraction pattern formed on the ground. This blurring reduces the width of the scintillation frequency spectrum, and also reduces the scintillation index. Both phenomena are in use as indicators of angular size, and both have been described at length in the literature.

4) Observing very faint sources by IPS.

Finally, we describe recent work performed at Cambridge in which the method of IPS has been combined with confusion analysis (p(D), or background deflexion analysis) to determine the average scintillation properties of radio sources whose flux densities at 81.5 MHz lie in the range 15 to 1.5 Jy.

Observations were made during the period 1981 August to 1982 October, using the Cambridge 36 000 m^2 array. This was operated in a number of different modes to sample source structure at different flux density levels between 2.4 and 1.5 Jy, and between declinations of 20° and 61°.

The data were processed to remove interference, solar breakthrough, the effects of the ionosphere and so on, and then analyzed to give histograms of p(D), where p is the probability of seeing a deflexion D in the scintillating output signal. The p(D) data give information principally about sources at the confusion level (i.e. sufficiently numerous that brighter sources occur, on average, once per beam area), whereas direct observations of individual sources are reliable only at flux densities 10 to 15 times greater. The p(D) distributions were analyzed to yield the rms scintillation index m_0 of the sources at the confusion level, for two ranges of solar elongation, 30°-50° and 60°-80°.

From these values of m_0, the IPS parameters R (the compactness, equal to the fraction of the total flux originating in the scintillating component) and θ (the angular diameter of the scintillating component) were deduced. The variation of m_0, θ and R with flux density S are shown in fig. 2, together with points for S = 15 Jy derived from the survey of 3000 discrete sources due to Purvis et al. It can be seen from the figure that the scintillation indices in the two elongation ranges increase from 15 Jy to 2.4 Jy, and then decrease rapidly to 1.5 Jy. The compactness R shows an increase from 0.3 at 15 Jy to 0.6 at 2.4 Jy, and an insignificant increase thereafter. The angular size θ increases from 0.35 arcsec at 15 Jy to 1.0 arcsec at 1.5 Jy.

The interpretation of these trends of R and θ with flux density sheds light on a number of important cosmological questions. Here we summarize the range of possible explanations in table 2. This logically divides all possibilities into four categories, according to whether faint sources are (a) further away or (b) less luminous, and to whether (a) θ and R are true representations of source structure or (b) they are affected by 'blending', in which slightly extended parts of a source scintillate dependently of the compact part, causing distorted values of θ and R to be observed. Each box of the table describes the straightforward implication of the data, and then lists effects which could cause such behaviour. For example, in the upper right-hand box, the angular sizes of the lobes decrease with increasing redshift; this could be explained by the inverse Compton effect.

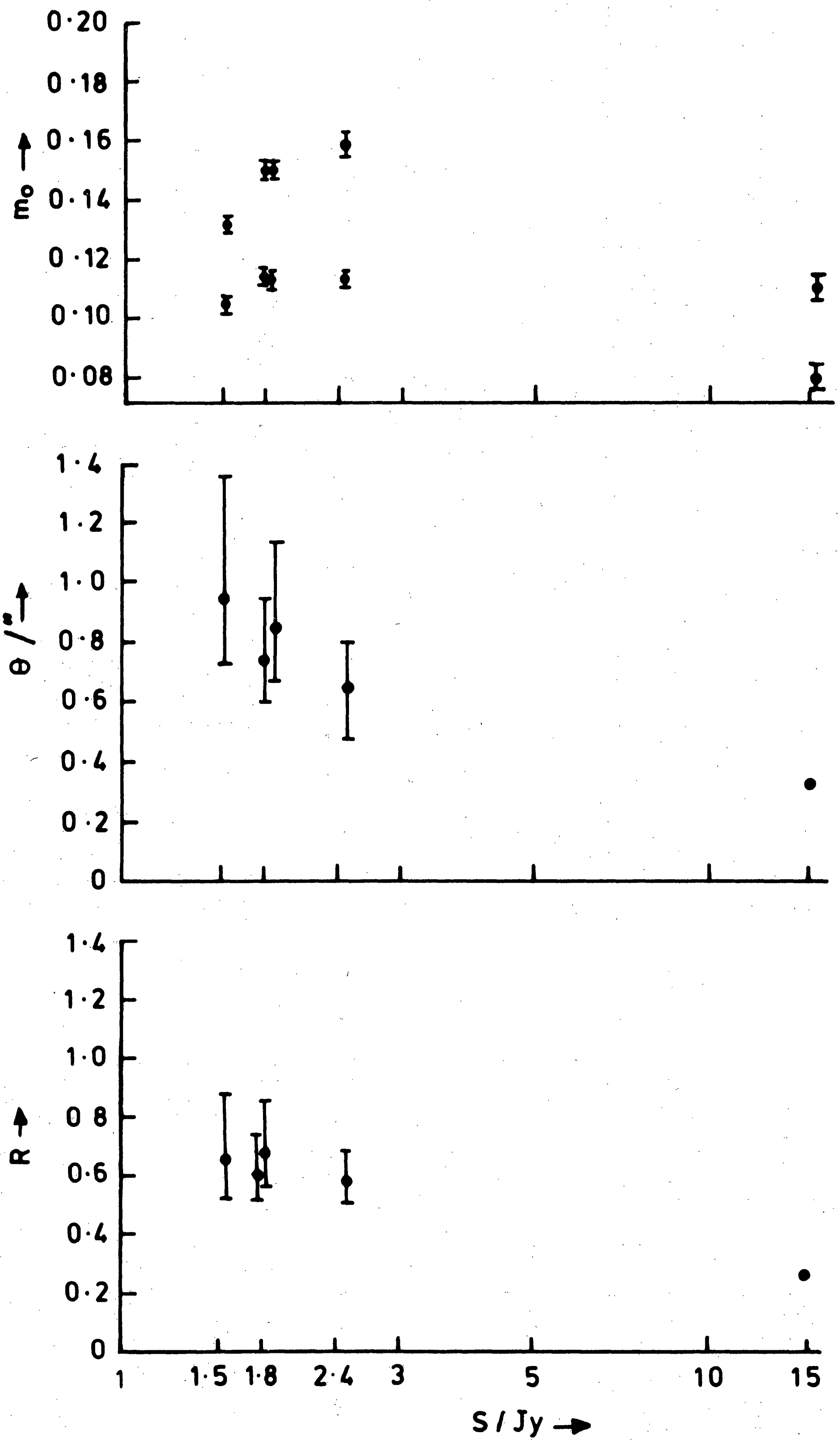

0·20
0·18
0·16
0·14
0·12
0·10
0·08
m_o
1·4
1·2
1·0
0·8
0·6
0·4
0·2
0
θ /″
R
1
1·5
1·8
2·4
3
5
10
15
S / Jy

Figure 2

Table 2

The range of possibilities implied by our measurements

	$\bar{\Theta}$ corresponds to true hotspot sizes	$\bar{\Theta}$ is affected by blending with lobes
Sources have same luminosities	Hotspot size increases with increasing z - *intergalactic scattering* - *qo = 0.8 if hotspots have same physical size*	Blending increases with z - *angular size of extended lobes decreases with increasing z*
Sources are at same redshift	Hotspot sizes increase with decreasing luminosity	Blending increases with decreasing luminosity - *physical sizes of extended lobes decrease with luminosity*

OBSERVATIONS OF STEEP SPECTRUM RADIO SOURCES FROM 30 TO 300,000,000,000 MHZ

D. E. HARRIS, Center for Astrophysics
I. McHARDY, University of Leicester
P. E. DEWDNEY and C. H. COSTAIN,
Dominion Radio Astrophysical Observatory

This written version will cover just a few bands of the frequency spectrum defined in the title: the participants of the workshop were not so lucky, as I was able to devote only 2 nanosec to each MHz. I should also mention at the outset that A. G. Willis and G. K. Miley are also collaborators on this project which has been receiving various amounts of our time for the last 5 years. Over this period, we have accumulated radio data from the DRAO (1420 MHz), the VLA (mostly 1420 MHz), WSRT (610 MHz), and most recently, from CLRO (57.5 and 30.9 MHz). Almost all of our fields were also observed with the Imaging Proportional Counter (IPC) of the Einstein Observatory (EO) and this is the basic reason that the radio observations were pursued. We also obtained optical spectra for redshift determinations of a few candidate identifications. Results for Abell 566, Abell 754, and 4C 08.66 have already been published.

Two EO Guest Projects formed the basis of this study. That of Willis et al. selected sources with steep spectra in the cm band, in order to isolate distant clusters of galaxies. In the proposal of Harris et al. sources with steep spectra below 100 MHz were chosen in order to increase the probability of selecting sources with a large number of low energy electrons (γ, the Lorentz energy factor = 2000). A further selection criterion was the absence of interplanetary scintillations, insuring that most of the flux density originated in structures greater than 1", a condition favoring weaker magnetic field strengths. These two conditions are the desirable characteristics for sources to be observable as "IC/3k" radiators: i.e. relativistic electrons scattering 3k background photons up to x-ray energies.

An allied, but more general question is "What happens to old electrons?" There are at least three possibilities. First, we have adiabatic expansion; but this cannot dominate in all cases because there are many extended sources which are still powerful radiators and thus must have survived the crippling early phases of expansion losses ($dE/dt=-v*E/r$ where v is the velocity of expansion and r is the characteristic radius). Next there is confinement, which describes the fate of dead radio lobes entrapped in a confining thermal gas (as in a rich cluster of galaxies).

Here we expect the E^2 losses (synchrotron or inverse-Compton) to progressively degrade the energy of the electrons, producing the well-known steep spectrum radio sources in clusters such as that in Abell 566. Finally there is diffusion out of the volume of space containing a reasonably strong magnetic field i.e."spreading the ashes to the winds" rather than being "locked in a steel casket". Figure 1 is an example of trying to show too many relationships at once,

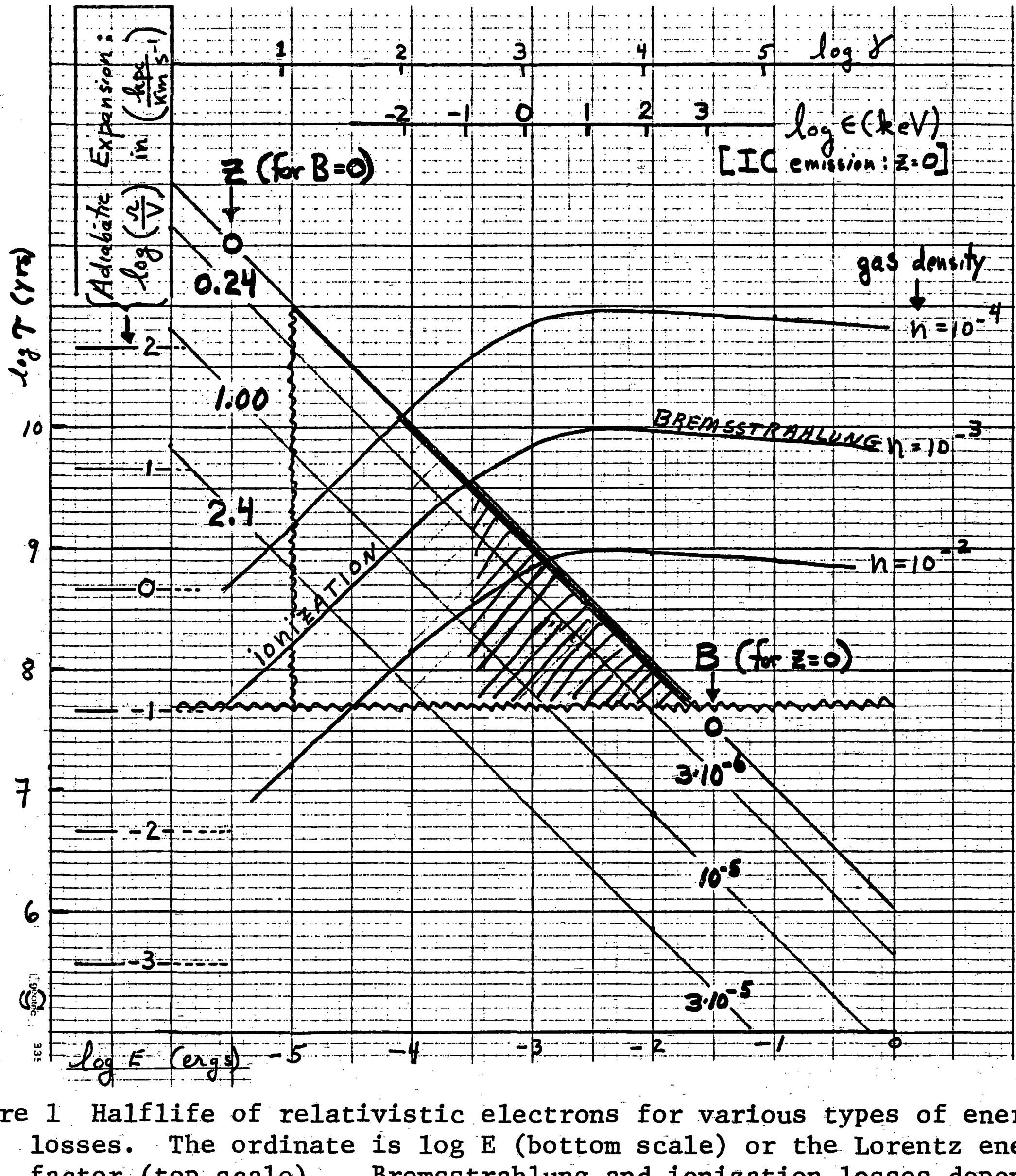

Figure 1 Halflife of relativistic electrons for various types of energy losses. The ordinate is log E (bottom scale) or the Lorentz energy factor (top scale). Bremsstrahlung and ionization losses depend on the ambient gas density, n ($/cm^{-3}$). Synchrotron and inverse Compton losses go as E^2 and are shown as the straight lines. Adiabatic expansion affects electrons of all energies equally: for a source expanding at 1 km/s with a characteristic radius of 1 kpc, log (r/v) is zero and all electrons lose half their energy in $5 \cdot 10^8$yrs. The electrons of interest for the present discussion are those with gamma=2000 (IC emission in the EO band) which attain ages of 10^8 yrs for the parameters indicated by the shaded region.

but, with some perseverence, it serves to summarize and quantize these notions.

The upshot of this discussion is that in the search for IC/3k x-ray emission, we are looking for large radio sources or remnants of radio sources 10^8 years after injection ceased: we are searching for all the relativistic electrons which ever radiated in a particular source!

METHODS OF USING THE DATA

We use the observed flux densities in the radio and the upper limit (or actual values if available) of the x-ray flux to determine the magnetic field strength, B, necessary to explain the x-ray emission (or limit) on the IC/3k model. Since part or all of any coincident x-ray emission may arise from thermal bremsstrahlung emission rather than from IC emission, B so derived is always a lower limit. In any event, this B is compared with B(eq), the field strength for equipartition, or B(min P), the field necessary for minimum non-thermal pressure within a radio feature. This is a circuitous route to assess the likelihood of IC/3k detection, but so far it has been extremely difficult to find convincing evidence for IC/3k emission from similar morphologies or from similar values of the spectral index (in the radio and x-ray bands). Most sources of interest are unresolved with the 90" FWHM IPC beam and with the small number of photons available from short observations, the x-ray spectral index is also poorly determined.

To study confinement and aging, we estimate the gas pressure from the x-ray data and the minimum non-thermal pressure, P(m), for various resolved or unresolved structures in the radio sources. Although we have no assurance that the radio source is actually embedded in the hot gas (rather than lying just beyond the high density regions), we smile when the gas pressure is greater than P(m) and frown when the situation is reversed. In a few cases (e.g. A566) we are able to obtain estimates of the time elapsed since injection ceased from the curvature of the radio spectrum.

FOUR FIELDS FROM THE OLD 26 MHZ SURVEY OF VINER AND ERICKSON

For sources with normal spectra, the flux density limits of the Viner and Erickson (VE) survey were such that any source detected should also be in the 4C catalogue. For this reason, we selected four sources from VE which were without 4C counterparts. Below we summarize the data and results in a very cursory way. The final study should be submitted to the Ap.J. in the first half of 1985.

CL0713+37

In this field we find two steep spectrum sources separated by a degree in declination (see Fig 2). The CLRO 26 MHz position is situated midway between them and the flux densities are such that it is highly likely that the VE entry represents a case of confusion. The northern source has a spectral index α=1.4. It has an "L" type radio morphology (i.e. a rather complex Wide Angle Tail) and is probably associated with an uncatalogued cluster of galaxies with m_V=18 to 19 mag. Unfortunately, this source was outside the field of the IPC. The southern source is a morphological twin to 3C 465, with a steep spectrum below 200 MHz, but with a strong core which dominates the spectrum above 200 MHz. It is identified with a galaxy (z=0.07) in a cluster. An extended X-ray source (outside the rib shadows of the IPC) is coincident, but there are too few counts to place a meaningful value on the x-ray size. If the two radio

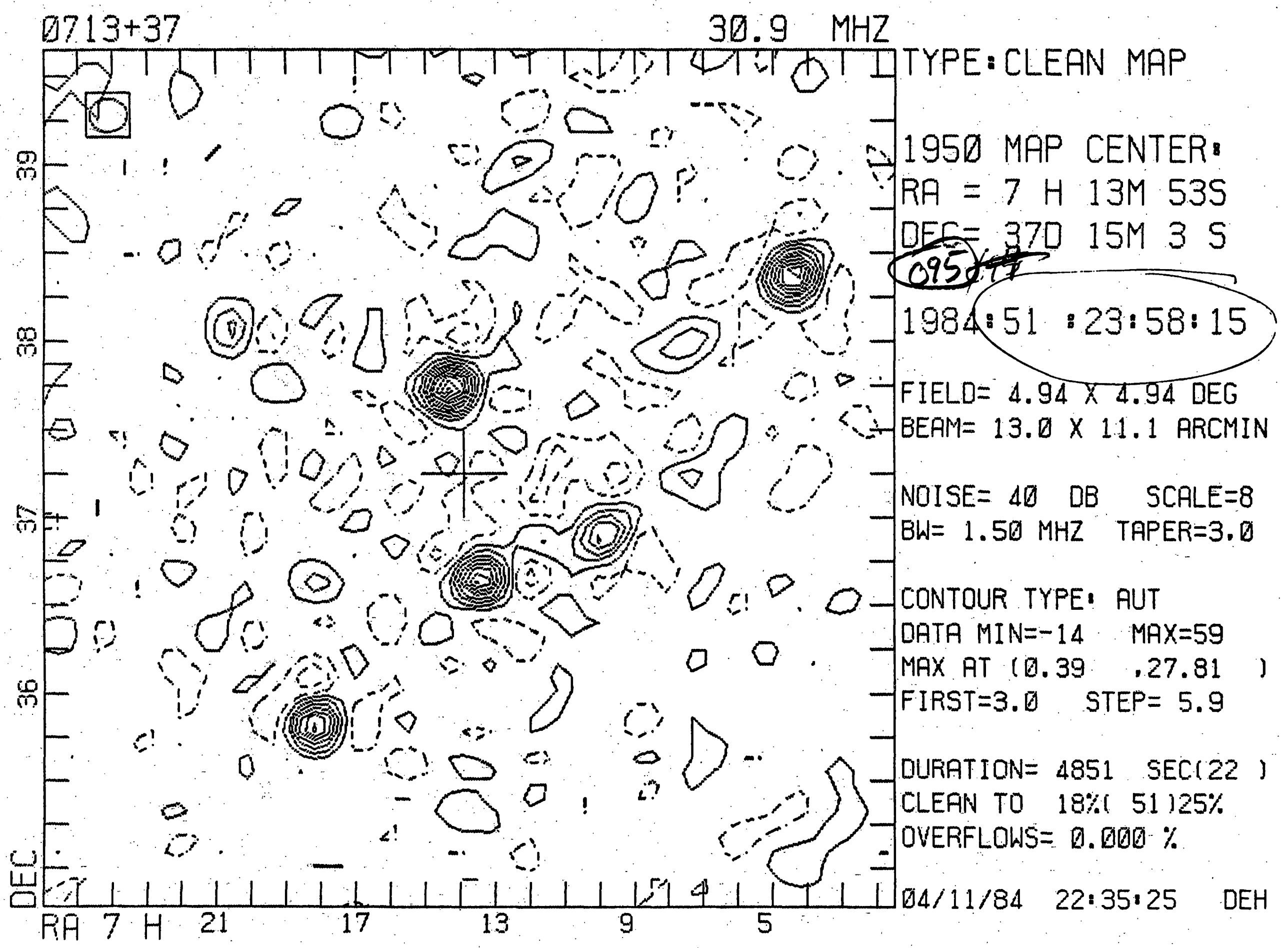

Figure 2 CL0713+37 at 30.9 MHz. The two sources discussed in the text are N and S of the field center (cross). The lowest contour is 1.2 Jy/beam and higher levels are at 10% intervals of the peak intensity which is 24.5 Jy/beam. The beam (insert) is 13'x11'.

spectral components correspond to the two spatial components (low frequency component=tails, high frequency component=core) then the IC calculation gives B(IC/3k)>0.4 μ Gauss. A rough estimate of the field required for minimum non-thermal pressue in the tails is B(min P)=0.7 μ Gauss.

CL1244+26

The CLRO 26 MHz source is resolved into two components separated by 2.5′ arcmin in RA, which is a significant fraction of the 4C fringe separation of 7.4′. No optical identification has been found and no x-ray emission was detected.

CL1530+41

The bulk of the low frequency emission comes from an unidentified source with α=1.0. However, 6′ to the NE is an extended radio source (α=0.9) identified with a 17.5 mag galaxy and an x-ray source.

CL1718+26

In this field we find a source with α=1.4, identified with an uncatalogued cluster of galaxies at z=0.162 which is also an X-ray source. The new CLRO obarvations (Figure 3) demonstrate the power of the TPT to distinguish spatially and spectrally the source of interest.

CONCLUSION

As most of us are aware, there has been a general neglect of the art and science of "low frequency" radio astronomy. The studies outlined here demonstrate several interfaces with other disciplines of astrophysics. An accurate knowledge of the spatial and spectral distribution below 100 MHz is necessary for success in these undertakings. First, we have the difficult and perhaps slightly exotic effort to detect IC/3k emission. Second is the more mundane (observationally speaking) but important problem of pressure confinement and aging effects in the environment of rich clusters and in regions of lower density. Is the conventional wisdom correct in this area? For what classes of radio sources and X-ray clusters does it hold? Finally, what is the eventual fate of old, tired electrons?

REFERENCES

This was a workshop: references are forbidden. However, there will be a substantial list in the Ap. J. article!

(a)

(b)

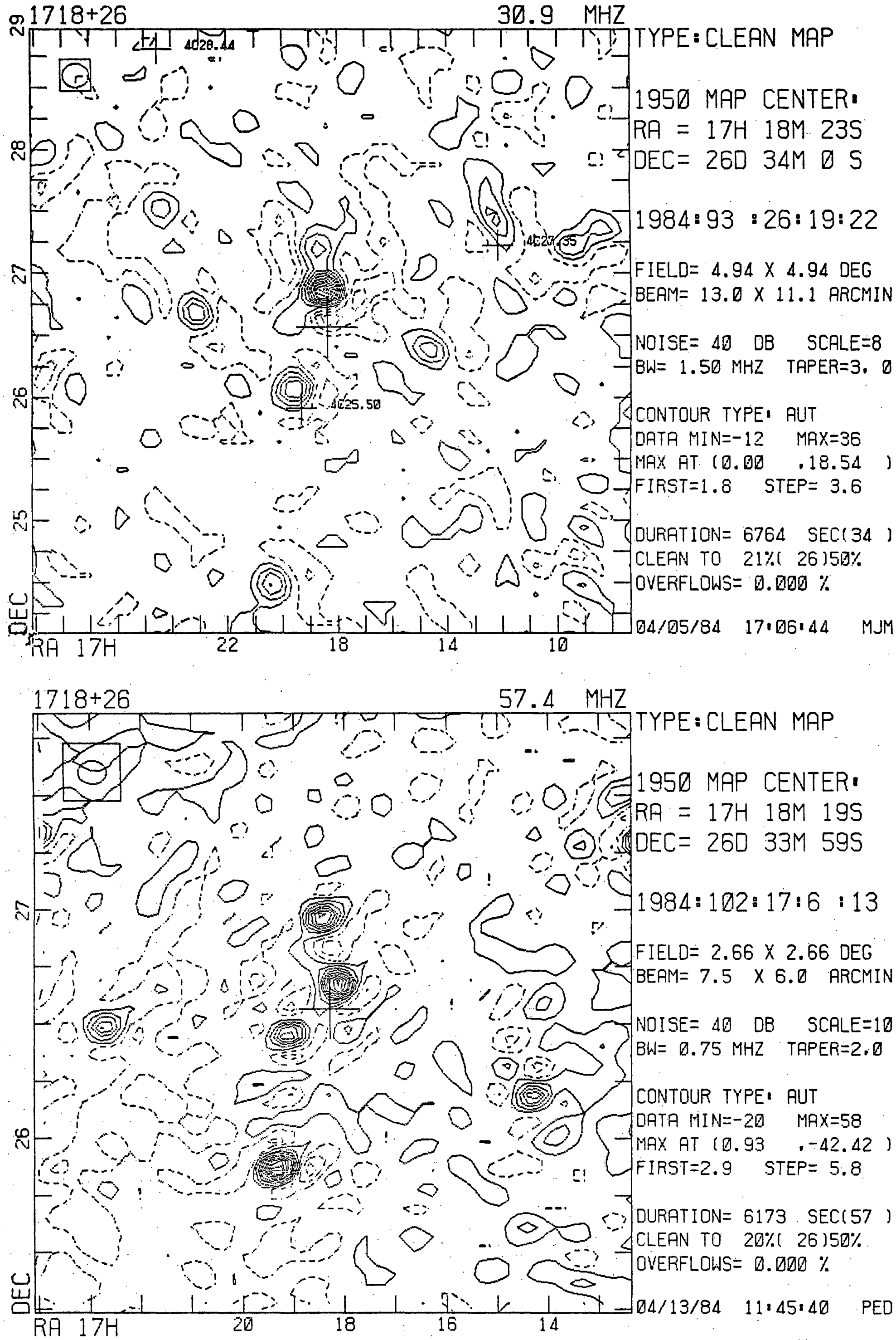

Figure 3 Contour maps of CL1718+26. The steep spectrum source is just north of the field center: compare the relative intensities of adjacent sources.
a) 30.9 MHz: the first contour is 0.75 Jy/beam and successive levels are at 10% intervals of the peak = 15 Jy/beam.
b) 57.4 MHz: the first contour is 0.44 Jy/beam and higher levels are at 10% intervals of the peak = 8.7 Jy/beam. The central source has a flux density of 7.6 Jy.

OBSERVATIONS OF M31 AND EDGE-ON SPIRAL GALAXIES

H. V. CANE, Laboratory for High Energy Astrophysics,

NASA/GFSC

W. C. ERICKSON, Clark Lake Radio Observatory,

University of Maryland

Summary

We have made low frequency (<60 MHz) observations of four normal galaxies; M31, NGC 891, NGC 4565 and NGC 4631. Our purpose was to look for emission which could be attributed to galactic radio halos. For none of the galaxies did the data require the presence of a radio halo. However, the data for NGC 4631 are compatible with the presence of a halo with the intensity of emission as discussed by a number of authors. Our observations of M31 at frequencies below 50 MHz reveal the nuclear source and enable us to derive its spectrum.

One of the major motivations for studying spiral galaxies is the hope of gaining information which will aid in the understanding of our own Galaxy. Our Galaxy is, of course, the easiest Galaxy to observe but since we are immersed in the system it is often difficult to interpret the observations. In particular, it is difficult to determine the distribution of interstellar material and, especially, its scale height.

The concept of a halo around the Galaxy was originally introduced from two different viewpoints. First, a halo was invoked (Shklovskii, 1952) to explain the bright radio emission observed out of the plane of the Galaxy. Second, Pikelner (1953) introduced the concept of a physical halo as the volume filled by cosmic rays. The question of the confinement region of cosmic rays remains unanswered. However, it is clear that much of the high latitude radio emission can be attributed to local (<1 kpc) structure and the separation of a true halo component is essentially impossible. Thus one is forced to study external systems which are similar to the Galaxy.

The closest object is M31 and the first observations were made with a 2 degree beam in 1951 (Hanbury Brown and Hazard). Subsequent observations by Baldwin (1954) were interpreted in terms of a disk component and a spherical component, the latter containing two-thirds of the total flux density. It was this result which for many years was used as supporting evidence for a radio halo in our Galaxy. Observations by Pooley (1969) showed that there were more than 200 discrete objects in the field of M31 and that these could account for the structure seen in earlier maps. However it was not possible to rule out the presence of a low luminosity extended region.

Since the radio emission from any external galaxy's halo presumably has a steeper spectrum than its disk emission (and the foreground Galactic disk emission), its detectability should be greatest at low frequencies. The Clark Lake TPT (Erickson et al., 1982) is the only instrument which operates at frequencies less than 100 MHz with adequate resolution to search for halos. We observed

M31 at 25.6, 30.9 and 57.5 MHz in January 1984. Further measurements were made in August 1985 when some additional data were also taken at 38.5 MHz.

Figures 1, 2 and 3 are three maps of the M 31 region at 25.6, 30.9 and 57.5 MHz. On the 30.9 MHz map we have marked the known sources. Figure 4 is our 30.9 MHz map convolved to the same beam (27x47 arc-min) as that used by Artyukh and Ogannisyan (1984) at 103 MHz. We find that there are essentially no differences between the 30.9 MHz and 103 MHz maps, apart form those due to external sources with different spectra. The distribution is also comparable to that

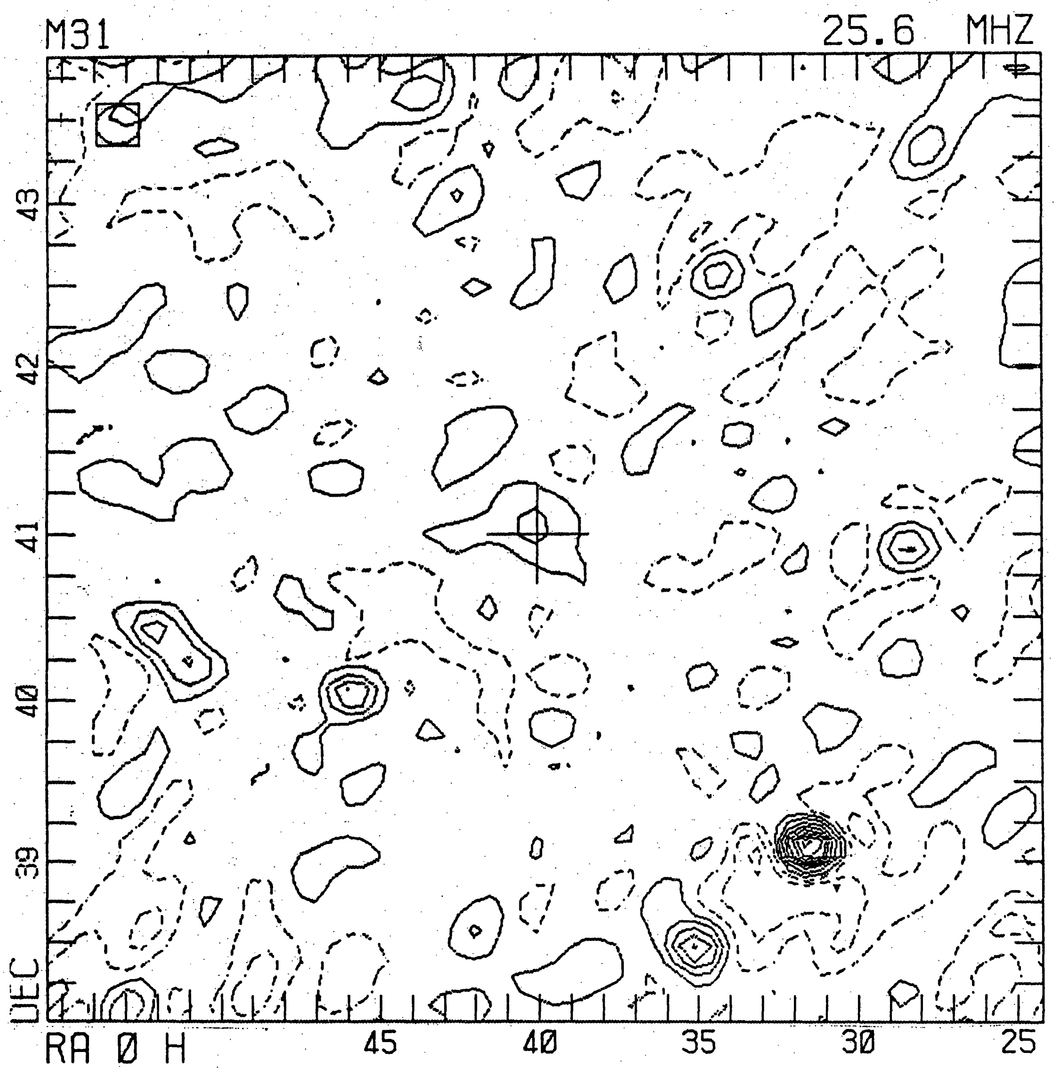

Figure 1

seen in the 408 MHz map (Haslam et al., 1974) obtained with a beamwidth of 37 arc-min. The resemblances of all three maps suggest that no halo emission is perceptible at 30.9 MHz.

Artyukh and Ogannisyan (1984) find a scintillating source 13 arc-min from the nucleus of M31 and identify this with the supernova, S Andromedae, which occurred in 1885. This source is probably 5C3.107 and is the source seen near the center of the 57.5 MHz map (Figure 1). At 30.9 MHz (Figure 2) the spectrum of this source has turned over but at 25.6 MHz there is another source of about 5.5 Jy near the map center which we identify with the nucleus

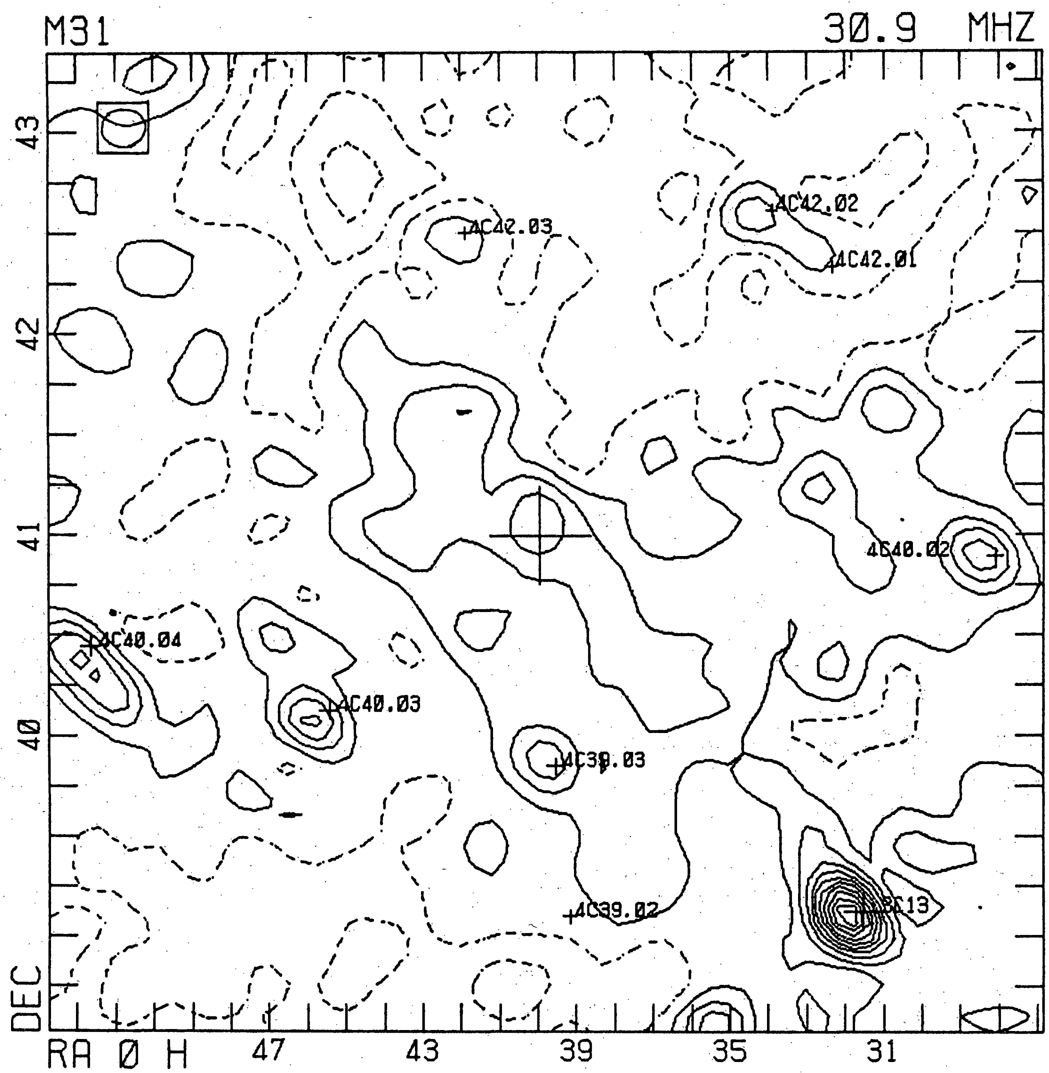

Figure 2

of M31. Our estimates for the flux density of this nuclear source at 25.6, 30.9 and 38.5 MHz are consistent with the measurements of Pooley (1969) and imply a spectral index of -0.6 with some steepening of the spectrum at low frequencies. Clark Lake data indicate that the Galaxy also has a steep-spectrum source associated with its nucleus (LaRosa and Kassim, 1985).

Apart from searches for extended structure another way of investigating the presence of radio halos is to look for steep spectrum components in unresolved sources. Given that cosmic rays have their origin in galactic disks, the old age of those cosmic rays

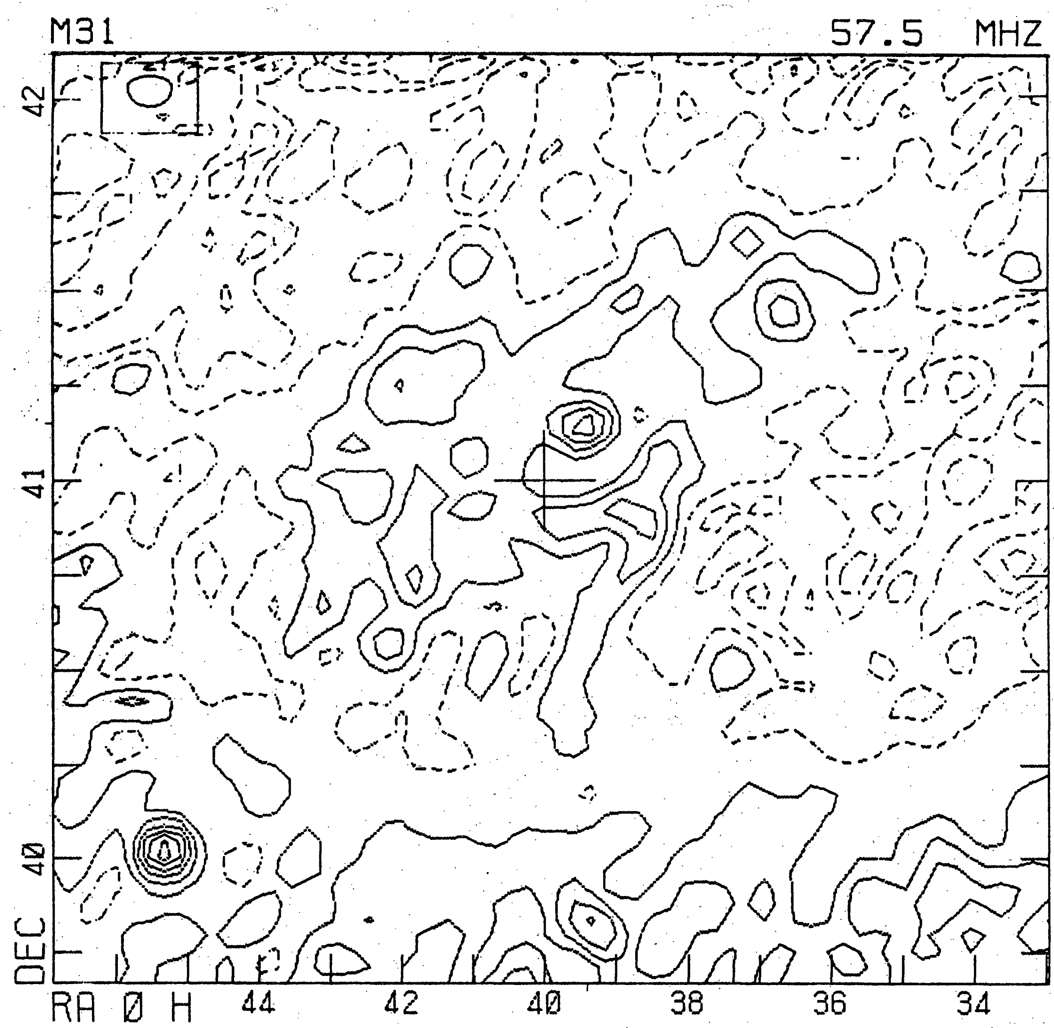

Figure 3

that diffuse out into a halo region will produce a radio spectrum that will be steeper than that of the disk. This property was invoked by Webster (1975, 1978) who, in recent years, is the only researcher to address the question of a Galactic radio halo. Unfortunately, in the Galaxy the technique can not be applied unambiguously. In his analysis it was necessary for Webster to assume that the spectral index of the disk was everywhere constant. This is not expected because of local inhomogeneities and is inconsistent with observations (Bridle, 1967; Cane, 1978). Meanwhile, attention has been directed at the few spiral galaxies which are edge-on and close

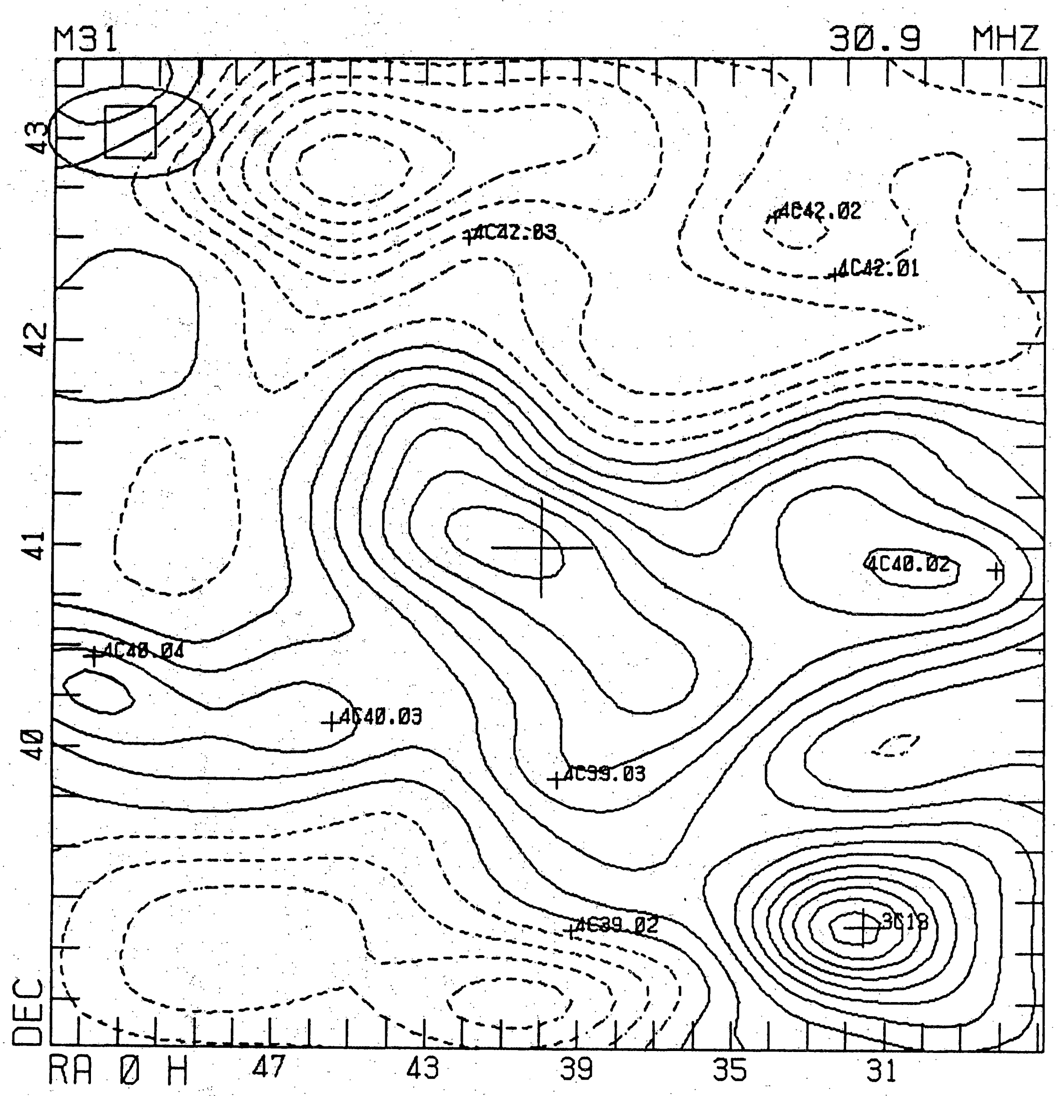

Figure 4

enough to be resolved at centimeter wavelengths. There are less than half a dozen such galaxies, the most favorable ones are NGC 4631 and NGC 891. A third suitable galaxy is NGC 4565. We observed these galaxies at Clark Lake with the following results:

	NGC 891	NGC 4565	NGC 4631
30.9 MHz	< 3.0 Jy	< 1.0 Jy	9 to 25 Jy
38.0 MHz	---	---	< 10 Jy
57.5 MHz	4.5±2.0 Jy	< 3.1 Jy	12.4±4.0 Jy

Figures 5, 6, and 7 show the integrated spectra of these three edge-on galaxies. The flux densities were obtained from compilations in the following papers: NGC 891 - Allen et al. (1978); NGC 4565 - Hummel et al. (1984); NGC 4631 - Pooley (1969), Sukumar

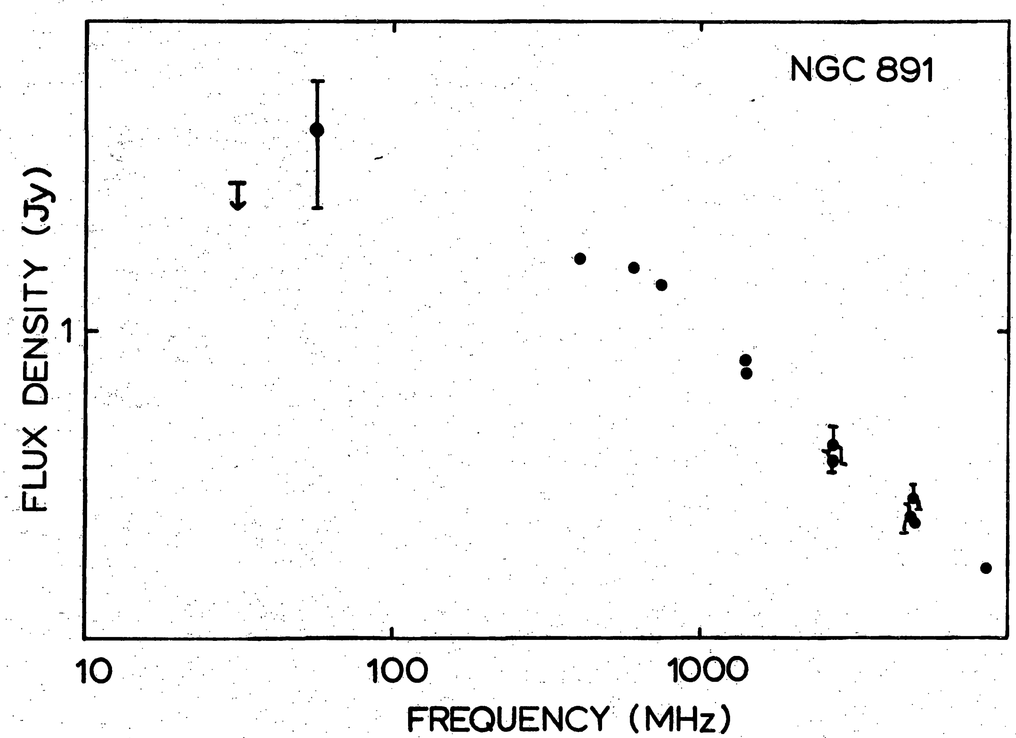

Figure 5

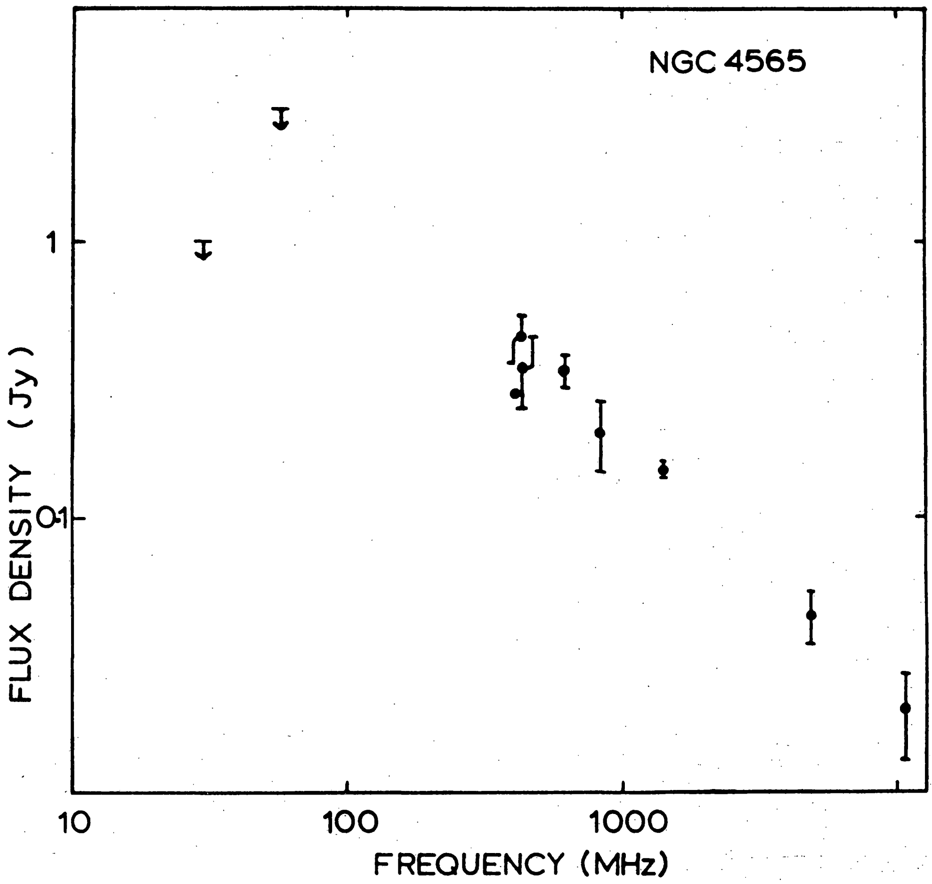

Figure 6

and Velusamy (1985). Combining our 57.5 MHz measurements with those at higher frequencies we obtain spectral indices of −0.75 and −0.95 for NGC 891 and NGC 4565 respectively. For both these galaxies the 30.9 MHz upper limits are well below the spectra extrapolated from higher frequencies. We assume that such turn overs are caused by free-free absorption; the existence of a turn-over caused by free-free absorption implies that the associated emission is generated predominantely by a disk component rather than a halo component. Low frequency observations of our Galaxy would suggest that the spectrum of its disk component would also turn over somewhere near 30 MHz (Cane, 1978) if viewed from an edge-on direction.

We made two independent measurements of NGC 4631 at 30.9 MHz and

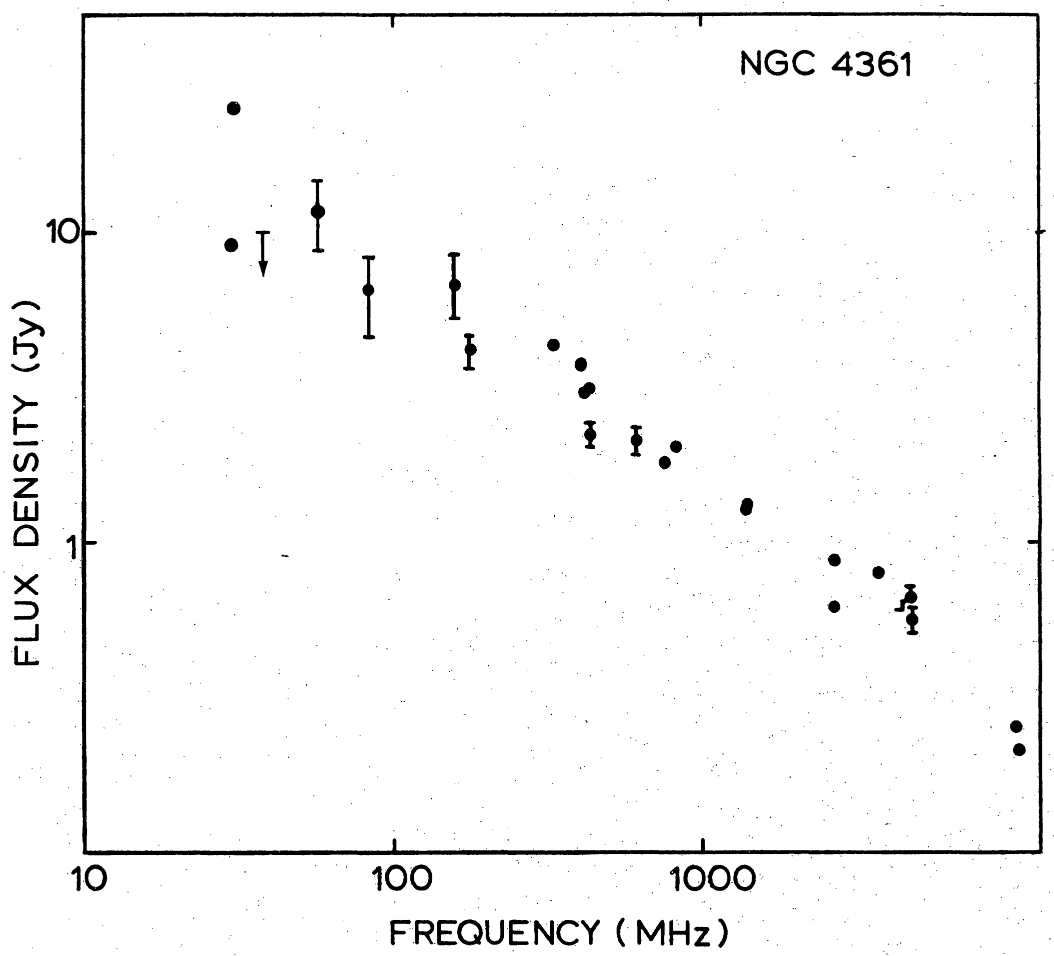

Figure 7

obtained inconsistent total flux densities of 9 and 25 Jy. The galaxy is partially resolved at 57.5 MHz. Its peak flux density was 8.5 Jy/beam and its integrated flux density is estimated to be 12.4 Jy. The 38 MHz data suggest a flattening of the spectrum below 57.5 MHz but the possibility that this may be followed by a rise at lower frequencies cannot be ruled out. Thus the shape that one expects from a galaxy with two components viz. a disk component with emission and absorption, and a halo component which dominates at low frequencies is allowed by our measurements. The integrated spectrum using the 327 MHz core-halo flux densities and spectral indices estimated by Sukumar and Velusamy (1985) is in reasonable agreement with our measurements.

This work was supported by the National Science Foundation under Grant AST 8416179.

REFERENCES

Allen, R.J., Baldwin, J.E. and Sancisi, R., Astron. Astrophys. 62, 397, 1978.

Artyukh, V.S. and Ogannisyan, M.A., Sov. Astron. 28(4), 375, 1984.

Baldwin, J.E., Nature 174, 320, 1954.

Bridle, A.H., Mon. Not. R. astr. Soc. 136, 219, 1967.

Brown, R. Hanbury, and Hazard, C., Mon. Not. R. astr. Soc. 111, 357, 1951.

Cane, H.V., PhD thesis, University of Tasmania, 1978.

Erickson, W.C., Mahoney, M.J. and Erb, K., Ap. J. Suppl. 50, 403, 1982.

Haslam, C.G.T., Wilson, W.E., Graham, D.A. and Hunt, C.G., Astron. Astrophys. Suppl. 13, 359, 1974.

Hummel, E., Sancisi, R. and Ekers, R.D., Astron. Astrophys. 133, 1, 1984.

LaRosa, T.N. and Kassim, N.E., Astrophys. J. Lett. 299, L13, 1985.

Pikelner, S.B., Dokl. Akad. Nauk SSSR 88, 229, 1953.

Pooley, G.G., Mon. Not. R. astr. Soc. 144, 101, 1969.

Pooley, G.G., Mon. Not. R. astr. Soc. 144, 143, 1969.

Sukumar, S. and Velusamy, T, Mon. Not. R. astr. Soc. 212, 367, 1985.

Shklovskii, I.S., Astron. Zh. 29, 418, 1952.

Webster, A., Mon. Not. R. astr. Soc. 171, 243, 1975.

Webster, A., Mon. Not. R. astr. Soc. 185, 507, 1978.

Wielebinski, R., Astron. Astrophys. 48, 155, 1976.

Observations of Pulsars with the Gauribidanur Radio Telescope

A.A. Deshpande, Ch.V. Sastry & V. Radhakrishnan
Raman Research Institute, Bangalore-560080.

The pulsars PSR 1919 + 21 and PSR 0950 + 08 were observed with the Gauribidanur Radio Telescope at 34.5 MHz which has a collecting area of 250 λ^2 and beamwidths of 26' x 40'. The observations were made using the recently installed tracking system which permits tracking of a source for 42 secδ minutes.

Observations of PSR 0950 + 08 were made using a bandwidth of 30 KHz and a post detector time constant of 10 msecs, while PSR 1919 + 21 was observed using a 16-channel receiver (BW 60 KHz and channel separation of 40 KHz) and post detector time constant of 100 msecs.

Analysis and Results

The detector outputs were directly recorded on a magnetic tape unit. The data from each channel were then folded over a two period stretch. In the case of PSR 1919 + 21, the folded outputs of the 16-channels were added after appropriate shifts in time. Average pulse profiles of the even and odd pulses in the two period stretch were added to get the final average profiles and are shown in Figure 1.

These profiles were used to estimate (1) the average energy

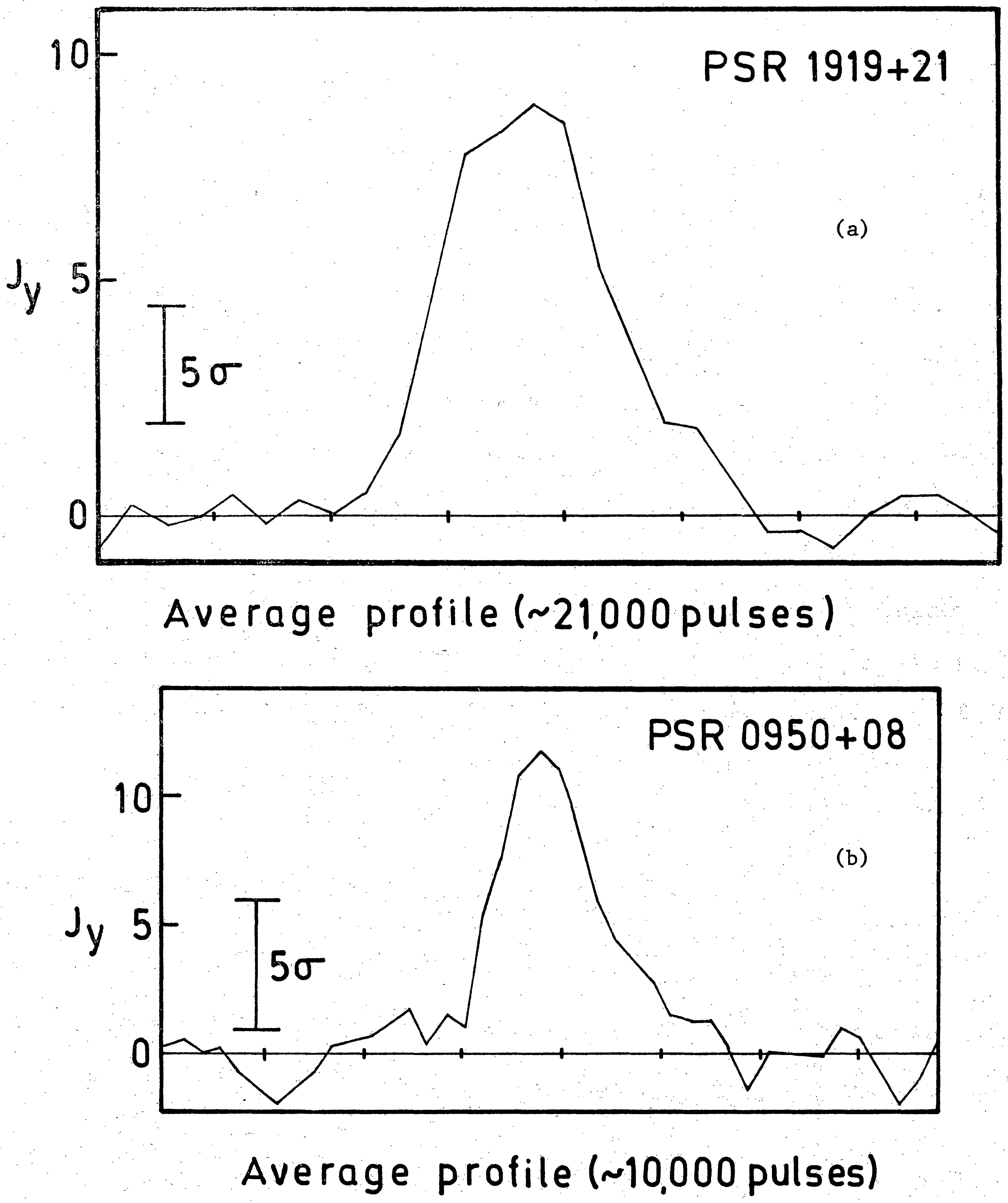

Figure 1

per pulse, (2) the amount of interstellar scattering in the pulsar direction at 34.5 MHz.

The average energy per pulse for PSR 1919 + 21 at 34.5 MHz was (2550 $\pm$ 400) $10^{-29}Jm^{-2}Hz^{-1}$ and that for PSR 0950 + 08, was (480 $\pm$ 140) $10^{-29}Jm^{-2}Hz^{-1}$. The spectra of these pulsars were compiled by Bruk et.al. (1978) in the frequency range 16.7 to 1420 Mhz. The average spectra of these pulsars including our values are shown in Fig. 2. In the case of PSR 1919 + 21 the measured energy

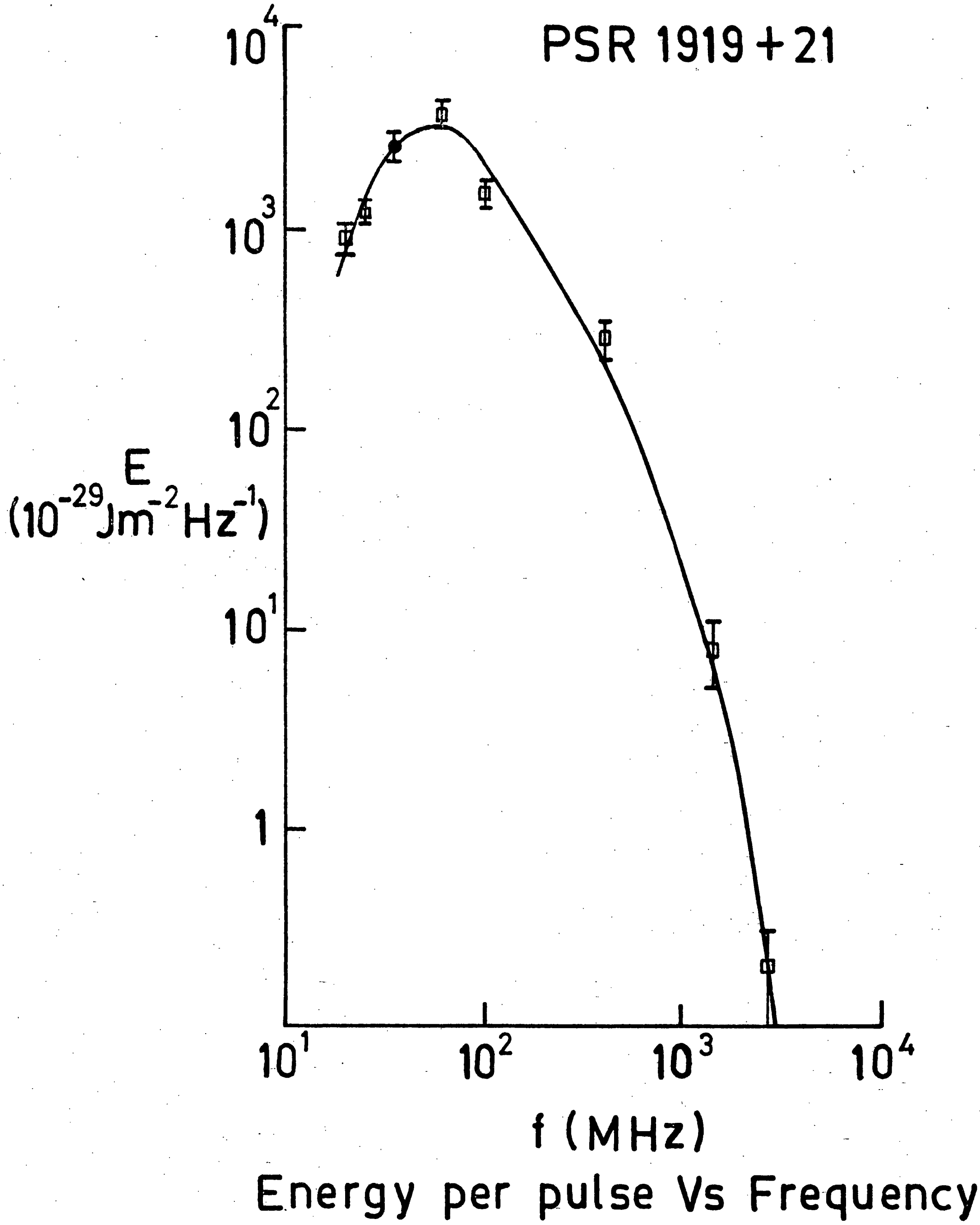

Figure 2(a)

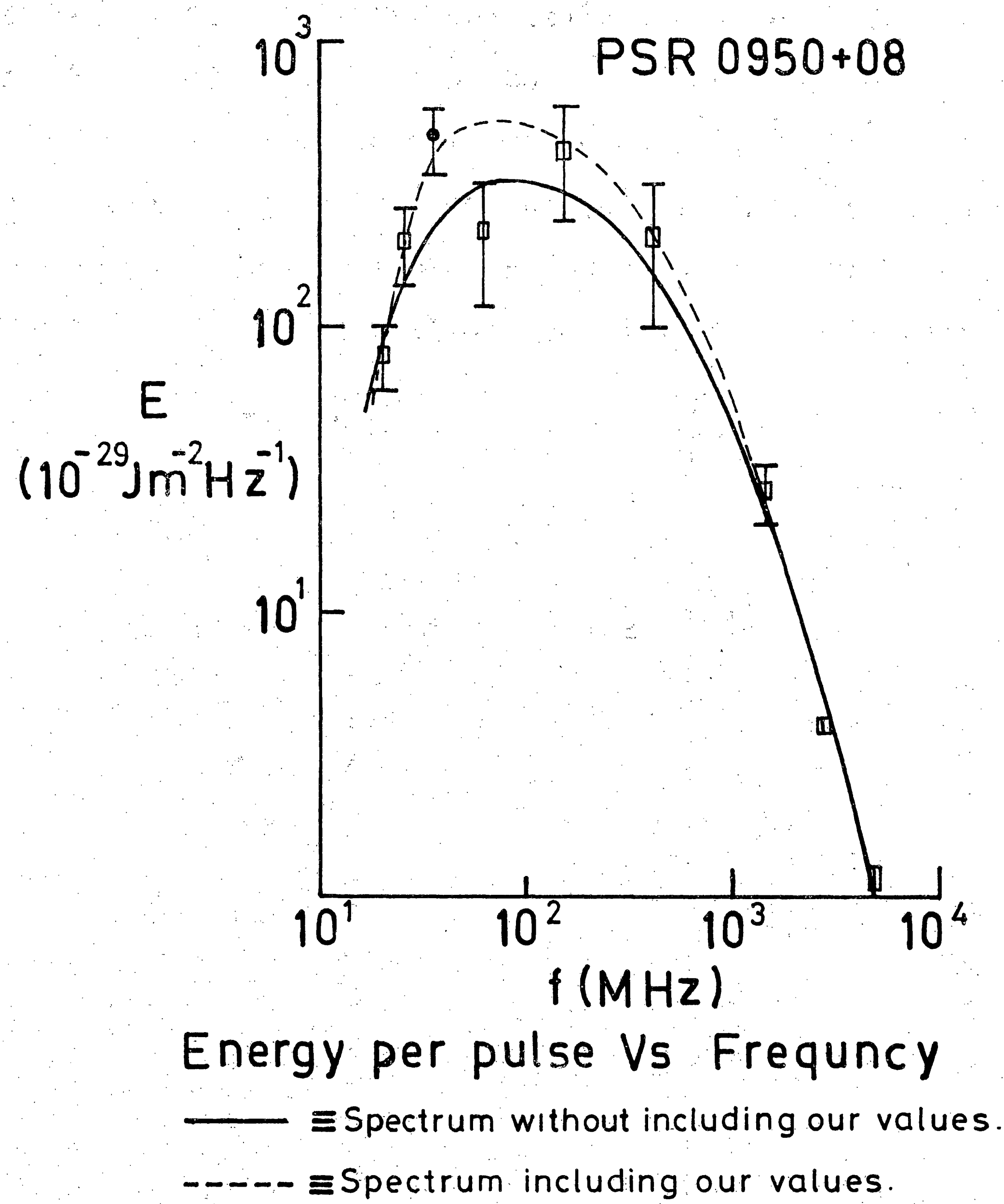

Figure 2(b)

at 34.5 MHz fits reasonably well with the spectrum given by Bruk et.al. (1978) but for PSR 0950 + 08 it appears that the pulse energy at 61 MHz quoted by V.A. Izvekova et.al. (1979) is an underestimate, possibly due to inadequate smoothing of interstellar scintillations.

The amount of interstellar scattering was estimated by finding the best fit f(t) for the average profile using the CHI-square test. The function f(t) used had the form

$$f(t) = p(t) * s(t) * d(t) * i(t)$$

where $p(t)$ = A Gaussian pulse of width

$$W_{0.5} = W_{0.5}(\text{at } 400\,\text{MHz}) \times (34.5/400)^{-0.25}$$

$s(t)$ = A truncated exponential, with τ_s as the characteristic time constant, representing scattering impulse response of the interstellar medium.

$d(t)$ = Dispersion function as a function of DM and pre-detection filter band shape.

$i(t)$ = A truncated exponential with a characteristic width equal to the post-detection RC time constant.

$*$ = Convolution

From this analysis, we estimate τ_s to be 67 $\pm$ 22m sec, in the case of PSR 1919 + 21, and $9.0 \pm^{5.5}_{4.5}$ m sec in the case of PSR 0950 + 08. The main sources of error in these estimates, apart from noise, are the uncertainties in the determination of d(t) because of the inaccuracies in band shape determination.

In the case of PSR 0950 + 08, this error is minimal because of the accurate determination of the predetection filter band shape.

The value of τ_s obtained here are much larger than those expected from the decorrelation band-width ($\Delta\nu$) measurements at high frequencies, if the two relations $2\pi\Delta\nu\tau_s = 1$, Sutton (1971) , and $\tau_s \propto \nu^{-4}$ are assumed. As discussed by Sutton, if the condition of multiple scattering is barely satisfied, then it will cause $\Delta\nu$ to exceed its theoretical value, while τ_s derived from pulse shapes averaged over many scintillation features will be unaffected. Most probably, the condition of multiple scattering is barely satisfied for near-by pulsars. Further, the condition of strong scattering is also not quite satisfied for nearby pulsars. Therefore the relation $2\pi\Delta\nu\tau_s = 1$ is almost certainly inappropriate in the case of nearby pulsars. If, in general, $2\pi\Delta\nu\tau_s = K$, then K has the value $\simeq$ 17 for PSR 1919 + 21 and $\simeq$ 70 for PSR 0950 + 08.

Such large values for K, call for further investigations into the validity of the ($\tau_s \rightarrow \Delta\nu$) relation for nearby pulsars and generally for low DM pulsars. However, it should be borne in mind that the estimates of τ_s could have large errors if the intrinsic pulse widths at low frequencies are very different from the values obtained by extrapolation from high frequencies.

No interpulse feature is obvious in either of the two pulsars. We plan further observations to improve on the signal to noise ratio achieved here.

LONG-BASELINE INTERFEROMETRY AT 81.5 MHz

by P. J. Duffett-Smith, M. J. Spinks, and W. G. Rees.

1. Introduction

The need for long-baseline interferometry at 81.5 MHz arose as a natural extension to interplanetary scintillation (IPS) studies at Cambridge. Measurements with the 3.6-hectare Array over a number of years have provided a body of high-quality data on nearly 2000 individual radio sources (Purvis et al., in preparation), besides statistical evidence for variations in average angular size and compactness with flux density between 15 and 1.5 Jy (Rees and Duffett-Smith, in preparation; see also the contribution by Rees et al. in this volume). One of the clearest results from IPS is that many sources which are compact at high frequencies are extended at metre wavelengths, with a significant proportion of their total emission arising in structure >> 2 arcsec (Duffett-Smith, 1980; see also VLBI measurements at 81.5 MHz by Hartas et al., 1983; Laing, 1981; Perley et al., 1980). A range of resolving powers from arcminutes to less than 1 arcsec at 81.5 MHz is required to measure such sources accurately, and this is available only by interferometry with baselines from a few hundred metres to more than 1000 km. We have therefore embarked on a programme of long-baseline interferometry at this frequency with a view to mapping radio sources brighter than about 5 Jy.

There are a number of difficulties. First, few if any antennas are available at this frequency within 1000 km of Cambridge. While MERLIN is now operating at 150 MHz, its maximum baseline is presently limited to about 150 km and its minimum to about 6 km, although the incorporation of another element at Cambridge will make significant contributions at both ends. Second, the 81.5 MHz band (or any other below 150 MHz) is not protected for radio astronomy except by local agreement within 30 km of Cambridge. Third, differential Faraday rotation in the ionosphere between the two ends of the interferometer becomes serious for baselines greater than about 50 km. Fourth, as in all VLBI measurements, the local oscillators are incoherent except over relatively short times. Fifth, and most serious, is the difficulty imposed by the effects of celestial plasmas on the phases of the signals propagating through them, especially the ionosphere, the interplanetary medium, and the interstellar medium. Nevertheless, it _is_ possible to make useful measurements, and we now describe the manner in which we have attempted to overcome these difficulties.

2. The interferometer

We have converted the large fixed element of the 4C interferometer to work as a tracking antenna at 81.5 MHz (Rees & Duffett-Smith, 1984). A line feed of 256 half-wave dipoles at the focus of a cylindrical trough reflecting screen can be phased electrically to track sources north of declination -5 degrees for at least 6 hours. It has a geometrical collecting area of 9600

m^2, sufficiently large that it can be combined with a much smaller antenna the other end of the baseline to give a useful interferometer sensitivity. We use a portable array of Yagi antennas at the remote station which, in principle, we can position to give any desired baseline. Since only a few hundred square metres of ground are required for a few days at a time, there is not usually much difficulty in finding suitable sites. The receiving, timing and recording equipment for the remote antenna is housed in a motor caravan which also serves to tow the antenna trailer between locations and to house the observer in reasonable comfort when necessary.

Signals are received in a total bandwidth of 1 MHz, subdivided into 8 contiguous channels of 125 kHz. Simple double-sideband receivers are used having sine/cosine (quadrature phase) outputs which are recorded on standard video cassette tapes. Two recorders are used at each terminal to cover the full 6-hour tracking period. They are switched by a microprocessor so that a single observer can operate the interferometer by himself provided that he can drive from one end to the other within a few hours. Subdividing the receiving band into a number of smaller channels helps to overcome the problem of interference. This is usually man-made, narrow band, and very strong. If the full band of 1 MHz were to be sampled and recorded with one-bit representation (as is usual in VLBI) a strong signal anywhere within the band would obliterate all the data. In the multi-channel case, the same signal affects only one of the channels.

The recorded tapes are played back and correlated using a purpose-built play-back system. The cross-correlation function is measured in fifteen delays in cosine and sine phases in each polarisation in each of the 8 frequency channels. Geometric fringe rate and delay corrections are applied so that the data can be integrated for 1 second before recording on magnetic tape for subsequent processing. A full six-hour run takes about 9 hours to process sufficiently that it may be passed to the mapping package. We generally correlate each day's data within 24 hours of recording.

The large fixed antenna at Cambridge receives signals in one linear polarisation. For baselines larger than about 50 km, differential Faraday rotation (DFR) in the ionosphere becomes significant. Observations by Rees & Duffett-Smith (1985) on a baseline of 130 km at latitude 51° N indicate that the rms DFR is about 25° at 81.5 MHz, being more than 45° about 10 per cent of the time. DFR is expected to scale roughly as the square of the wavelength and as the baseline length up to about 100 km. Two arrays of yagi antennas are used at the remote station, set to receive in orthogonal linear polarisations. When DFR is expected to be serious, both polarisations can be recorded at once, though with a small reduction in overall sensitivity.

The interferometer is synchronised using low-frequency radio transmissions. MSF Rugby (National Physical Laboratory) on 60 kHz provides time-coded signals for automatic time transfer to within a few hundred microseconds. Hence we do not need to keep our clocks operating continuously to preserve time, but can switch on from 'cold' and achieve synchronisation in a few minutes. Fine adjustment to within 5 microseconds is made using the LORAN-C (US Coastguard) transmissions on 100 kHz.

The local oscillators at each site are locked to rubidium frequency standards (which also supply the reference signals for the clocks). These units have a coherence time of about 15 minutes at 81.5 MHz, but coherence over the full six-hour tracking period might be achieved by locking the standards themselves to low-frequency ground-wave transmissions. The short-term stabilities of the rubidium standards are preserved, but their longer-term variations are reduced. This method requires that both stations are locked to the same LF signal and that there is no significant differential variation in the propagation paths from the transmitter to either station. Hence it is essential to select ground-wave signals only. We use the LORAN-C transmissions for this purpose. Our automatic tracking receivers provide, as a by-product, a signal proportional to the accumulated phase error between the LORAN-C ground wave and rubidium references. We use this to vary the magnetic field inside the rubidium cavity, thereby making fine adjustments to the resonant frequency. Early results indicate that it is possible to maintain phase coherence by this method to within 90^{o} over 6 hours on the shorter baselines.

3. Celestial plasmas

(i) The ionosphere

Irregularities of refractive index cause phase and intensity scintillations on a length scale of about 5 km and a time scale of about 10 s. These sometimes result in appreciable decorrelation of the interferometer signals, but can usually be ignored when the ionosphere is in its 'quiescent' state. Much more serious are the phase errors introduced by quasi-periodic travelling ionospheric disturbances. Rees and Duffett-Smith (1985) recorded up to 24 radians of differential phase at 81.5 MHz across their baseline of 130 km on a time scale of 20 minutes. This is entirely consistent with observations at 151 MHz by the Cambridge 151-MHz Array, and with other studies of ionospheric conditions. The phase is expected to scale roughly with baseline length to about 100 km. There are several ways in which the effects of such disturbances might be overcome.

a) A point source in the field, resolved in interferometer delay or accessible by fast nodding, may be used as a reference to correct the interferometer phase.

b) If the source under observation is bright enough, it may be possible to use the frequency dependence of the refractive index of the plasma to correct the observed phase. The interferometer phase, ϕ_i, inserted by the plasma is given by

$$\phi_i \simeq -\frac{\nu}{\Delta\nu}\,\Delta\phi_i$$

where $\Delta\phi_i$ is the difference in phase measured across the observing bandwidth $\Delta\nu$ at frequency ν. With a 1 per cent bandwidth, a signal/noise ratio in excess of 100 in a few minutes of integration should be sufficient to correct the phase to within 90°. Note that it would be necessary to search in fringe-rate space before carrying out the integration as the geometric fringe rate would be significantly perturbed.

c) With three or more baselines operating simultaneously, the closure phase can be measured (Rogers et al., 1974). It is important, however, to be able to measure the phase on each baseline separately, but with one large antenna and two smaller portable outstations the full sensitivity can only be realised on two of the baselines. It then becomes necessary to apply some sort of global fringe-fitting technique (Moran et al., 1973) so that a large enough integration period can be applied to the third baseline.

d) There is some evidence to suggest that the presence of travelling ionospheric disturbances may be reflected in microfluctuations of barometric pressure at ground level. Monitoring the pressure at each station may at least allow the detection of the waves and might be used in some circumstances to correct the phase variations. We are investigating this possibility.

(ii) The interplanetary medium

Scattering in the interplanetary medium at 81.5 MHz is weak for solar elongations greater than 35°. The diffraction pattern then has a scale size of about 200 km and causes scintillations on a time scale of about 1 second. Rees & Duffett-Smith (1984) measured the effect of the scintillations on the interferometer fringe visibility, finding negligible effect for solar elongations greater than 50°. At 20°, the fringe visibility was reduced by 40 per cent on a baseline of 130 km (see Figure 1).

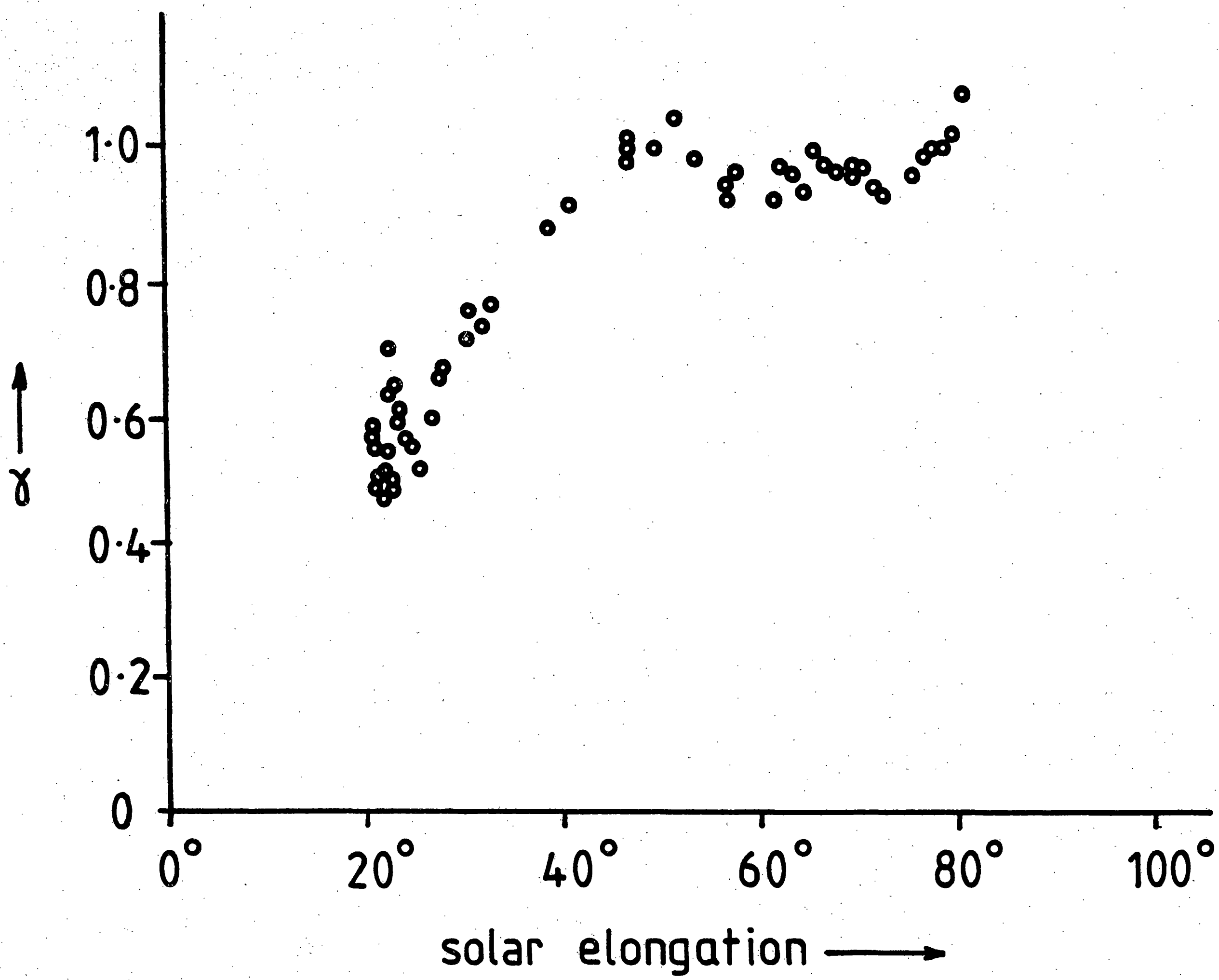

Figure 1. The effect of the interplanetary medium on the fringe visibility, γ .

(iii) The interstellar medium

The scattering in the interstellar medium is strong at metre wavelengths and scales as λ^2. Measurements at a number of frequencies suggest that the scattering on lines of sight perpendicular to the galactic plane is about 0.2 arcsec (see eg. Readhead & Duffett-Smith, 1975; Dennison et al., 1983). This becomes significant for baselines more than about 2000 km. Figure 2 shows a map of the average angular size of scintillating radio sources measured using IPS during a recent radio survey (Rees & Duffett-Smith, in preparation). The data are provisional; in particular the reality of the feature at the bottom right-hand corner of the map has yet to be confirmed. The map does show, however, that the scattering increases near the galactic plane and that it is patchy. Note that the intrinsic mean angular size of the sources, $\bar{\theta}_i$, is 0.5 - 0.6 arcsec, so that the scattering only shows up clearly where it exceeds this amount. If $\bar{\theta}_o$ is the observed mean angular size, then the scattering angle is given by

$$\theta_s^2 \simeq \bar{\theta}_o^2 - \bar{\theta}_i^2$$

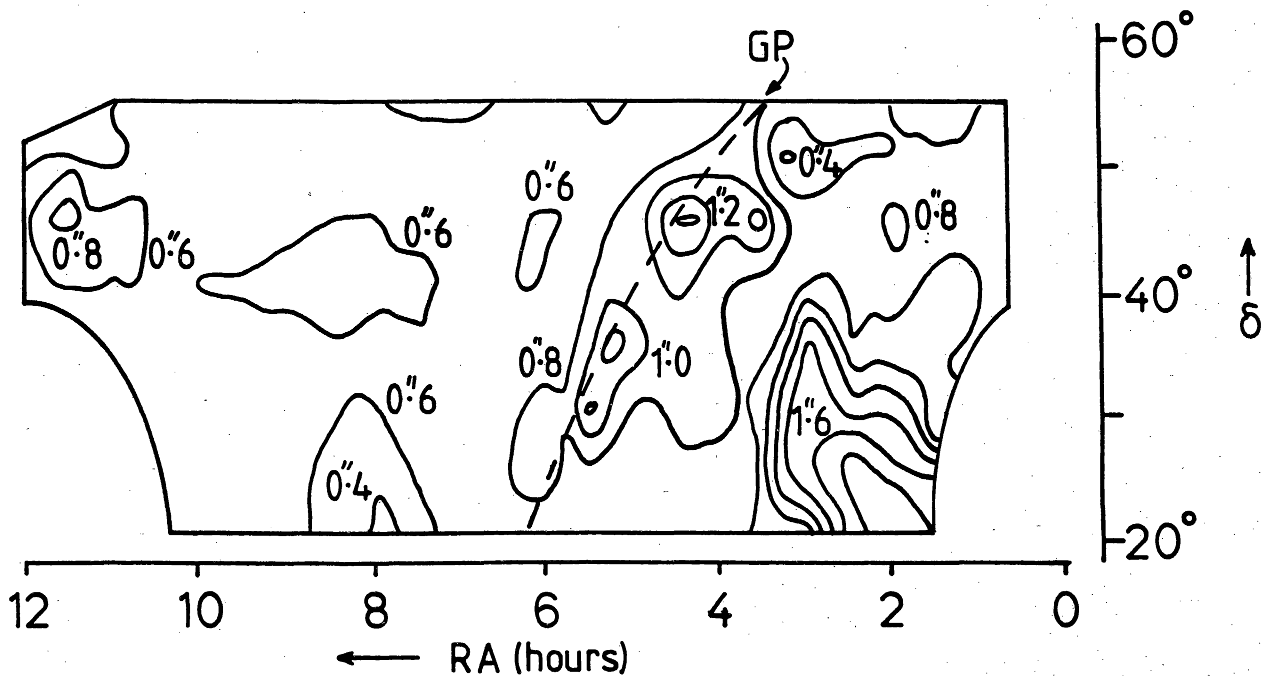

Figure 2. A map of the average angular sizes of radio sources measured by IPS at 81.5 MHz. The dashed line GP indicates the galactic plane.

4. Concluding remarks

At the time of writing (May 1985), observations of Cygnus A were in prgress at Cambridge using the two-element interferometer described above. Measurements had been made at 14 sites on baselines from 250 m to 23 km. At least two observations were made at each location 24 hours apart. We found that the data were reproducible to within a few percent and that the overall effects of interference from man-made transmissions was almost always negligible, even when one end of the interferometer was stationed in the middle of the City of Cambridge itself. We expect to add a second recording terminal and further correlators to the play-back system to give us a three-baseline capability by early 1986. Meanwhile, our results to date, taken together with the pioneering efforts of Hartas et al. (1984), confirm that this sort of experiment is relatively straightforward, providing a powerful means of complementing other low-frequency techniques.

References.

Dennison B., Thomas M., Broderick J. J., Brown R. L., & Condon J. J., 1983. IAU Symp. 110, p 309.

Duffett-Smith P. J., 1980. Mon. not. R astr. soc., 192, 41.

Hartas J. S., Rees W. G., Scott P. F., & Duffett-Smith P. J., 1983. Mon. not. R astr. soc., 205, 625.

Laing R. A., 1981. Mon. not. R astr. soc., 194, 301.

Moran J. M., et al., 1973. Ap. J., 185, 535.

Perley R. A., Fomalont E. B., & Johnston K. J., 1980. Astron. J., 85, 649.

Readhead A. C. S., & Duffett-Smith P. J., 1975. Astron. Astrophys., 42, 151.

Rees W. G., & Duffett-Smith P. J., 1984. Mon. not. R astr. soc., 205, 759.

Reas W. G., & Duffett-Smith P. J., 1985. Mon. not. R. astr. soc., 212, 463.

Rogers A. E. E., et al., 1974. Ap. J., 193, 293.

INDIA'S PLANS FOR GIANT METER-WAVELENGTH RADIO TELESCOPE*

D.S. BAGRI **

RADIO ASTRONOMY CENTER, OOTY, INDIA

SUMMARY

India is planning to construct giant meter-wavelength radio telescope (GMRT). The telescope is designed to work at 38, 150, 327 and 610 MHz and would consist of a number of parabolic cylinders distributed over an area of about 25km having a total effective collecting area of approximately 65×10^3 sq.m. This report briefly describes the plan for the telescope. Present design of the telescope is preliminary and needs to be optimized.

I. INTRODUCTION

Large man made interference, labor intensive construction and ionospheric scintillations have generally discouraged building large meter wavelength telescopes. In India the problem of man made interference is less serious and labor is relatively much cheaper compared to western countries. Further, with recent developments in radio astronomical techniques, the problem of ionospheric scintillation can be largely overcome by suitable design of the telescope and data processing techniques. These considerations and our experience in working at meter wavelengths at Radio Astronomy Center, Ooty, have lead us to propose construction, in India, of a high sensitivity, high resolution telescope operating at meter wavelengths. This would fill a very important gap in available radio astronomical facilities in the world.

*This report is based on Giant Meter-Wavelength Radio Telescope- A proposal by G. Swarup, Radio Astronomy Center TIFR, Ooty, India 1984.

**Present Address: NRAO-VLA, P.O. Box 0 Socorro, N.Mex. 87801

II. OBJECTIVES OF THE TELESCOPE

Major objectives of the telescope are:

(1) High resolution (a few arcseconds) studies of galactic and extragalactic radio sources with high dynamic range.

(2) Deep searches for a variety of celestial objects such as pulsars (including millisecond pulsars), proto-galaxies and proto-clusters, variable radio sources (both galactic and extra-galactic) etc. that require searching over a wide field of view using multi-beam, multi-filter receivers.

(3) Exploitation of the techniques of inter planetary scintillations (IPS) and lunar occultation (LO) to obtain very high angular resolution (fraction of arcsecond) at meter wavelengths.

III. DESIGN CONSIDERATIONS

Effective Collecting Area Required: To achieve a significant improvement in the available sensitivity for observing weak radio sources, it is essential that the total effective collecting area of the telescope exceeds at least fifty thousand sq. m. It is also necessary that each element of the array has an effective collecting area of about two thousand sq. m. in order to be able to use methods of closure phase and closure amplitude for mapping the sky with high dynamic range.

Relative Cost of Parabolic Dishes Versus Cylindrical Antennas: For operations at meter wavelengths it is relatively easy to construct parabolic cylindrical antennas. The cost of cylindrical antennas is roughly $110/m^2 for a 35m wide cylinder and approximately linearly proportional to the length of the cylinder. This is at least an order of magnitude lower than the cost of a parabolic dish of 25m diameter. Thus, even with additional cost of electronics and some sacrifice in terms of system temperature etc. for cylinders, their effective cost is almost an order of magnitude cheaper compared to dishes.

East-West (EW) Versus North-South (NS) Orientation of Parabolic Cylinders: The NS orientation of the cylindrical antennas would allow hour-angle (HA) coverage of about $\pm 90^o$ and declination (δ) coverage from roughly $(45+\lambda)^o$ to $-(45-\lambda)^o$, where λ is the latitude of the observing station. For the EW orientation, the coverage would be only about $\pm 45^{\circ}$ in hour angle and from $+90^{\circ}$ to $-(90-\lambda)^{\circ}$ in declination. Thus, although the NS orientation would have a restricted declination capability, it has full hour angle coverage which is very important for aperture synthesis mapping and also helpful in obtaining long integration time that would be required for weak radio sources. We have therefore preferred the NS orientation over the EW orientation.

The Antenna Configuration: Considering the various objectives described above, the following antenna configuration is proposed.

For achieving high angular resolution for sources both at high as well as low declination, the Y shaped configuration of the array of antennas used for VLA is well suited. It is proposed to have 13km for each arm of Y which provide good resolution for studying galactic and extragalactic radio sources.

For the second objective, it is required to have a minimum number of multiple beams covering a wide field of view which requires uniform element spacing. Further, the allowable integration time depends upon the size of the array. Considering these aspects, it has been planned to have a central square array of 16 elements with spacing between elements of approximately 300m.

For exploiting the techniques of lunar occultations and interplanetary scintillations to achieve subarcsecond resolutions at meter wavelengths, which is hard to obtain otherwise, requires a large collecting area. While the scintillation observations would be possible using both the Y array and the central square array, only the central array of about 1km may be used for the occultation observations. This is because the overall size of about 1km would not degrade appreciably the achievable resolution which is determined by the size of the array divided by its distance from the occulting object.

IV. ANTENNA SYSTEM

As shown in Figure 1, the proposed GMRT consists of

(a) A 1km x 1km square array (the central array) consisting of 16 steerable parabolic cylindrical antennas, each of size 92m

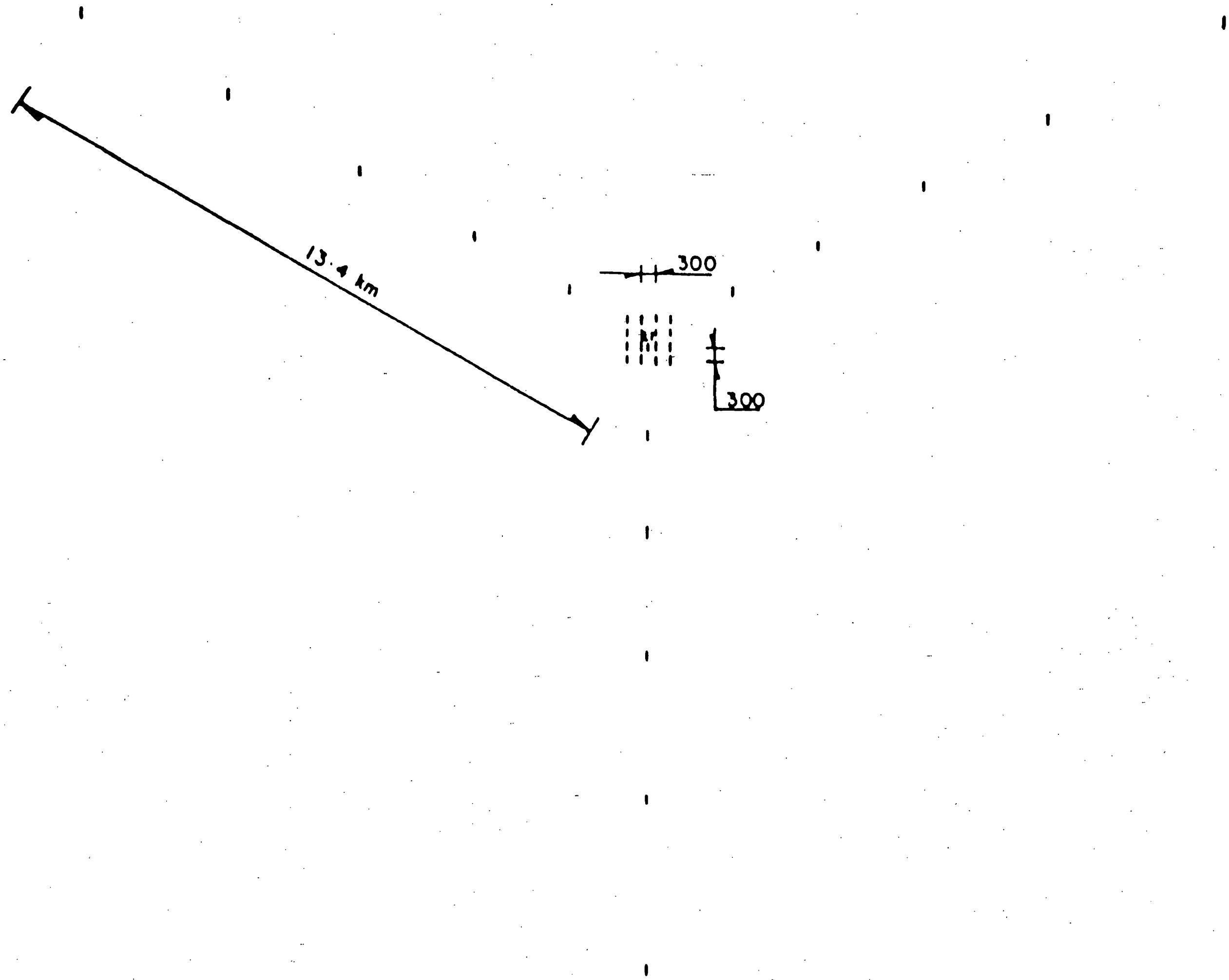

FIG:1 GIANT METRE WAVELENGTH RADIO TELESCOPE (GMRT)
Consisting of 34 parabolic cylinders of size
92m (NS) x 35m (EW) each.

long (NS) x 35m wide (EW) placed about 300m apart,

(b) Fifteen parabolic cylindrical antennas each of size 92m x 35m, placed along the 3 arms of a Y, with 5 cylinders in each arm. Several of the 16 antennas of the central square array also lie in the direction of the Y array. Starting from a distance of about 630m from the center of the square array, the antennas in each arm of the Y are placed progressively further apart so that the distance of the nth antenna from the center is about $n^{1.7}$ as in the VLA (Napier et al. 1983), and

(c) Three 92m x 35m NS oriented cylinders are placed near the center of the square array for obtaining the low spatial frequencies necessary for mapping extended regions.

The total physical area of the 34 cylindrical antennas would thus be about $109,000 m^2$ and the total effective area about $65,000 m^2$ (giving $24^{o}k/Jy$). Brief specifications of the proposed antenna system and electronics are summarized in Table 1. The length and width of each antenna would be optimized during the detailed design phase, considering the cost of the structural, mechanical, electrical and electronics system.

Table 1: Tentative Specifications of GMRT

1. Antenna System : 34 parabolic cylindrical antennas, each 92m(NS) x 35m(EW), placed as follows:
   a) 3 antennas at the corners of a triangle with sides of 140m. lengths,
   b) 16 antennas in a central square with separation of 300m between adjacent antennas and
   c) 15 antennas in a Y-shaped array with a length of 13.4km of each arm.

2. Total Effective Area: $65,000 m^2$
3. Antenna Sensitivity: $24^{o}K/Jy$
4. Steerability : HA $\pm 90^{o}$
   DEC -30^{o} to $+55^{o}$(3 dB points)
5. Parameters

Frequency (MHz)	Total No. of dipoles*	T_{sys} ^{o}K	Field of view of each antenna NS x EW ($arcmin^2$)	Resolution of Y-array (arcsec)	RMS Noise $f=4MHz$ $\tau=10hours$ (mJy)
38	1500	12,000	265x930	75	4.0
152	6000	400	65x235	18	0.13
326	12000	120	31x108	8	0.04
610	24000	90	17x58	4	0.03
	43500				

* total for both polarization

6. Bandwidth (Computer Selectable) } 1, 4, 12 MHz
7. Digital Correlator : Minimum 4096 channels, preferably 8192 or larger.

All the 34 parabolic cylindrical antennas will be mounted with their long axes in the horizontal direction. The tracking of a radio source would therefore require simultaneous east-west mechanical rotation of the 34 NS antennas, and appropriate beam steering in the NS direction by phasing of the dipole arrays along the focal lines. The entire tracking operation would be computer-controlled.

Frequency of Operation: The radio telescope would operate at the four frequency bands which are protected internationally for radio astronomy observations in the metre-wavelength region, namely, 37.75-38.25, 150-153, 322-328.6 and 608-614 MHz.

As shown in Figure 2, electrically-steerable dipole-arrays for reception at the four different frequencies will be placed along the four faces of a square-shaped steel trusses running along the focal line of the parabolic cylinders. The desired frequency of observation will be selected by appropriate rotation of the steel trusses using electrical motors. By rotating the trusses differently on different sets of antennas one could even make observations at 2 or more frequencies simultaneously if necessary. One could for instance use the central square array and the Y array for two independent scientific programmes at different frequencies simultaneously.

Dual Polarization: The reflecting surface of the parabolic cylinders is proposed to be formed by a square mesh of 2cm x 2cm size, made of stainless steel (S.S.) wires of 0.38 or 0.44mm diameter. The cross wires of the mesh would be electrically welded at each joint. The mesh surface is to be tensioned using long north-south S.S. wires of about 3 or 4mm diameter placed every one metre apart. The crossed mesh would allow polarization measurements by placing orthogonal dipoles along the focal line of the cylindrical antennas connected to two independent receiver systems. The dipoles would be placed at $\pm 45^{\circ}$ to the NS axis of each cylinder. This should lead to a highly symmetric placement of the dipoles with respect to the cylindrical antenna, and would therefore minimize cross-polarization of the waves received by the orthogonal dipoles.

For ease of servicing the dipole array, it is proposed to make the parabolic cylindrical antenna semi-asymmetric (Fig. 3),

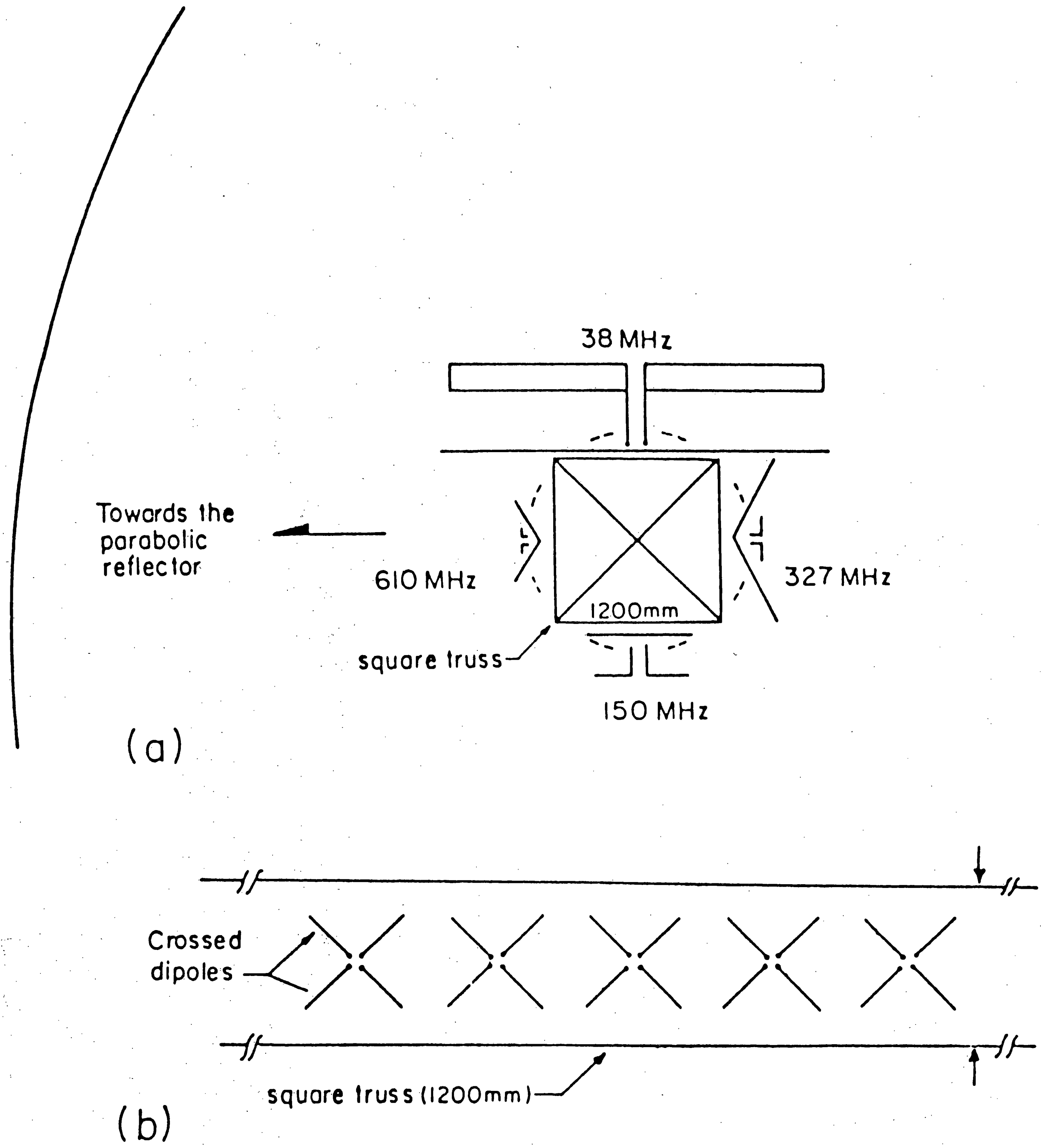

Fig. 2 (a) Placement of the dipole arrays at 38, 150, 327 and 610 MHz along the four faces of the rotatable square truss placed near the focal line of the cylindrical antenna.

(b) At each frequency orthogonal dipoles are placed $\pm 45^{\circ}$ to the long axis of the parabolic cylinders; in this figure are shown the dipoles for 150 MHz, each backed up by a reflector.

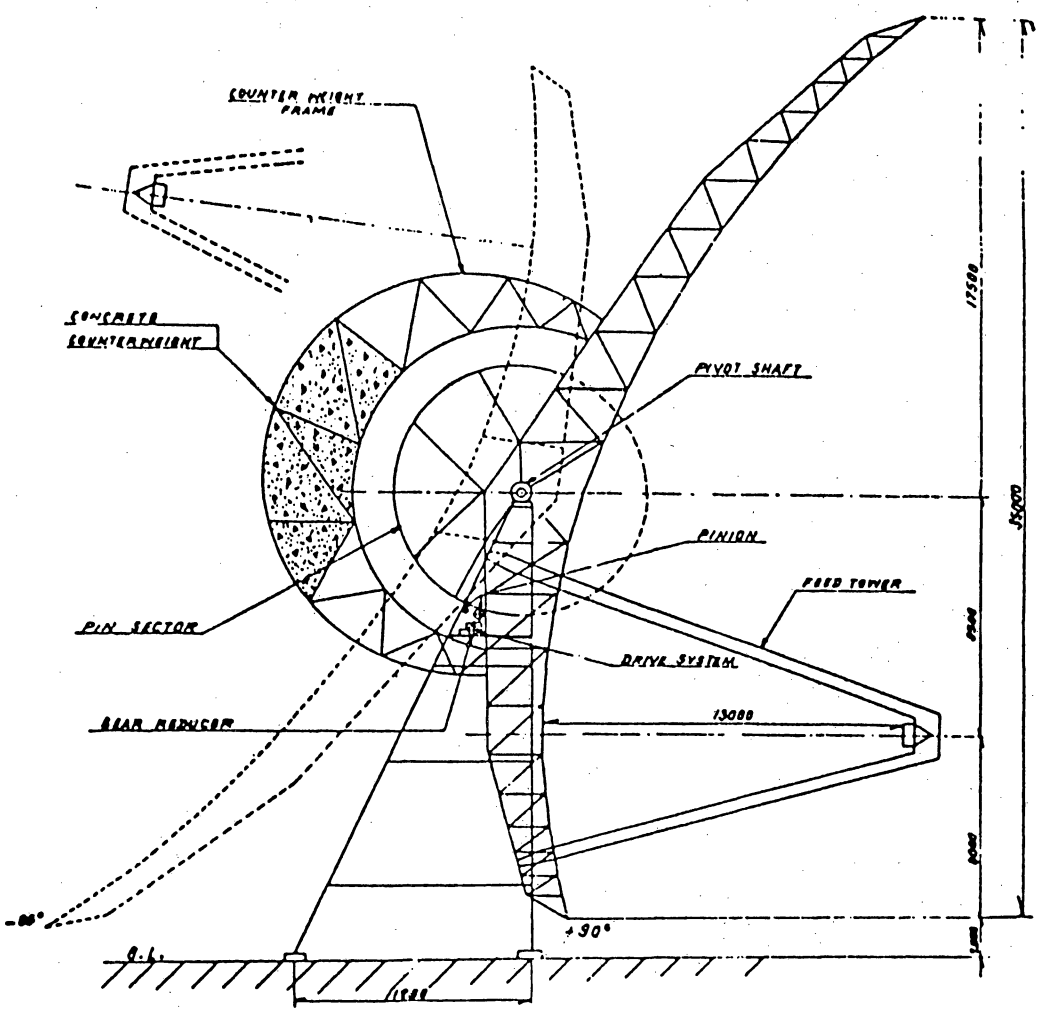

Fig 3(a) TYPICAL PARABOLIC FRAME

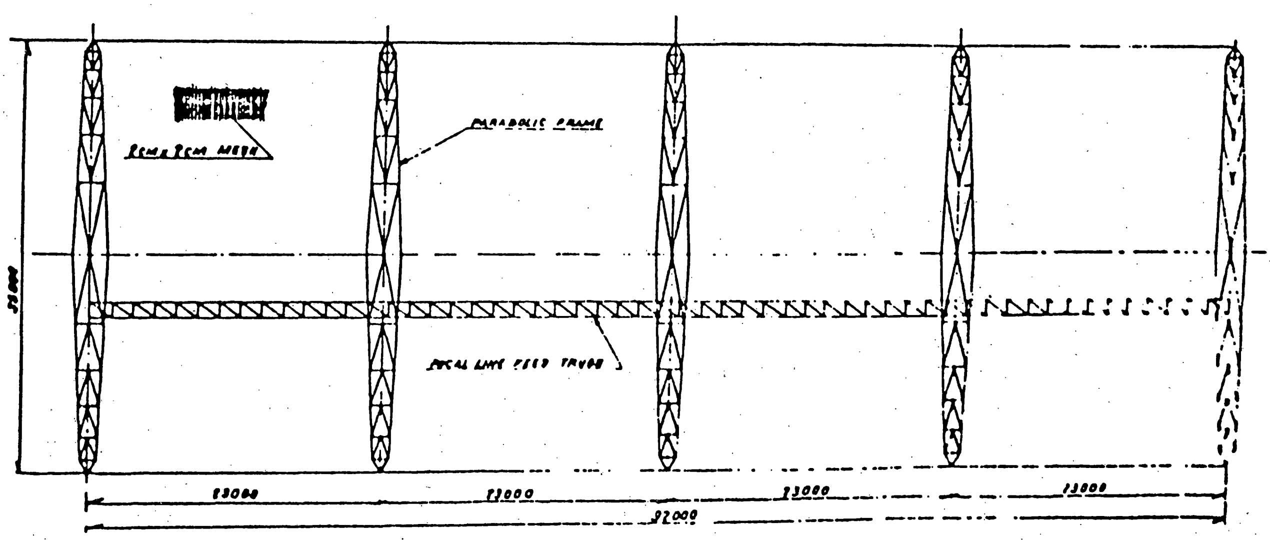

Fig.3(b) Plan of each parabolic cylindrical antenna
(92m NS x 35m EW of GMRT)

so that the height of the focal line from the ground is only about 11m when the antennas are driven to eastern or western horizons. One could then easily reach the focal line using a "cherry picker" type of mobile vehicle.

V. ELECTRONICS SYSTEM

The proposed electronics of the telescope is conventional. The system would consist mainly of:

(1) Phased dipole arrays including a low noise amplifier, a variable phase shifter and attenuator after each dipole: A total of about 44,000 dipoles are required for operation at the four frequency bands. Output from each dipole would be connected to an RF unit consisting of a low noise RF amplifier, a digitally controlled phase shifter and a variable attenuator. The phase shifters may be placed in the local oscillator path rather than RF path, if a mixer and an IF amplifier are placed after each dipole but would depend on the cost and relative advantages.

(2) Rapid check out system for the phased dipole array: In view of the large number of dipoles, RF amplifiers, phase shifters, attenuators and mixers required for GMRT, it would be essential to develop and install a suitable check out system for measurement, adjustment and fault finding. A scheme as shown in Fig. 4 and described below is proposed for this purpose. Near the center of each of the parabolic cylindrical antennas four oscillators, operating at center of the four operating bands, are placed which excite probes suitably placed near the center line of the surface of the parabolic cylinder. Signals picked up by each dipole can be compared with a suitable reference and thus amplitude and phase of each dipole can be adjusted under computer control.

(3) Multi Frequency Phase Stable Local Oscillator and IF System: Output from 12 or 16 dipoles would be suitably combined and given to a mixer and IF amplifier before combining signals from all dipoles of a cylinder. Combination of fiber optics and co-axial cables are planned for distribution of local oscillator signals and bringing IF signals from all antennas to a central place for correlating. It is planned to use round trip phase measuring

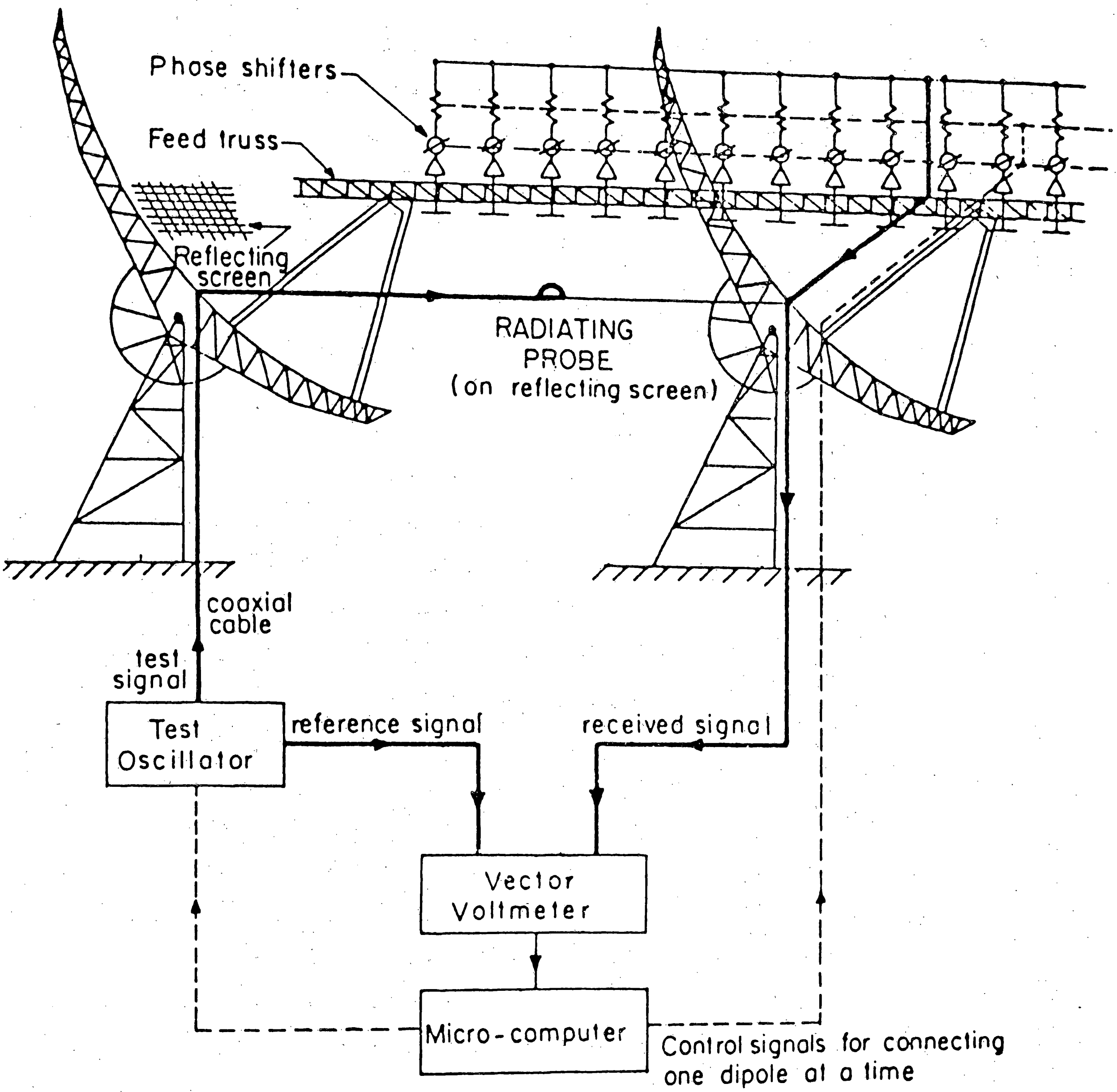

Fig.4 A schematic diagram showing that a test signal is radiated by a standard Probe, received by one dipole at a time through the RF amplifier, phase shifter and attenuator, and then its amplitude and phase measured by a vector volt meter.

technique for stabilizing local oscillator and IF.

(4) Correlator System: Signals received from the 34 antennas would be correlated in suitable analog and digital correlators.

(5) Control and Monitor System: A micro-computer at each antenna with a central on-line computer to control and monitor

the entire array and receiver system including data acquisition and calibration of the array is being planned.

VI. SITE SELECTION

The occurance of spread-F irragularities in the equatorial ionosphere gives rise to considerable ionospheric scintillations at sites close to the magnetic equator. Observations with the Ooty telescope (327 MHz) show that the rms value of the scintillation index $\gtrsim 0.1$ for about 3 hours a day. Even in the absence of noticeable ionospheric scintillation a phase variation of $\approx 5^{o}$ to 10^{o} rms are observed across 4 km baseline of the Ooty synthesis radio telescope. Although self calibration techniques using closure amplitude and closure phase should be able to correct for this, it would still be desirable to locate GMRT at a site appreciably farther away from the magnetic equator. On the other hand, it would be desirable to locate GMRT as far south (in India) as possible for ensuring good coverage of the southern sky (especially galactic center region around $\delta \sim -30^{o}$).

Considering (i) ionospheric scintillation and (ii) coverage of southern sky as well as (a) low interference (away from industrial complexes, protection by low lying hills etc.) (b) logistics of construction and running the array and (c) possible future expansion, two potential sites have been located:

(i) A site about 100km north of Bangalore - Lat$\sim$13.5N (geomagnetic Lat$\sim 6^{o}$)

(ii) A site about 250km south of Bombay -Lat$\sim 17^{o}$N (geomagnetic latitude$\sim 10^{o}$)

Various tests about ionospheric scintillation etc. are being carried out to choose a site.

VII. COST ESTIMATE AND TIME SCHEDULE

The cost of GMRT is estimated to be equivalent of U.S. $20 million with a foreign exchange content of about ten percent. The cost of the telescope is roughly half in structural, mechanical and civil, one third in electronics and the balance in miscellaneous. It is proposed to construct GMRT over a seven year period from 1985-92 with major design optimization for the antenna system during mid 1985 to mid 1986 and for the electronics during 1985-87.

REFERENCES

Napier, P.J., Thompson, A.R., and Ekers, R.D. (1983), Proc. I.E.E.E., 71, 1295

Self-Calibration at Meter Wavelengths

FREDERIC R. SCHWAB

National Radio Astronomy Observatory,[a] Charlottesville, Virginia 22901

In ordinary self-calibration one assumes that the observed visibility $\widetilde{V}$ on the i–j baseline at time t is related to the true radio source visibility V according to

$$\widetilde{V}(u_{ij}(t), v_{ij}(t), w_{ij}(t)) = g_i(t)\overline{g}_j(t)V(u_{ij}(t), v_{ij}(t), w_{ij}(t)) + \text{error}. \tag{1}$$

Here, the spatial frequency coordinates (u, v, w) along the baseline track have been parametrized by time, and the bar denotes complex conjugate. g_k, the so-called *antenna/i.f. gain* for antenna k of the array, is complex-valued; it can also be written as $g_k(t) = a_k(t)e^{i\psi_k(t)}$, with a_k real. $\psi_k \equiv \arg g_k$ is called the *antenna/i.f. phase*. Systematic amplitude errors are lumped together in the a_k, and phase errors due to unstable clocks, troposphere, ionosphere, etc., are lumped together in the ψ_k.

Now, the basic idea of self-calibration is that given a source *model* whose visibility function is $V^{\sharp}$, one can solve for the unknown g_k, say, by least-squares—minimize the quantity

$$S(\mathbf{g}) = \sum_{1 \le i < j \le n} \left| \widetilde{V}_{ij} - g_i \overline{g}_j V^{\sharp}_{ij} \right|^2. \tag{2}$$

Here, n denotes the number of antennas comprising the array, and $\widetilde{V}_{ij} \equiv \widetilde{V}(u_{ij}, v_{ij}, w_{ij})$. Also, the time-dependence has been omitted—in practice one assumes that the g_k are constant over short intervals of time, and the least-squares estimation procedure is applied separately to the data from each of a number of appropriately chosen time segments. What remains is to correct the data, make a map, and deconvolve the ideal point source response, in order to obtain an improved source model and its visibility function $V^{\sharp\sharp}$; and then iterate the entire process. This is all nicely described in a recent review article by Pearson and Readhead [**3**]. An essential point is that—once the source model has been specified—these least-squares problems often are nicely overdetermined: with an n element array there are only n unknown g_k, but $(n^2 - n)/2$ observations have been recorded during each integration period.

In the meter wavelength regime the ionospheric phase corruption is very severe. Because of this, and because interferometers operating in this regime respond to radio emission over a fairly large region of the sky, the model given by Eq. 1 is inadequate. To remedy this situation, let's forget the amplitude errors and consider only the ψ_k. We need to assume that they are functions of *position on the sky* (specified by direction cosines $(x, y, z \equiv \sqrt{1 - x^2 - y^2} - 1)$), as well as of time—i.e., functions $\psi_k(x, y, t)$. Let's divide the "field-of-view" of each antenna (we'll assume that each antenna has the same field-of-view) into some (hopefully small) number m of pieces, whose centroids

[a]The National Radio Astronomy Observatory (NRAO) is operated by Associated Universities, Inc., under contract with the National Science Foundation.

we'll denote by (x_l, y_l), $l = 1, \ldots, m$. Over any sufficiently small patch, termed an *isoplanatic patch*, ψ_k is essentially constant as a function of (x, y).

Having carved the field-of-view up into patches, if we know, for antenna k, and for each l, the phase corruption ϕ_{kl} that is suffered by a plane wavefront impinging from the direction (x_l, y_l), then we can approximate ψ_k anywhere within the field-of-view by forming an appropriately weighted sum of the ϕ_{kl}. So write (ignoring the time dependence)

$$\psi_k(x,y) \approx \widehat{\psi}_k(x,y) \equiv \sum_{l=1}^{m} \omega_l(x,y)\phi_{kl}\,.$$

If there are sufficiently many well-positioned patches, then ψ_k can be well approximated by an expression of this form.[1]

Very frequently in self-calibration, the model visibility $V^\sharp$ corresponds to a set of N CLEAN components (point sources) of flux p_q located at positions (l_q, m_q, n_q); i.e., $V^\sharp(u,v,w) = \sum_{q=1}^{N} p_q e^{2\pi i(ul_q + vm_q + wn_q)}$. So—assuming this to be the case—we can, in analogy to Eq. 2, solve for the nm unknowns ϕ_{kl} by minimizing the expression

(3)

$$S(\phi) = \sum_{1\le i<j\le n} \left| \widetilde{V}_{ij} - \sum_{q=1}^{N} p_q e^{\sqrt{-1}\left(2\pi(u_{ij}l_q + v_{ij}m_q + w_{ij}n_q) + \sum_{l=1}^{m} \omega_l(l_q,m_q)(\phi_{il}-\phi_{jl})\right)} \right|^2 .$$

Obviously, for all of the ϕ_{kl} to be well-determined, there must be modeled emission in each of the m patches.

The big problem is that there are m times more unknowns to solve for than in ordinary self-calibration. So clearly it is desirable to have a large number of antennas, observations that are of high signal-to-noise ratio, and a good initial model of the radio emission over the entire field-of-view. Fortunately for the proposed 75 MHz array, reasonable models ought to be available from 327 MHz VLA observations. The big remaining questions are:

(i) How do we hold this larger number, nm, of degrees of freedom in check?

and (ii) How can we make use of the space-variant antenna/i.f. phases in inversion (mapping/deconvolution)? (The visibility data cannot be corrected prior to mapping; the data correction must be applied, somehow, inside of the mapping/restoration process.)

[1] The specific functional form of the interpolation weights $\omega_l(x,y)$ is not important in the context of this discussion. One might choose simply to make $\widehat{\psi}_k$ piecewise constant, in which case $\omega_l(x,y)$ would be defined to be 1 everywhere within the lth patch, and 0 elsewhere. Another possibility is to incorporate a scattered data interpolation formula which is due to Shepard [2]. One form of Shepard's formula leads to the inverse-distance weighting (analogous to a $1/r$ gravitational law)

$$\widehat{\psi}_k(x,y) = \frac{\sum_{l=1}^{m} \phi_{kl}/\sqrt{(x-x_l)^2 + (y-y_l)^2}}{\sum_{l=1}^{m} 1/\sqrt{(x-x_l)^2 + (y-y_l)^2}}\,.$$

These $\widehat{\psi}_k$ resemble thin elastic membranes elevated by point supports of altitude ϕ_{kl} at the interpolation points (x_l, y_l).

The answer to question (ii) is easy: One can combine mapping and CLEANing in a *mosaicing* algorithm *à la* the AIPS program MX (MX is an implementation of the so-called *"battery-powered" CLEAN algorithm*). The patches must be CLEANed in parallel, because sidelobes from a source in any one patch fall into each of the other patches. MX occasionally recomputes the residual map over each mosaic patch by re-gridding the difference between the data and the model. At this step in the algorithm, one would simply apply space-variant phase corrections when computing the residual visibilities.

In regard to question (i), there are a number of ways to control the large number of degrees of freedom. First of all, one may incorporate an assumption of *spatial* correlation of the antenna phases. This is reasonable to do because closely spaced antennas see a given patch of the sky through nearly the same tropospheric/ionospheric path. A straightforward way to appropriately constrain the least-squares solutions is by use of a penalty function added to S (Eq. 3). For example, one might add the term

$$\lambda \sum_{\substack{i \neq j \\ 1 \leq l \leq m}} \frac{(\phi_{il} - \phi_{jl})^2}{r_{ij}},$$

where r_{ij} is given by some monotone increasing function of the separation (or the projected separation) of antennas i and j. λ would be chosen so as to achieve a reasonable balance between the influence of the χ^2 error term and the penalty. This technique could be applied, as well, in ordinary self-calibration—it would be useful, e.g., for VLA observations done in the compact C- and D-array configurations.

Secondly, one may incorporate an assumption of *temporal* correlation of the antenna phases. This assumption, in fact, is usually incorporated in ordinary self-calibration, through use of a data window (a time-window). A different approach is to incorporate another penalty function. Assuming that the data are processed sequentially in time, one might assume a Gaussian prior distribution for ϕ_{kl}, of mean μ_{kl} equal to some running mean of the solutions for earlier times. E.g., one might add the term

$$\lambda' \sum_{\substack{1 \leq k \leq n \\ 1 \leq l \leq m}} \frac{(\phi_{kl} - \mu_{kl})^2}{\sigma^2}.$$

A further refinement—in the same vein—would be to further constrain the ϕ_{kl} to be in accord with higher-order statistics of the ionospheric phase variations, accumulated over time. Armstrong and Sramek [**1**],[**5**], for example, characterize the *tropospheric* phase scintillations at *centimeter* wavelengths by means of a structure function which, at 5 and 22 GHz, they find is well-modeled by a power law. One might constrain the solutions so that the mean square variation of each computed antenna phase surface is in accord with some estimate of such a structure function.

In ordinary (phase-only) self-calibration, at each instant there are $n-1$ unknown antenna phases and $n(n-1)/2$ observations; hence, it can be said that the solutions are overdetermined by the factor $q = n/2$. In the present case—ignoring the penalty constraints—this ratio becomes $q = \frac{n(n-1)}{2(nm-1)}$, and so, for an overdetermined solution, one must have m, the number of patches, satisfy $m < r(n) \equiv \frac{n-1}{2} + \frac{1}{n}$. Two interesting cases are $r(27) = 13\frac{1}{27}$ and $r(50) = 24\frac{13}{25}$. Based on 327 MHz VLA observations, Perley and Erickson have estimated, I believe, that one might typically be dealing with ≈ 36 isoplanatic patches over a $1°$ field at 75 MHz—so clearly we may have a few extra degrees of freedom to hold under control.

To date, no attempt has been made at a practical implementation of the scheme presented here. One would probably want to combine all of this into a single computer program, or into a set of tightly-coupled programs, because the handling of space-variant effects within the steps of the procedure would have to be highly intertwined. A saving grace is that the map sizes required for the proposed 75 MHz array may be fairly small, so that the computing effort would be less heavily directed toward large images (than is customary for VLA data), and more heavily directed to intensive computing on relatively small chunks of visibility data.

My work is also described in [**4**], where additional details can be found.

References

1. J. W. Armstrong and R. A. Sramek, *Observations of tropospheric phase scintillations at 5 GHz on vertical paths*, Radio Science **17** (1982), 1579–1586.
2. W. J. Gordon and J. A. Wixom, *Shepard's method of "metric interpolation" to bivariate and multivariate interpolation*, Math. of Computation **32** (1978), 253–264.
3. T. J. Pearson and A. C. S. Readhead, *Image formation by self-calibration in radio astronomy*, Ann. Rev. Astron. Astrophys. **22** (1984), 97–130.
4. F. R. Schwab, *Relaxing the isoplanatism assumption in self-calibration; applications to low-frequency radio interferometry*, Astron. J. **89** (1984), 1076–1081.
5. R. A. Sramek, *VLA phase stability at 22 GHz on baselines of 100 m to 3 km*, VLA Test Memorandum No. 143 (1983).

MAXIMUM ENTROPY METHOD FOR LOW FREQUENCY MAPPING

R.K. Shevgaonkar
Indian Institute of Astrophysics, Bangalore 560034, INDIA.

Astronomy Program, University of Maryland, College Park
Md 20742, U.S.A.

ABSTRACT

An application of the Maximum Entropy Method to closure data is described here. It is shown by simulated examples that although the principle of the method is to obtain a brightness distribution which has highest entropy, the closure phases play a prominent role in giving the correct reconstruction especially when the sources are complex and the measurement errors are large. The method gives a faithfull reconstruction even upto phase errors of $\pm$ 150°. It appears that the method could be an alternative to the routinely used 'self calibration' technique for improving radio images obtained from phase unstable interferometers.

The method is further extended for low frequency imaging where the field of view is not isoplanatic. In this case the sum of visibility phases around a close loop of interferometers is not free from the systematic measurement errors. However, if we assume that the whole anisoplanatic sky can be divided into number of small isoplanatic patches and that there is only a small coupling among the different patches, it is possible

to obtain approximate closure relations for visibilities corresponding to the small patches. The uncertainty in the closure phases can be treated as a noise in the observation. It is suggested that the effect of the closure phase uncertainty can be compensated to some extent by making use of the relative entropy where one can bias the reconstruction by an *a priori* known distribution.

1. Introduction

In the past few years considerable progress has been made in the direction of improving the images obtained from unstable interferometers (Cornwell and Wilkinson 1981, Readhead and Wilkinson 1978, Readhead et.al. 1980). The success of these image improving technique lies in the use of so called 'closure' phase which provides an indirect information about the true visibility phases. The method which uses the closure phase information for refining the measured phase errors is called the 'self calibration' technique and the reconstructed maps are known as 'hybrid maps' (Baldwin and Warner 1976). The self calibration method is a combination of the image deconvolution method CLEAN (Hogbom 1974) and the closure phases. The method starts with a model distribution which is usually a CLEANed version of the initial dirty map. The method is quite sensitive to the choice of model distribution and at many occasions it has been observed that due to improper starting model the method gives a bad reconstruction. For the brightness distributions which are composed of point like sources the guess of model distribution could be relatively easy but for the extended distributions, especially when the errors are large, it is not always possible to predict the correct starting model. Further, due to repetitive use of the CLEAN the method becomes quite expensive in computer time for large fields of view (Cornwell and Evans 1984).

The Maximum Entropy Method has shown a new promise in the field of astronomical image reconstruction. In radio astronomy the method has so far been used as an image deconvolution technique. However, in other fields like crystallography, the method has been applied to the phase refinement problem (Narayan and Nityananda 1981, 1982). In crystallography problems where the sources are well isolated point like sources (atoms) the maximization of the entropy alone can provide reasonably good reconstruction. However, in radio astronomy where the presence of extended sources is common, only maximization of the entropy does not give good image reconstruction if the measurement errors are large. The reliability of the reconstruction can be increased by providing an additional information about the visibility phases through the closure relations. We discuss here an application of MEM combined with the closure phases to the phase refinement problem in radio astronomy. Strictly speaking, in low frequency imaging the assumption that the sky is isoplanatic over the field of view is not satisfied. However, just to initiate the problem, in the first part of the paper we have assumed that the sky is isoplanatic over the entire field of view. The method is then extended to accommodate the anisoplanatic nature of the sky at low frequencies.

2. Closure Relations

For strong sources which have a high signal-to-noise radio the phase errors could be mainly introduced by the changes in the path lengths due to variable atmosphere and the temperature sensitive electronics, and the positional accuracy of the interferometer elements. The concept of closure phase which is free from all these errors was first introduced by Jennison in 1958. The statement of the closure phase is, 'the sum of visibility phases around a close loop of interferometers is free from all systematic measurement errors'. For a system of N elements i.e., N(N-1)/2 visibilities, the total number of loops and therefore the total number of the closure phases is

$$N_c = {}^{N}C_3 + {}^{N}C_4 + \cdots + {}^{N}C_N \qquad (1)$$

However, it should be noted that all the N_c closure phases are not independent. For an N element interferometer system there could be maximum N errors associated with the N(N-1)/2 visibilities. Further, since the phase measurement is always relative, any one of the interferometer elements can be taken as a reference element giving the maximum number of phase errors of only (N-1). This gives the error-free quantities or the independent closure phases atmost $\{N(N-1)/2 - (N-1)\} = (N-1)(N-2)/2$. The number of visibility phases is always greater than the total closure relations and therefore there are infinite distributions which satisfy the closure relations. To obtain a unique solution we need to have more information about the distribution along with the closure phases. In self calibration the additional information about the source is provided in the form of a model distribution. In the Maximum Entropy Method, among the infinite solutions given by the closure relations, we propose to accept that solution which maximizes the entropy of the observed brightness distribution. In this method the closure conditions are the essential conditions, whereas the maximization of the entropy is a desirable condition.

3. MEM for Closure Data

The observed brightness distribution, B(x,y) in the sky is related to the complex spatial visibility function, ρ_{mn} ($= |\rho_{mn}| \exp(i\phi_{mn})$) through a Fourier transform relationship i.e.

$$B(x,y) = \sum_m \sum_n \rho_{mn} \, e^{i2\pi(mx+ny)} \qquad m,n \in M,N \tag{2}$$

where,

$$\rho_{mn} = \iint_{-\infty}^{\infty} B_{true}(x,y) \, e^{-i2\pi(mx+ny)} \, dx\,dy \tag{3}$$

where x,y are the sky coordinates and m,n are the spatial coordinates on the earth. $B_{true}(x,y)$ is the true brightness distribution in the sky.

The entropy of the brightness distribution could be defined in the most general form as (Nityananda and Narayan 1982)

$$\mathcal{E} = \iint f\{B(x,y)\}\, dx\, dy \tag{4}$$

where 'f' can be one of the conventional entropy functions, ln B, -B ln B (Gull and Daniell 1978, Gull and Skilling 1984) or other functions like $B^{1/2}$, $B^{3/2}$ etc.

Since the brightness distribution is real the visibility function ρ_{mn} is hermitian i.e., $\rho_{mn} = \rho^{*}_{-m-n}$ (* represent the complex conjugate). With this modification eqn. (2) can be rewritten as

$$B(x,y) = \rho_{00} + \sum_m \sum_n |\rho_{mn}|\, e^{i\phi_{mn}}\, e^{i2\pi(mx+ny)} + \sum_m \sum_n |\rho_{mn}|\, e^{-i\phi_{mn}}\, e^{-i2\pi(mx+ny)} \tag{5}$$

To maximize the entropy with respect to the unknown phases $\partial\mathcal{E}/\partial\phi_{mn}$ should be equal to zero giving,

$$\frac{\partial \mathcal{E}}{\partial \phi_{mn}} = 2\,|\rho_{mn}|\,|\sigma_{mn}|\,\sin(\alpha_{mn} - \phi_{mn}) = 0 \tag{6}$$

where, $$|\sigma_{mn}|\, e^{i\alpha_{mn}} \equiv \iint f'\{B(x,y)\}\, e^{i2\pi(mx+ny)}\, dx\, dy \tag{7}$$

and f'(B) is the derivative of f(B) with respect to B. Equation (6) is similar to the one obtained by Narayan et.al. (1984).

Considering the cyclic nature of the phase, it is clear that eqn. (6) has multiple maxima and depending upon the starting condition the solution may converge to the nearest maximum. The positivity of the map can certainly be utilized to restrict the choice of the solutions. Obviously, beside the positivity if we have more a priori information about the brightness distribution the chances of obtaining the correct solution go on increasing. One of the indirect ways which provides an additional information about the brightness distribution is the closure phase. The choice of solution becomes much more restricted when along with the positivity of the map the visibility phases have to satisfy the closure relations.

Since, eqn. (6) gives gradient of the entropy with respect to the unknown phases through one Fourier transform, it is relatively straightforward to maximize the entropy by any of the iterative gradient techniques. Starting from the observed distribution the visibility phases are shifted in the direction of the gradient subject to the observational constraints until the entropy is reached to the maximum. If the closure phases were not there, the obvious choice would be to shift the unknown phases in the direction of the gradient defined by eqn. (6). However, in the presence of the closure relations all the phases cannot be shifted along the gradient. Since, the closure relations must be satisfied at every stage of iteration, the changes in the visibility phases should be in such a way that the sum of the changes around a close loop of interferometers is equal to zero. Mathematically this can be written as

$$\underline{\underline{A}} \cdot \underline{\Delta\phi} = 0 \tag{8}$$

where, $\underline{\underline{A}}$ is a p x q (p < q) rectangular matrix which defines the closure relations and contains elements 0 or ± 1; $\underline{\Delta\phi}$ is a vector of q elements denoting the changes in the q unknown visibility phases. Since, p < q i.e., number of closure relations is less than the number of unknowns, eqn. (8) represents a surface in a q-dimensional space. Any vector $\underline{\Delta\phi}$ lying in this surface satisfies the closure conditions. However, for maximization of entropy we take that vector which is closest to the entropy gradient vector or in other words we compute a vector $\underline{\Delta\phi}$ on the closure surface which has smallest distance to the gradient vector. The scalar distance between the gradient vector and a vector $\underline{\Delta\phi}$ is

$$S = |\underline{\phi_g} - \Delta\phi| = \left\{ \sum_{j=1}^{q} (\phi_{gi} - \Delta\phi_i)^2 \right\}^{1/2} \tag{9}$$

Since, the q unknowns are coupled through only p closure equations, any (q-p) unknowns can be chosen independently. For S to be minimum with respect to the (q-p) independent variables

$$\frac{\partial S}{\partial \Delta\phi_j} = 0 \quad ; \; j = 1, 2, \cdots (q-p). \tag{10}$$

These (q-p) equations along with the p closure relations form a set of simultaneous algebraic equations which can be solved uniquely to give $\underline{\Delta \phi}$.

4. Computational Simulations and Results

A simple gradient method is implemented for the maximization of the entropy. A flow diagram of the algorithm is given in Figure 1. First, a suitable entropy function is chosen in the form of f' directly (e.g. for entropy function ln B, f' = 1/B). The observed map is lifted by a suitable constant to make it positive definite at every point. Taking f' of the lifted distribution the gradient of the entropy is computed by a fast Fourier transform (FFT) of the f'. Combining the gradient with the closure relations the direction of the phase shift is computed. The unknown visibility phases are rotated by the computed phase changes. New refined distribution is obtained by Fourier transforming the modified visibilities. The method iterates until the convergence is reached.

The method has been successfully tried on arbitrary simulated distributions. One of the examples is shown in Figure 2. From the variety of simulated examples the main features of the method can be summarized as follows. (For detail discussion see Shevgaonkar, 1985)

(i) The method gives faithfull reconstruction for phase errors upto $\pm 150^{\circ}$.

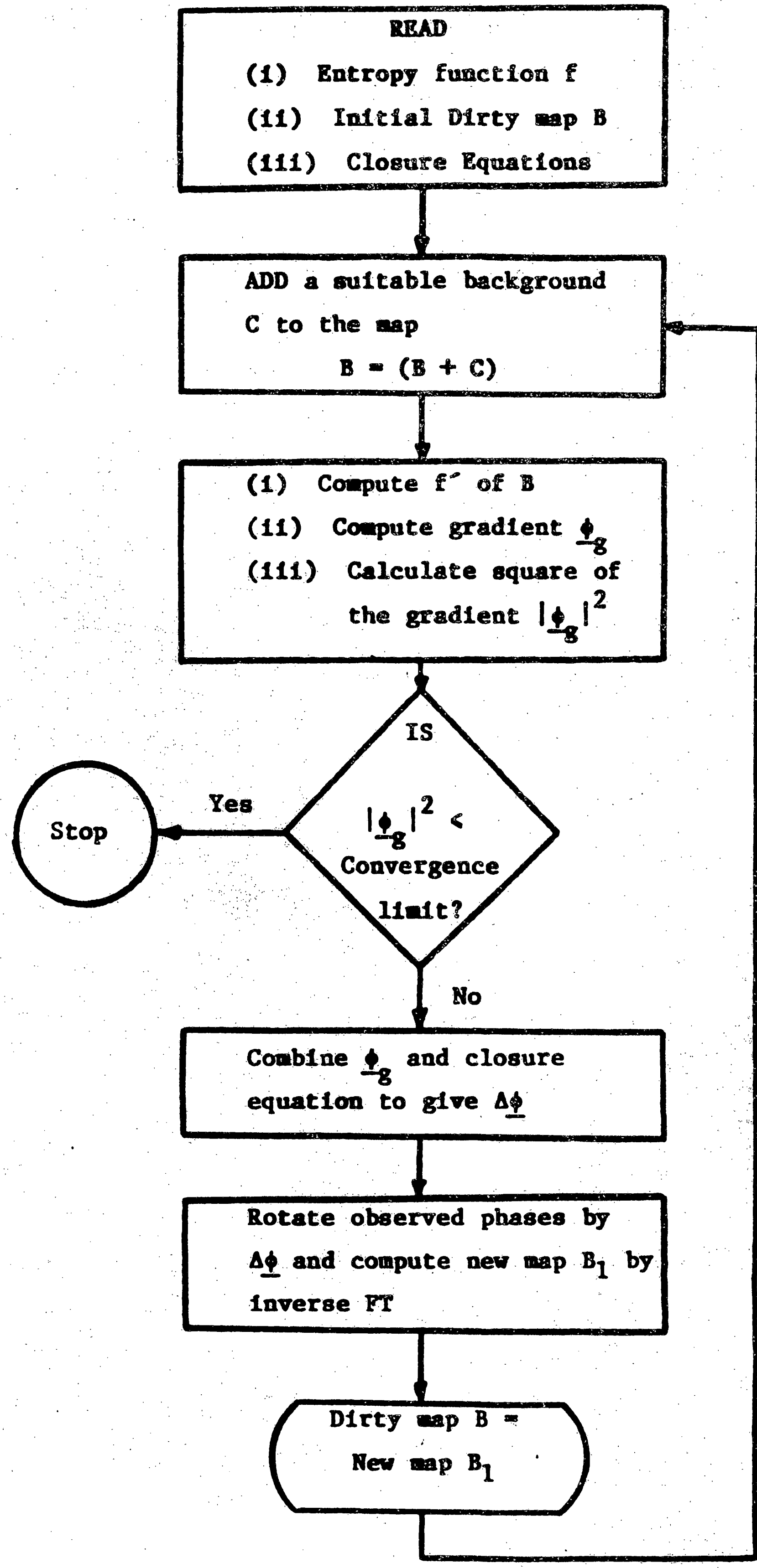

Fig 1. A flow diagram of the algorithm.

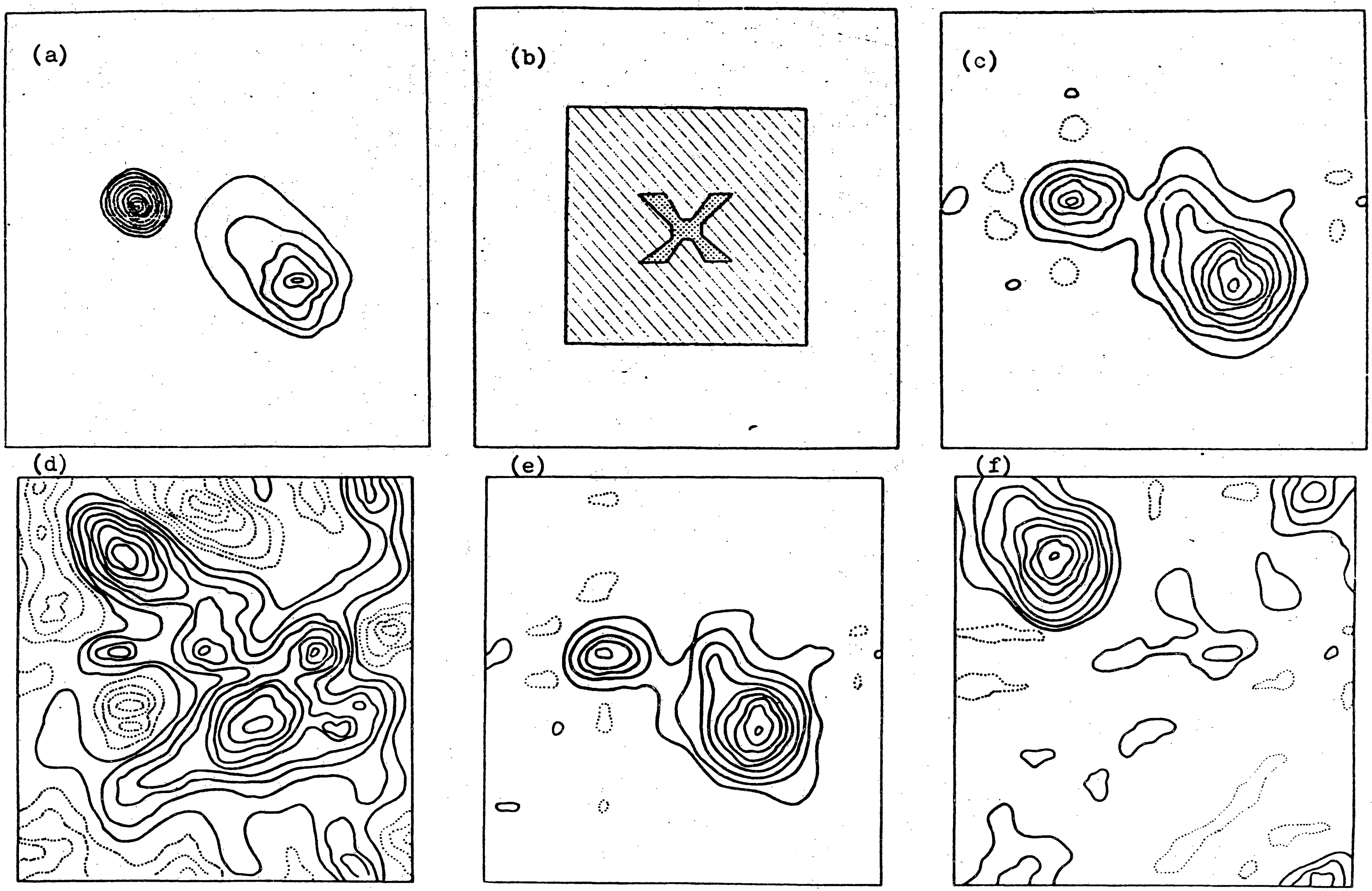

Fig. 2 (a) A model distribution (b) Simulated u-v diagram; in dotted region both visibility phases and amplitudes are measured accurately whereas, in the hatched region the phases have a random error of ± 150°. In the outer empty area the visibilities are completely unknown. (c) Map which one should get if there are no phase errors. (d) Actual dirty map (e) MEM restoration with closure constraints (f) MEM restoration without closure constraints.

(ii) For small phase errors the maximization of the entropy alone can provide reasonably good reconstruction whereas, for large phase errors if the distribution is complex, the use of the closure relation is rather essential.

(iii) Even for large phase errors if the distribution consists of well isolated point sources, it is possible to obtain a good phase refinement without the closure relations.

(iv) The gradient method works satisfactorily and convergence is reached in 20–40 iterations which in other words gives a computational time of 40–80 FFT's.

(v) The method could be used as an alternative to the routinely used self calibration method.

5. Relaxing the Condition of Isoplanatism

The success of the phase refinement technique to some extent lies in the closure phases which restricts the choice of distributions given by maximization of the entropy. However, at low frequency it is not possible to obtain the closure phases which are free from all the systematic measurement errors. Due to different ionospheric conditions in different directions of the sky the radio signals arriving from different parts of the sky are subject to different phase errors. Since the measurement error is a function of the sky coordinates it can be seen easily that it is not possible to absorb this error in the antenna phase and therefore it is not possible to obtain the closure phase which is an error-free quantity. The problem of finding closure phase seems to be impossible in the most general case of the low frequency mapping. However, if we make a simplifying assumption (as made by Schwab 1983) that the anisoplanatic field of view can be divided into number of small isoplanatic patches the observed visibility function can be written as

$$\rho_{mn} = \sum_{\ell=1}^{L} \rho_{mn}^{\ell} \, e^{i\phi_{mn}^{\ell}} \qquad (11)$$

L=Total isoplanatic patches

where ρ_{mn}^{ℓ} and ϕ_{mn}^{ℓ} are amplitude and phase respectively of the Fourier transform of the brightness distribution in the ℓ^{th} patch of the sky. (It should be noted that the different patches need not be identical and they could be of any arbitrary size and shape). With this assumption we see that although ρ_{mn} cannot give the closure relations, the visibility phase ϕ_{mn}^{ℓ} corresponding to the individual patches do satisfy the closure relations as

$$\underline{\underline{A}} \cdot \underline{\phi}^{\ell} = \underline{\phi_c}^{\ell} \qquad (12)$$

The visibility phases ϕ_{mn}^{ℓ} of the individual isoplanatic patches although satisfy the closure relations, cannot be measured explicitly. If we take the Fourier transform of the observed brightness distribution in the ℓ^{th} patch assuming that the remaining sky is empty, we obtain a visibility function for that patch which in general is not equal to the true visibility function i.e.,

$$\rho'^{\ell}_{mn}\, e^{i\phi'^{\ell}_{mn}} \equiv \rho^{\ell}_{mn}\, e^{i\phi^{\ell}_{mn}} + e^{\ell}_{mn} \tag{13}$$

The complex error term e^{ℓ}_{mn} is mainly due to two effects (i) Finite size of the isoplanatic patch which introduces a sudden discontinuity in the distribution (ii) interference from the other patches in the sky. Obviously, the magnitude of the error, e^{ℓ}_{mn} depends upon how far away the boundary of the patch is from the distribution within it and also upon how bad the interfering sidelobes of the synthesized beam are. If we make one more simplifying assumption that the different patches have low coupling among themselves, the magnitude of the error term e^{ℓ}_{mn} will be small compared to the true visibility and the eqn. (13) can be approximated to

$$\rho'^{\ell}_{mn}\, e^{i\phi'^{\ell}_{mn}} = \rho^{\ell}_{mn}(1+\Delta\rho^{\ell}_{mn})\, e^{i(\phi^{\ell}_{mn}+\Delta\phi^{\ell}_{mn})} \tag{14}$$

If we replace $\underline{\phi}^{\ell}$ by $\underline{\phi}'^{\ell}$ in the closure eqn. (12) we get

$$\begin{aligned}\underline{\underline{A}}\cdot\underline{\phi}'^{\ell} &= \underline{\underline{A}}\cdot\underline{\phi}^{\ell} + \underline{\underline{A}}\cdot\underline{\Delta\phi}^{\ell}\\ &= \underline{\phi_c}^{\ell} + \phi^{\ell}_{c\ error}\end{aligned} \tag{15}$$

The second term in the eqn. (15) can be treated as an uncertainty in the closure phase due to observational noise.

It is shown in the previous section that for simple distributions and for moderate phase errors the quality of the reconstruction is mainly due to the maximization of the entropy alone and the closure phases play a relatively less important role. Therefore, in these type of situations at least the method should be able to give a reasonable low frequency image reconstruction. For large errors and for complex distributions where the reconstruction is mainly governed by the closure relations the reliability of the method can be increased by the use of relative entropy

$$\mathcal{E}_{rel} = -\iint B \ln (B/B_0)\, dx\, dy \qquad (16)$$

where one can bias the reconstruction with a prior knowledge about the distribution.

Acknowledgement: The part of the work was supported by NSF grant ATM 81-03089.

REFERENCES

Baldwin, J.E. and Warner, P.J., 1976, Mon. Not. R. Astr. Soc., 175, 345.

Cornwell, T.J. and Evans, K.F., 1984, To appear in Astr. Astrophys.

Cornwell, T.J. and Wilkinson, P.N., 1981, Mon. Not. R.Astr. Soc., 196, 1067.

Gull, S.F. and Daniell, G.J., 1978, Nature, 272, 686.

Gull, S.F. and Skilling, J., 1984, Proc. IAU/URSI Symposium on 'Indirect Imaging', Ed. J.A. Roberts.

Hogbom, J.A., 1974, Astr. Astrophys. Suppl., 15, 417.

Jennison, R.C., 1958, Mon. Not. R. Astr. Soc., 118, 276.

Narayan, R. and Nityananda, R., 1981, Curr. Sci., 50, 168.

______________ 1982, Acta. Crystallogra., A38, 122.

Nityananda, R. and Narayan, R., 1982, J. Astrophys. Astr. 3, 419.

Readhead, A.C.S. and Wilkinson, P.N., 1978, Astrophys. J., 223, 25.

Readhead, A.C.S., Walker, R.C., Pearson, T.J. and Cohen, M.H., 1980, Nature, 285, 137.

Schwab, F., 1983, VLA Scientific Mem., 151.

Shevgaonkar, R.K., 1985, To appear in Astr. Astrophys.

EVENING DISCUSSION OF THE 75-MHz VLA PROPOSAL

An evening discussion on November 16 and the final discussion focused upon the 75-MHz VLA proposal. The original proposal envisioned free-standing 75 MHz antennas and a narrow-band correlator system separate from that of the present VLA. A spare channel of the VLA waveguide would be used to transmit the data from the antennas to the control building. The rationale was that the major cost of any meter-wavelength system with the aperture of the VLA is in the signal transmission system. This system already exists at the VLA site. On the other hand, meter-wavelength observations are often destroyed by ionospheric scintillation and by terrestrial interference. The scheduling flexibility of a system independent from the present VLA is essential. As originally proposed, the 75-MHz would operate completely independently of the 25 meter dishes. However, from our discussions it became clear that the funds required to build this system (about $1,000,000) could not be obtained in the near future. Also, there are some questions about how difficult it will prove to be to correct for ionospheric image distortions using self-calibration techniques.

It was concluded that before pursuing the original proposal for an independent 75-MHz system, we should instrument the 25 meter dishes for 75 MHz and use the existing correlator. This can be accomplished at very low cost (about $100,000) and it will provide a viable system at this frequency. It will have comparable collecting area and capabilities to the free-standing system. It will allow us to carry out interesting science at this frequency and to prove that the necessary ionospheric corrections can be made.

On the other hand, it is extremely inefficient to tie up the expensive 25 meter dishes and 50 MHz bandwidth correlators for 75 MHz observations. The dishes are only six wavelengths in diameter and provide no more collecting area than a simple array of dipoles. The observing bandwidth near 75 MHz will be limited by terrestrial interference to 1-2 MHz. The deletion and re-observation of data destroyed by ionospheric disturbances will represent a painful waste of VLA time. Therefore, it was concluded that we should implement the original proposal for an independent system as soon as it is financially feasible.

LOW FREQUENCY OBSERVATIONS OF SUPERNOVA REMNANTS

M.J. Mahoney

Clark Lake Radio Observatory
University of Maryland
College Park, MD 20742

INTRODUCTION

The Clark Lake Radio Observatory's TPT synthesis radio telescope (Erickson, Mahoney and Erb 1982) is ideally suited for mapping old supernova remnants (SNRs). Because of their large angular size, most of these objects have only been mapped using single dish observations at centimeter wavelengths. The TPT telescope operating at decametric wavelengths has a comparable resolution to many of these single dish measurements and thus provides a very convenient means to look for spectral index variations over differents parts of the remnants. In addition it provides the only means for observing SNRs at long wavelengths with sufficient resolution to say something about their structure.

Many old SNRs have now been mapped, or are being mapped, using the TPT telescope. This paper will present a combination of preliminary and final results for four of these objects which have been observed in collaboration with either Bill Erickson or Namir Kassim. Table I summarizes some of their physcical parameters.

Table 1. Some characteristics of the observed SNRs

SNR	l	b	Distance(Kpc)	Radius(pc)	Spectral	Index
IC443	190	5.0	2.3	13.7	-0.36	
HB21	89	5.0	1.0	14.5	-0.40	
VRO42.05.01	166	4.5	5.5	25.0	-0.40	wing
					>0.00	shell
W50	40	-2.0	3.0	25.0	-0.42	SNR
					-0.60	SS433

Before discussing each of the remnants individually, it is appropriate to make a few general comments. The most important is that the low frequency maps look virtually identical to the maps observed as much as two decades higher in frequency at comparable angular resolution. This implies, contrary to many previous reports, that the spectral index does not vary within these SNRs, as would be the case if there were localized electron acceleration. Presumably the SNRs are populated by electrons with a differential energy spectrum characterized by an unique spectral index. In addition it also appears that the spectral index is significantly flatter than what would be obtained if the cosmic ray electron energy index seen at high galactic latitudes is extended to the plane.

IC443

The results of observations of IC443 (3C157) at 73.8, 57.1, 38.5 and 30.9 MHz have recently been published (Erickson and Mahoney 1985). As can be seen in Figure 1, the spectrum is fitted by single power law from 20 MHz to 11 GHz with a spectral index of -0.36 +- 0.02. There is no evidence for steepening at high frequencies due to relativistic electron energy losses, nor is there evidence for internal free-free absorption. According to the theory of Blandford and Cowie (1982), interstellar clouds are compressed by the hot gas of an expanding SNR to the point where free-free absorption can occur. In the case of IC443 the slight turnover at the lowest frequencies can easily be accounted for by absorption external to the remnant. In addition it can be seen that the spectrum of IC443 is significantly different from the -0.5 spectrum predicted for synchrotron emission from electrons accelerated by strong shocks, if such shocks have a compression ratio of four. This implies that either the cosmic ray electron energy spectrum is different in the plane than was measured at high latitudes, or that compression ratios greater than four are possible. The latter would be possible if there were particle and/or thermal losses (Ellison et al. 1983).

Figure 2 shows our 73.8 MHz map of IC443 and the 2.8 cm map of Kundu and Velusamy (1972) which have similar angular resolutions. It is clear that there is little change in the brightness distribution of the SNR over more than two decades in frequency. This strongly supports the idea that IC443 has a global electron energy spectrum independent of the properties of the SNR.

HB21

Our conclusions regarding HB21 (Mahoney and Kassim 1985) are similar to those for IC443. As seen in Figure 3, the spectrum of HB21 can also be fitted by a single power law of spectral index -0.405 +-

0.030. Again there is no evidence for either low frequency absorption or high frequency steepening. In Figure 4 we compare our 40.0 MHz map to the 1420 MHz map of Hill (1974). It is clear that the maps are very similar, again implying little or nor variation in the differential electron energy spectrum throughout the remnant. As indicated on the 40.0 MHz image, there are three sources within HB21 which are unrelated to the SNR: 3C418, for which HI absorption gives a distance of 7.5 Kpc, 4C50.52, which is a double radio source of 2 arcmin separation at a position angle of 43 degrees, and 4C51.44. A fourth source, 4C51.53, is not clearly detected. The flux density contributions of these sources have been removed in deriving the integrated flux density for HB21 at 40.0 MHz.

Several authors have in the past noted a flattening in the northern part of HB21, presumably due to the interaction of the expanding remnant with a denser region of the ISM. In fact there is a dense HI cloud in this area. We see this feature as well, but in addition our map also shows a loop of emission even further to the north. We attribute this to a combination of 4C51.44, the galactic background, and a spur seen in the 1420 MHz map of Hill (1974), which is also suggested in the 610.5 MHz map of Yang and Dickel (1965).

VRO 42.05.01

Figure 5 compares our preliminary 50.0 MHz map of VRO42.05.01 to the 1420 MHz map of Landecker et al. (1982). Obviously this is a very spectacular object, suggesting the possibility that it might be either two SNRs, or a single SNR breaking into a less dense region of the

ISM. All previous images of this object (for example, Dickel, McGuire and Yang (1965) at 610.5 MHz and Willis (1973) at 2.7 GHz) were unable to resolve the smaller shell component, and in fact made it appear much larger by blending in the three strong sources, labeled A, B and C, to the north-east. The 50.0 MHz map resolves these objects, which we find all have much steeper spectra than the remnant. An additional map at 30.9 MHz however indicates that the *spectrum of the* shell component is turning over relative to *that of* the western wing component. This might be due to free-free absorption within the shell if it were more dense, and would lend support to a model for VRO42.05.01 in which the wing component is a part of the shell bursting into a less dense ISM. Simple momentum arguments based on the observed component radii indicate that the shell is about four times more dense than the wing.

In determining whether or not the *spectrum of the* shell is turning over, all flux contributions due to obvious point sources in the 1420 MHz were removed. To do this we assumed typical extra-galactic spectra for these sources and extrapolated the 1420 MHz flux densities provided by Landecker (private communication).

W50 AND SS433

Figure 6 compares a 57.5 MHz CLRO map of W50 to a recent VLA composite map at 1420 MHz (Baum, private communication). Because the low frequency map has been scaled to the same angular size as the VLA map, the eastern lobe of the SNR has been lost off the field. Clearly all the other features such as the west radio lobe attributed to interaction of a radio jet from SS433 with the remnant's shell are very similar in both maps, as is the prominent northern ridge, and an additional ridge running south-west from SS433. As in the case of the ot~~h~~her SNRs discussed here, the similarity of maps at such widely separated frequencies strongly suggests that the radiating electrons within the SNRs are characterized by a single energy index.

REFERENCES

Baars,J.W.M.,Genzel,R.Pauliny-Toth,I.I.K. and Witzel,A. 1977, Astron. Astrophys. 61,99.

Blanford,R.D. and Cowie,L.L. 1982, Ap.J., 260, 625. Astron. Astrophys. 61,99.

Dickel,J.R., McGuire,J.P. and Yang,K.S. 1965, Ap. J.,142,798.

Ellison,D.C., Jones,F.C. and Eichler,D. 1983, Proc. 18th Int. Cosmic Ray Conference.

Erickson,W.C. and Mahoney,M.J. 1985, Ap.J.,290,596.

Erickson,W.C., Mahoney,M.J. and Erb,K. 1982, Ap. J. Suppl.,50,403.

Hill,I.E. 1974, Mon.Not.R.A.S.,169,59.

Kundu,M.R. and Velusamy,T. 1972, Astron. and Astrophys.,20,237.

Landecker,T.L.,Pineault,Serge,Routledge,D. and Vaneldik,J.F. 1982, Ap. J.,261,L41.

Mahoney,M.J. and Kassim,N.E. 1985, BAAS,16(4),zzz.

Willis,A.G. 1973, Astron. and Astrophys.,26,237.

Yang,K.S. and Dickel,J.R. 1965, A.J., 70, 300.

FIGURE CAPTIONS

Fig. 1. The integrated flux density spectrum of IC443. The solid dots refer to data that has been placed on the MPI flux scale (Baars et al. 1977). A single power-law spectrum of index -0.365 +- 0.024 fits these data. This differs significantly from the index of -0.5 which is predicted by some theories.

Fig. 2a. A map of IC443 at 73.8 MHz as observed with the CLRO TPT synthesis radio telescope. The contour levels are 5%(10%)95% of the map maximum. The beam size is 5.4x4.7 arcmin and is shown in the box.

Fig. 2b. A 10,700 MHz of IC443 as observed by Kundu and Velusamy (1972).

Fig. 3. The integrated flux density spectrum of HB21. The solid dots refer to data that has been placed on the MPI flux scale. A single power-law spectrum of index -0.405 +- 0.030 fits these data.

Fig. 4a. A map of HB21 at 40.0 MHz as observed at CLRO. The contour levels are 5%(10%)95% of the map maximum. The beam size is 10.0x9.3 arcmin and is shown in the box.

Fig. 4b. The 1420 MHz map of HB21 as obtained by Hill (1974) with the Half Mile telescope. The resolution is 3.0x3.9 arcmin. The source 3C418 has been removed from the map; not all contours are shown for the sources 4C50.52 and 4C51.44.

Fig. 5a. A preliminary 50.0 MHz map of VRO42.05.01. Because of the low surface brightness of this source, the first contour shown reprsents about 0.5 Jy/beam and successive contours steps of about 0.2 Jy/beam. All previous maps of VRO42.05.01 included the three sources labelled A,B and C as part of the remnant. The beam shown in the box is 8.0x6.9 arcmin.

Fig. 5b. A 1420 MHz map of VRO42.05.01 from Landecker et al. (1982). This was the first image of the SNR that clearly demonstrated its remarkable structure.

Fig. 6a. A 57.5 MHz map of W50 and SS433. Because this image has been scaled to the same angular size as Fig. 6b. the eastern lobe has been lost off the field. SS433 appears to be clearly detected, as are the other features of the remnant.

Fig. 6b. A preliminary VLA 1420 MHz composite map of W50 (Baum, private communication).

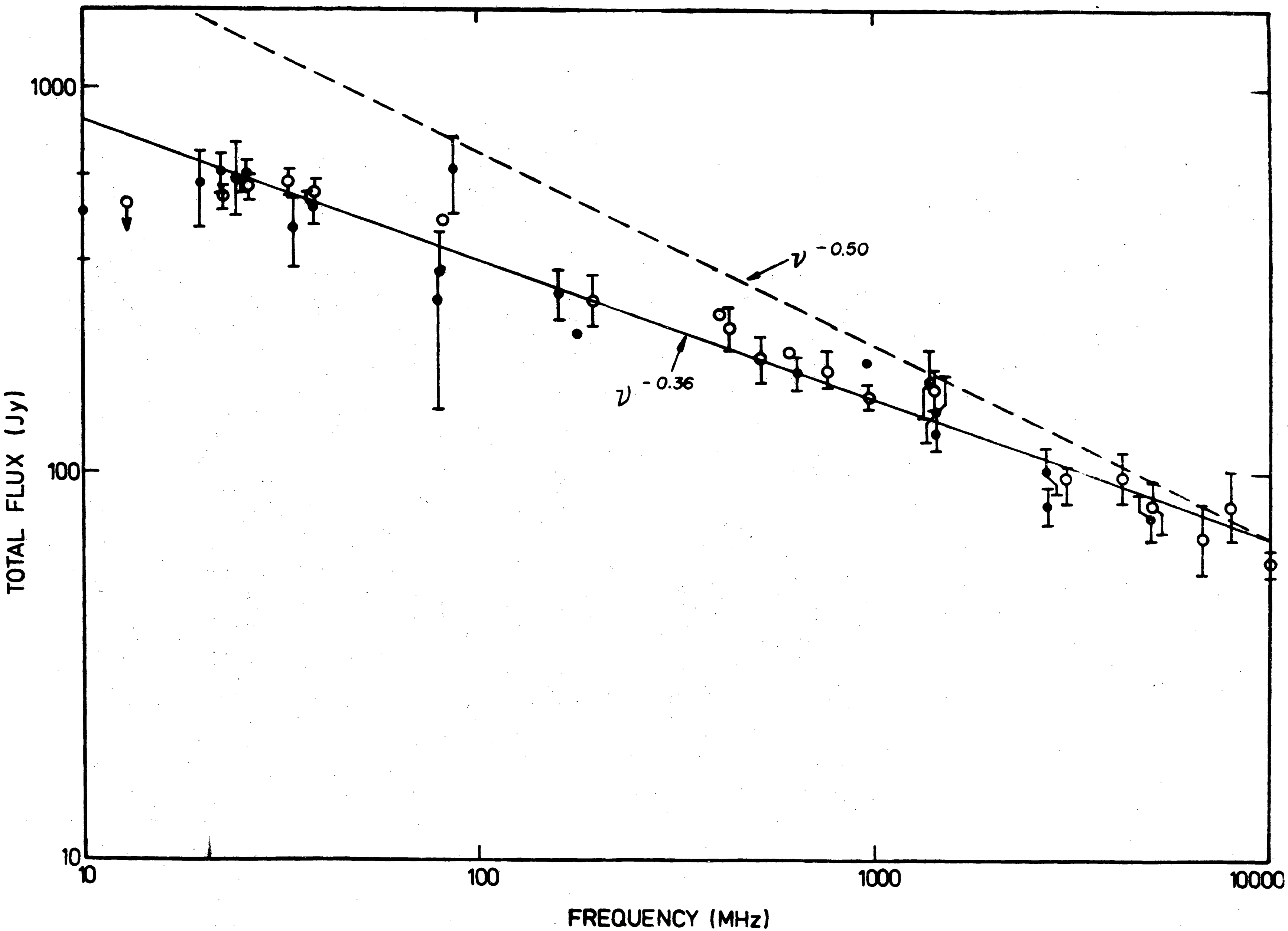
1000
100
10
10
100
1000
10000
TOTAL FLUX (Jy)
FREQUENCY (MHz)
$\nu^{-0.50}$
$\nu^{-0.36}$

Figure 1

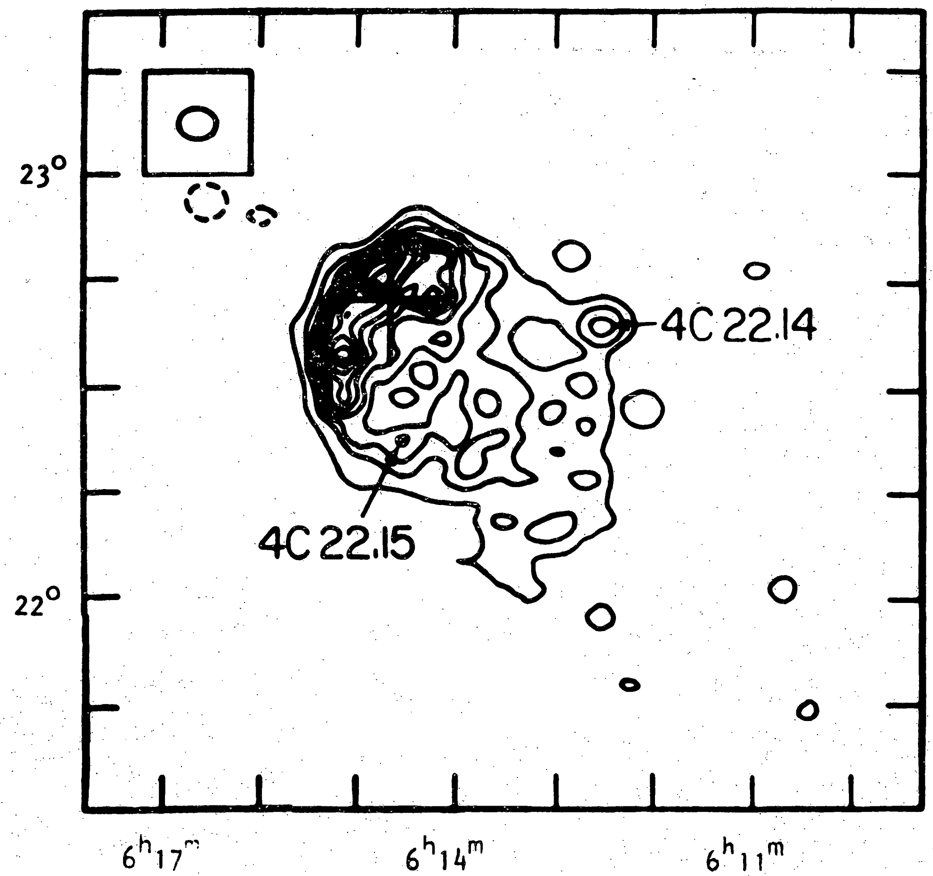

Figure 2a

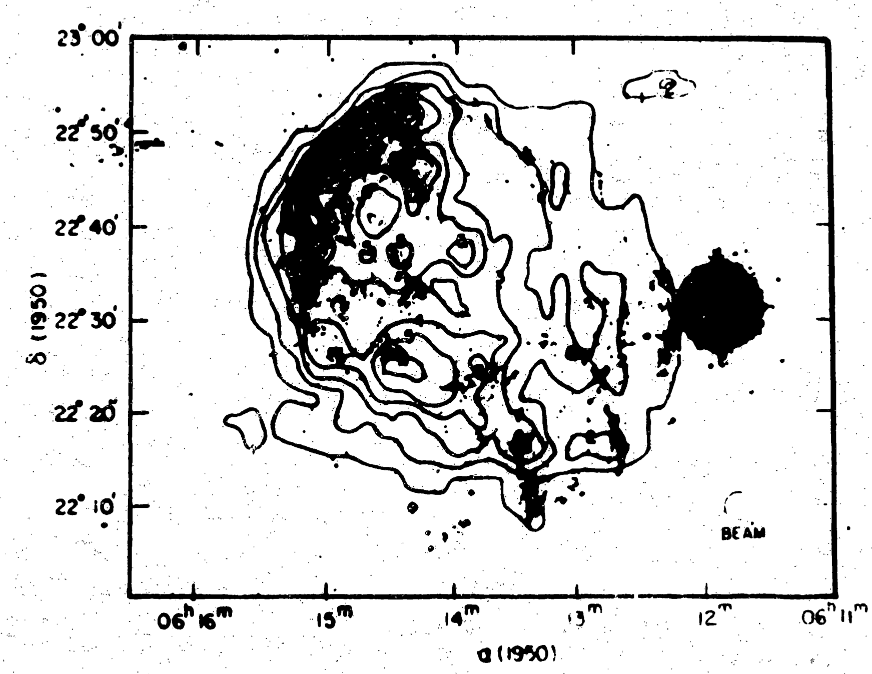

Figure 2b

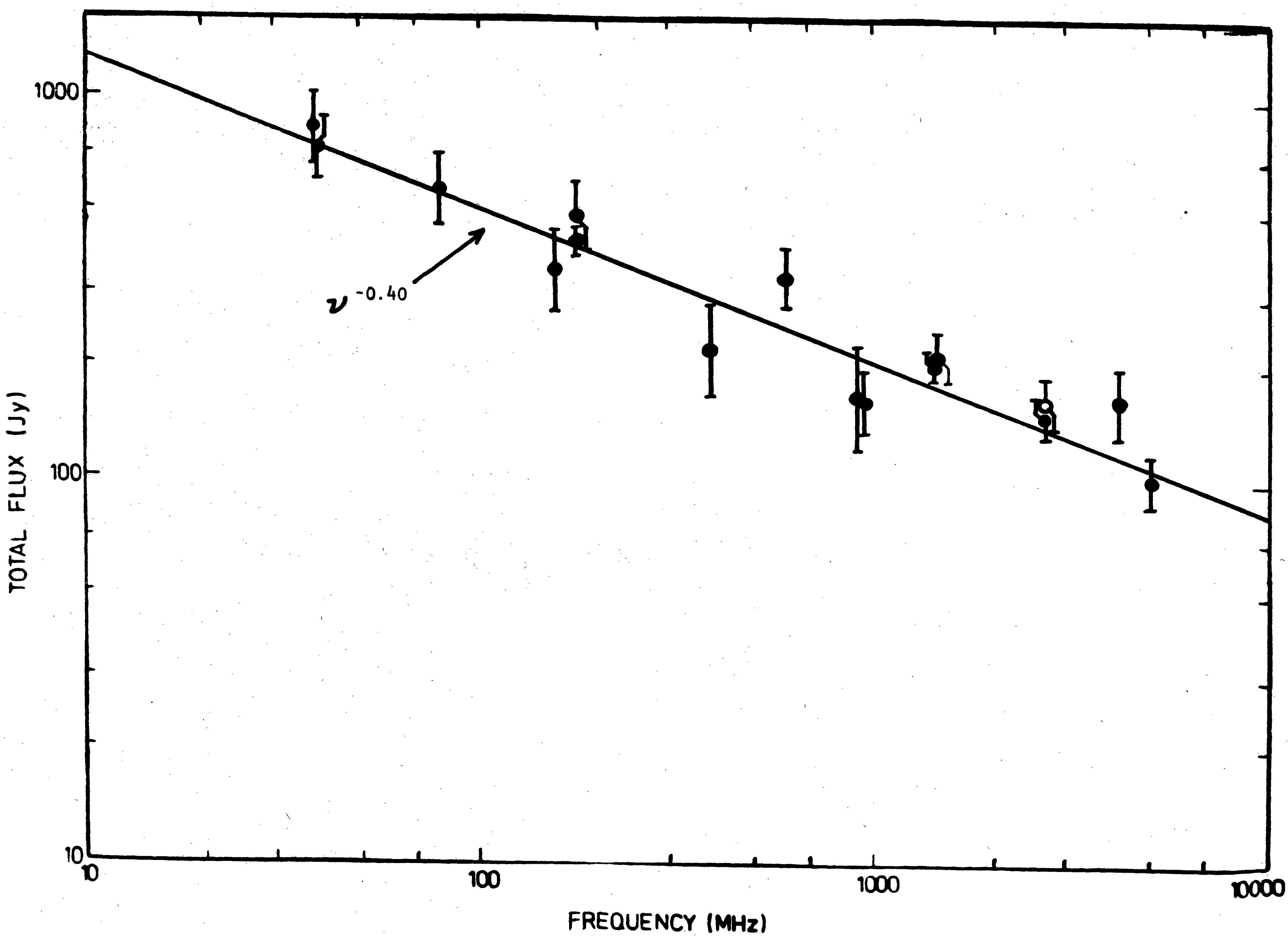
$\nu^{-0.40}$
TOTAL FLUX (Jy)
1000
100
10
10
100
1000
10000
FREQUENCY (MHz)

Figure 3

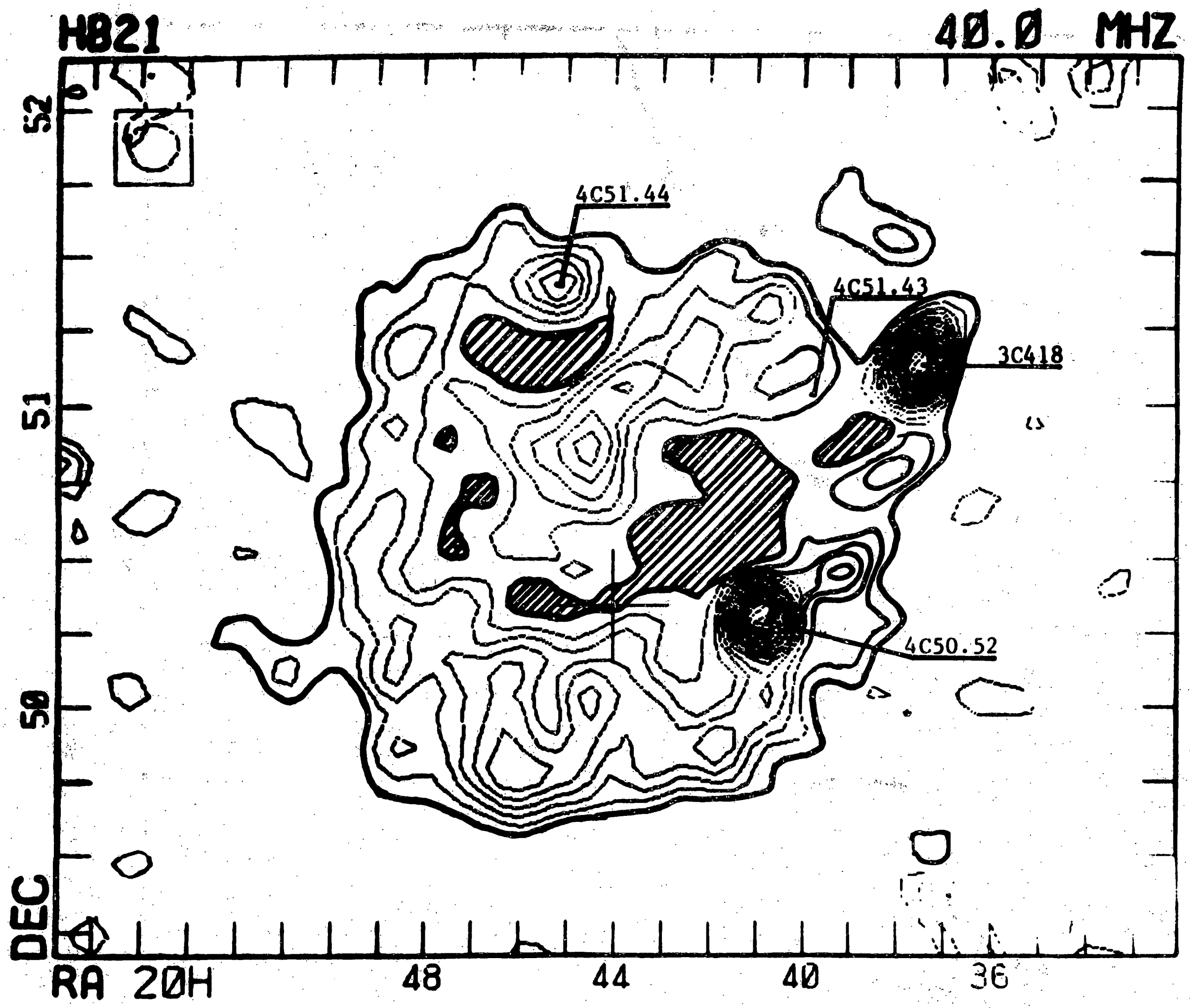

Figure 4a

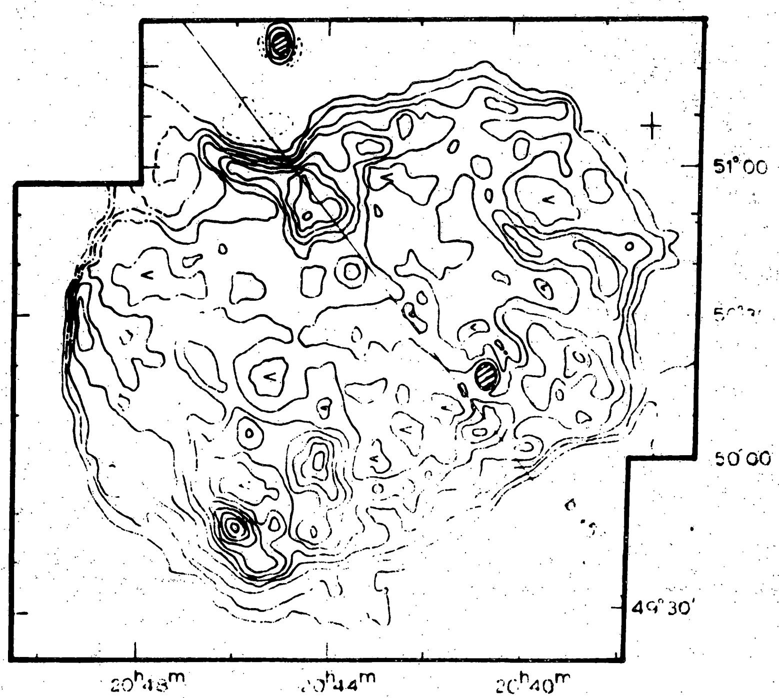

Figure 4b

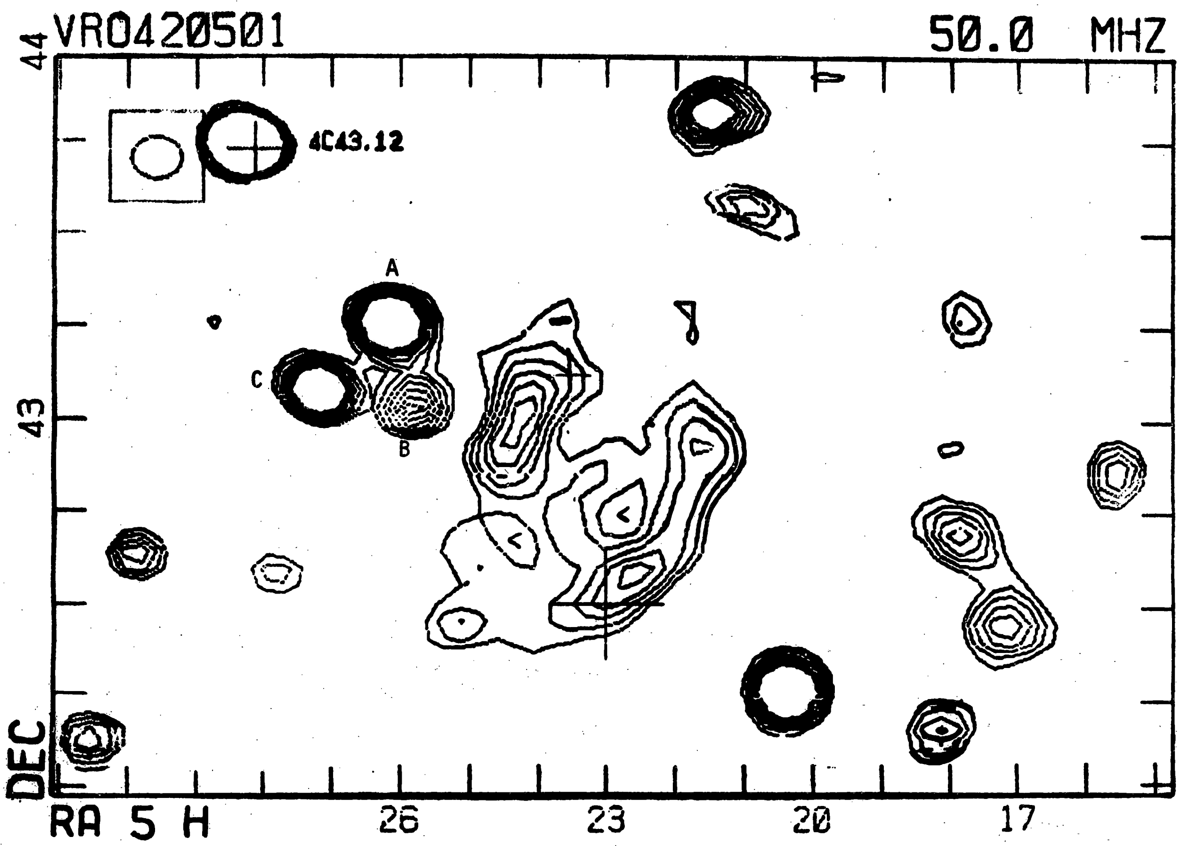

Figure 5a

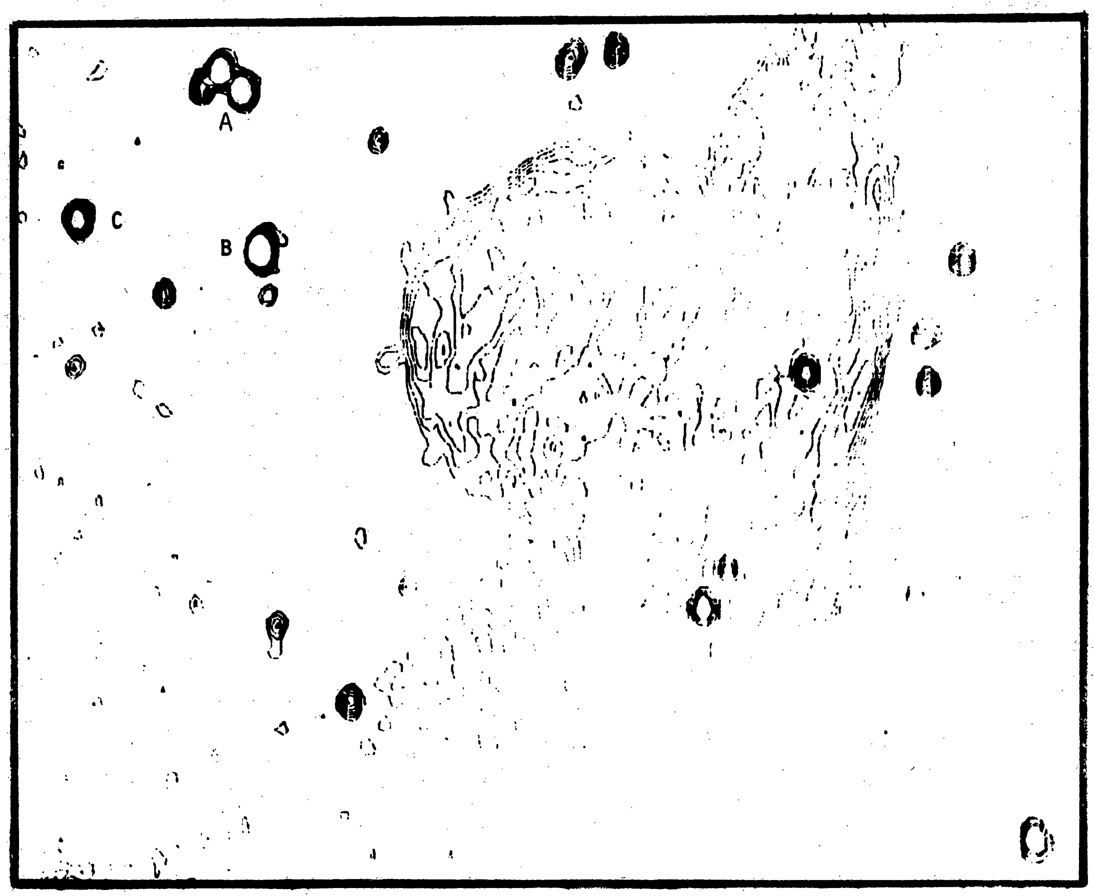

Figure 5b

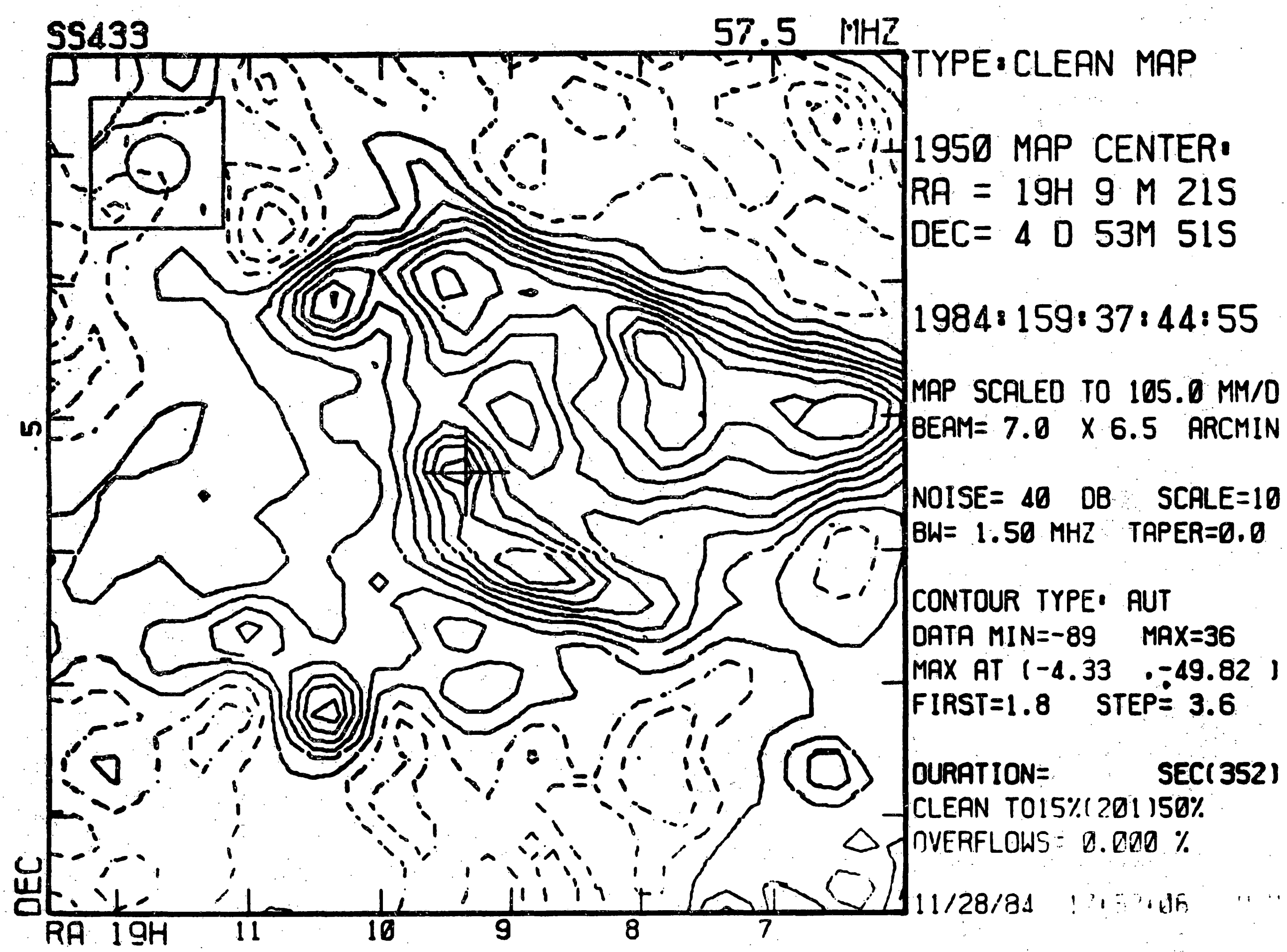

Figure 6a

VLA Composite Map of W50 (Baum, 1984) 1420 MHz

Figure 6b

LUNAR OCCULTATION OBSERVATIONS OF THE CRAB NEBULA AT METER AND DECAMETER WAVELENGTHS

A. G. Weisenberger, J. A. Phillips, S. T. Gottesman, and T. D. Carr
Department of Astronomy, University of Florida
Gainesville, FL 32611

Introduction

One-dimensional strip brightness distributions of the Crab Nebula at meter wavelengths are obtainable at resolutions of tens of arc seconds from lunar occultation observations made with single radio telescopes of sufficient size. The production of an unambiguous two-dimensional source brightness map usually requires several such strip distributions. While a comparable resolution may be obtained using interferometry, baselines of tens or hundreds of kilometers would be required. Few such interferometric observations have been made at meter wavelengths. Periodic lunar occultations have afforded an opportunity for investigating the Crab Nebula at meter wavelengths with high resolution, but the observations have not been systematic and the mapping has generally been fragmentary. A complete map derived from occultations of the Crab was produced, however, by Maloney and Gottesman (1979) at 114 MHz. Unfortunately, ionospheric and interplanetary sciltillation in the occultation records at such frequencies may create erroneous structure in the derived maps. A sufficient number of occultation observations is therefore required to reduce the effects of scintillation to an acceptable level. The situation at decameter wavelengths is even worse because of the increased ionospheric scintillation and the often severe interplanetary scintillation of the Crab Nebula pulsar, NP 0532. The published results of the few Crab occultations that have been observed at decameter wavelengths are not of high quality, in most cases because of scintillation and interference. There are times, however, when scintillation is negligible, even at decameter wavelengths. Occultations occurring under such conditions could produce good maps. Since occultations of the Crab are rare (occurring only at intervals of 8 or 9 years) it is important that full advantage be taken of these events whenever they can be observed by large meter and decameter wavelength telescopes. We report in this paper results from the most recent series of occultations, observed at four meter wavelengths and at one decameter wavelength.

Observations

We observed the occultation of the Crab Nebula on October 8, 1982 with the 1000 ft Arecibo radio telescope in Puerto Rico and with the 640-dipole, 26.3 MHz array of the University of Florida Radio Observatory (Desch, Carr and Levy, 1975). The Arecibo observations were made at the four frequencies 84, 111.5, 114.5, and 218 MHz. At each frequency, separate right- and left-hand circular polarization component outputs were recorded, each at two bandwidths (125 and 500 KHz), providing a total of sixteen channels. The Florida observations, at 26.3 MHz, were made at linear polarization and with a bandwidth of 260 KHz. Usable results were obtained from only the ingress at Arecibo, the Crab having passed beyond the Arecibo beam limit before the egress was complete, and from the egress at the Florida observatory, the ingress having been marred by radio station interference.

The plots in Figure 1 and Figure 2 are the occultation records of the ingress event for both polarizations at 84 and 218 MHz, respectively, at the 125 kHz bandwidth. Scintillation is apparent at 84 MHz, but is less severe at 218 MHz. The 26.3 MHz occultation egress record is displayed in Figure 3. Despite the scintillation in this

FIGURE 1

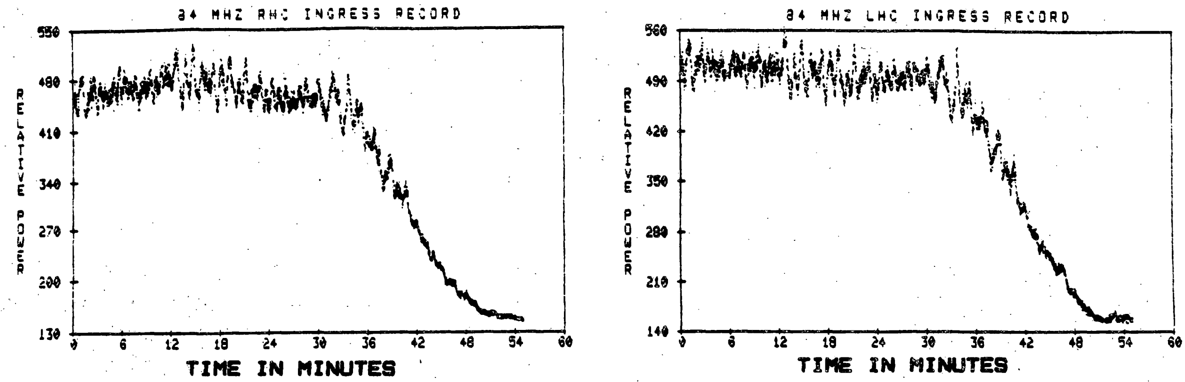

Arecibo occultation ingress records obtained on October 8, 1982 at 84 MHz with both right- and left-handed circular polarizations. On the time axis, t=0 corresponds to 8 hours 00 minutes Universal Time. Data points are 0.8 seconds apart.

FIGURE 2

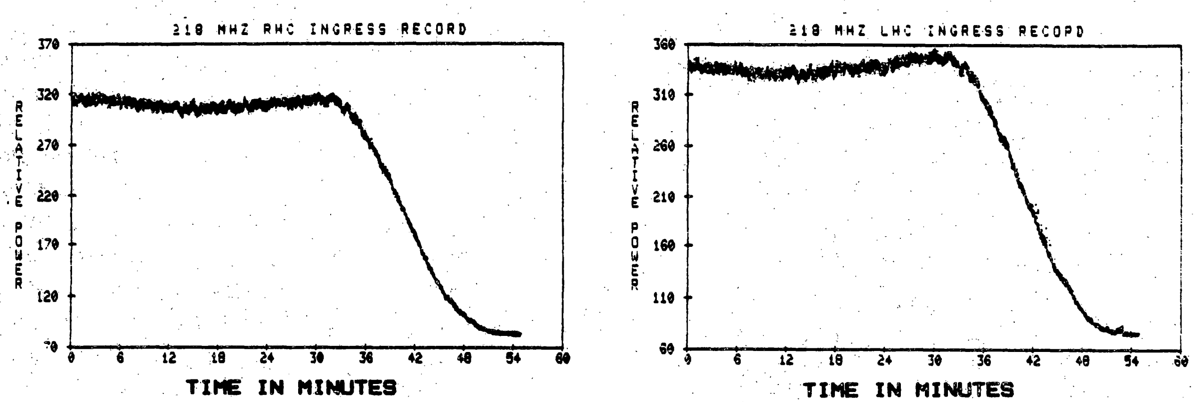

Arecibo occultation ingress records obtained on October 8, 1982 at 218 MHz with both right- and left-handed circular polarizations. On the time axis, t=0 corresponds to 8 hours 00 minutes Universal Time. Data points are 0.8 seconds apart.

FIGURE 3

Occultation egress record obtained on October 8, 1982 at 26.3 MHz from the University of Florida Radio Observatory. On the time axis, t=0 corresponds to 9 hours 28.4 minutes Universal Time. Data points are 0.25 seconds apart.

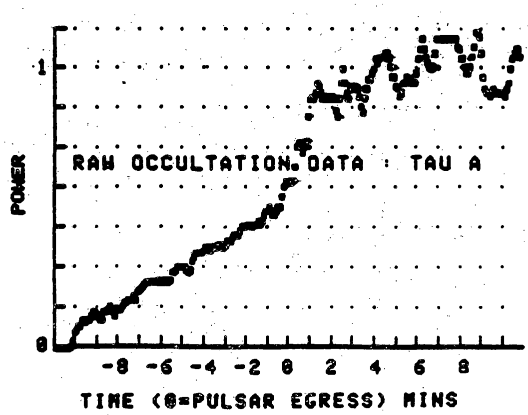

record, we believe its quality to be generally better than that of any other obtained yet from a Crab Nebula occultation below 40 MHz.

Analysis

The procedures of Scheuer (1962) have been employed to recover integrated strip brightness profiles from the occultation records. Figures 4 and 5 show the four strip scans recovered from the two polarizations of the 84 and 218 MHz records obtained at Arecibo. These scans correspond to an ingress position angle of 109 degrees. The resolution achieved for the 84 MHz strip scans is comparable to that of a radio telescope with a fan-shaped beam of Gaussian cross-section and a full width at half power of 38.4 arc seconds. The corresponding resolution for the 218 MHz profiles is 23.8 arc seconds. The maximum resolution that can be realized in each case is a function of the noise in the original occultation record. Since scintillation is more intense at 84 MHz that at 218 MHz, the resolution is poorer at the lower frequency.

An inspection of Figures 4 and 5 clearly reveals that there is resolved structure in the Nebula, and that it becomes more pronounced at the lower frequency. In addition, the strip scans for left-hand circular polarization appear to differ appreciably from those at right-hand circular polarization, particularly in the case of the feature about 2' east of the origin. This difference is evident at all the frequencies observed at Arecibo and may be an indication that some emitting regions in the Crab Nebula have a surprisingly high degree of circular polarization. On the other hand, the possibility that the observed polarization results somehow from scintillation or from instrumental effects cannot be ruled out at this early stage in our analysis.

The 26.3 MHz restored integrated strip brightness map is shown in Figure 6. This strip profile corresponds to an egress position angle of 281 degrees. The brightness distribution is equivalent in resolution to that obtainable with a fan-shaped radio telescope beam of 45 arc seconds full width at half power. The dominant feature of the brightness profile is a strong pointlike source (broadened in the smoothing process) centered on the known position of the pulsar, to the accuracy at which the time of the deflection maximum can be read. The peak is seen to arise from within the region of the nebula itself, which in turn rises well above the galactic background. The part of the nebula brightness distribution west (i.e., to the right on the diagram) of the pulsar is decidedly smoother than that to the east. The probable reason for this is that there was almost no scintillation as long as the pulsar was covered by the moon, but it became severe when the pulsar emerged from behind the moon. The structure of the nebula distribution to the right of the pulsar in Figure 6 is therefore much more reliable than that to the left, which was badly contaminated by the pulsar scintillation. A similar situation is probably encountered in the restored strip brightness distributions from most Crab Nebula occultations observed in the decameter band and, at a lower level, for the meter wavelength results reported here.

Our 26.3 MHz Crab Nebula occultation results have provided more detailed structural information than did the earlier observations (Costain, 1956; Andrew, Branson and Wills, 1964; and Matveenko, 1968), presumably as a result of better observing conditions and the use of a much larger antenna array. The degree of ionospheric scintillation at the time of our measurements was definitely below average, and there was no interference from radio stations or distant thunderstorms during the egress period. Frequent reference has been made in the literature to the "low frequency compact source" in the Crab Nebula, even since the discovery of the Crab pulsar. Our strip brightness profile in Figure 6 will reinforce the conclusion that the two are the same, since the peak of the curve is centered on the position of pulsar NP 0532. By

FIGURE 4

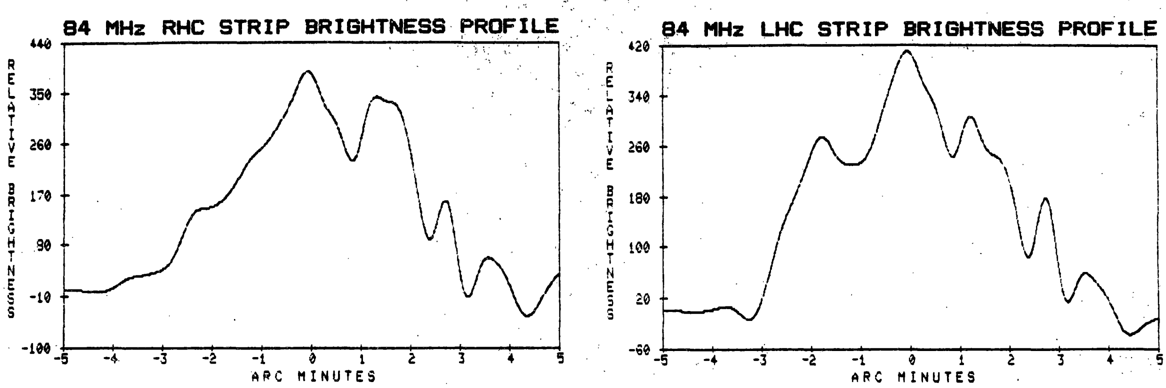

Restored 84 MHz strip brightness distributions. The origin of the abscissa is the location of the pulsar NP0532. West is on the right for both of the scans and the occultation position angle (measured eastward from north) is 109 degrees.

FIGURE 5

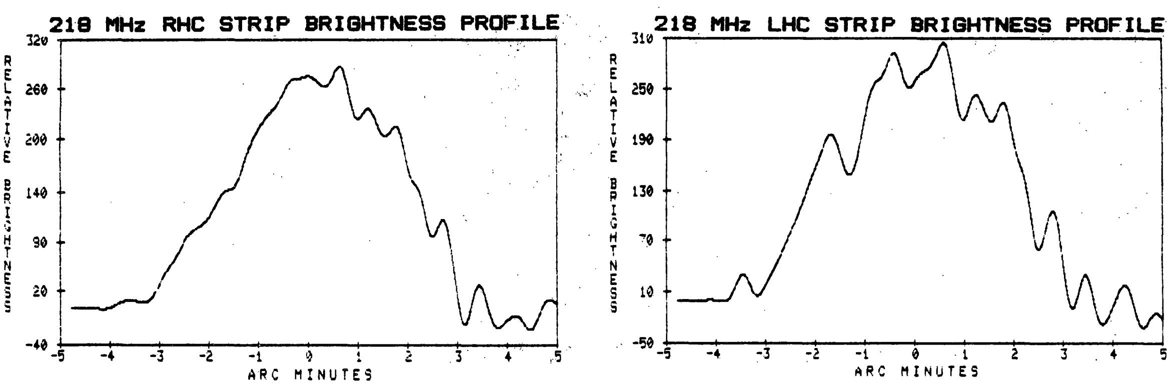

Restored 218 MHz strip brightness distributions. The origin of the abscissa is the location of the pulsar NP0532. West is on the right for both of the displayed scans. The occultation position angle (measured eastward from north) is 109 degrees.

FIGURE 6

Restored 26.3 MHz strip brightness distribution. The origin of the abscissa corresponds to the location of the pulsar NP0532. Like the scans displayed above, west is to the right in the 26.3 MHz brightness distribution. The occultation position angle is 281 degrees.

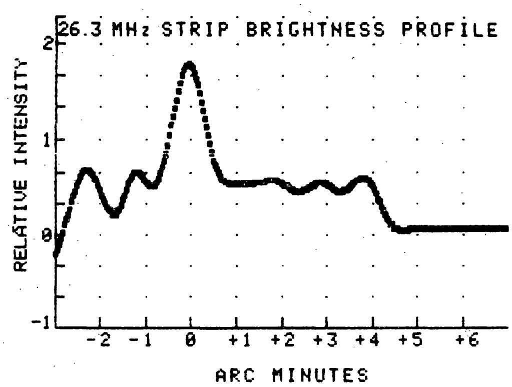

integrating the curve in Figure 6, we have found that the pulsar emits 25% of the observed Crab Nebula flux density at 26.3 MHz, with error limits +6, -10 %. Cronyn (1970) obtained the value 26% from interplanetary scintillation.

Conclusion

Maloney and Gottesman (1979) claimed that the Crab Nebula at a frequency of 114 MHz is composed of a broad envelope of emission with small scale structure. The structure was attributed to the non-negligible opacity of the major filaments at these wavelengths. This effect was expected to become more pronounced at even lower frequencies. The 1982 occultation observations, which we have reported here, confirm the presence of sub-minute-of-arc structure and that a substantial fraction of the total flux density at 26 MHz is emitted by the low frequency compact source (the pulsar). To our surprise, we have found that the meter wavelength emission from some of these features is relatively highly circularly polarized. However, the presence of scintillation makes this conclusion less than certain at this time. Before this project is completed, we plan to analyze more fully this apparent polarization phenomenon, and to determine the two-dimensional brightness distribution of the Crab at 114 MHz.

Finally, these meter and decameter lunar occultation observations have shown that it would be extremely useful to have a dedicated meter wavelength array of the kind proposed for the VLA. A system of high sensitivity with a resolution of better than 1' would be able to make repeated observations of the Crab and overcome, finally, the problem of confusion caused by scintillation. Notwithstanding, lunar ocultations at meter wavelength are a powerful tool for investigating the structure of strong sources in the ecliptic and for determining their low frequency spectral indices.

References

Andrew, B. H., Branson, N., and Wills, D., 1964. Nature, 203, 171.
Costain, C. H., 1956. Mon. Not. R. Astr. Soc., 116, 380.
Cronyn, W., 1970. Science, 168, 1453.
Desch, M. D., Carr, T. D., and Levy, J., 1975. Icarus, 25, 12.
Maloney, F. P., and Gottesman, S. T., 1979. Astrophys. J., 234, 485.
Matveenko, L. I., 1968. Sov. A. J., 12, 552.
Scheuer, P. A. G., 1962. Aus. J. Phys., 115, 333.

Addendum

We were informed recently by the Arecibo Observatory that the observations we have described were sensitive to linear rather than circular polarization.

Lower limits of solar burst source sizes at decameter wavelengths

T.E. Gergely

Astronomy Program

University of Maryland

College Park, MD 20742

The impact of a new decameter wavelength telescope, operating at spatial resolution and sensitivity two orders of magnitude higher than those achieved by current instruments is difficult to predict. In the following, I discuss the usefulness of such a telescope for solar research based on our current knowledge.

I assume that the telescope will have an angular resolution of ~ 20" at ~ 75 MHz. Long integration times are of relatively little usefulness for solar research. I assume therefore a 1 min integration time and a 2 MHz bandwidth. The sensitivity of the telescope would then be ~ 0.1 Jy. For some programs, even a one minute integration time may be too long and integration times of the order of a second or shorter may be desirable, further lowering the sensitivity. The 75 MHz plasma level is located in the mid-corona, ~ 0.6 $R_\odot$ above the photosphere. A resolution of ~ 20" corresponds to a size of ~ 0.02 $R_\odot$, or 1.5 x 10^4 km on the Sun. It is therefore natural to ask the questions:

1) Are there structures on this scale in the corona ~ 0.6 $R_\odot$ above the photosphere.
2) What source sizes are observed at decameter wavelengths with the resolution presently available?
3) Could "solar" type bursts that occur on nearby stars be observed at decameter wavelengths?

1) The angular resolution of presently operating coronagraphs (e.g. the C/P carried on board of the SMM satellite, or the ground based MK-III coronameter of HAO) is similar to that of the proposed decameter telescope, and is in no case better than $\sim 10''$. Filamentary structures, a few times the size of the resolution element are often seen on images of the quiet sun obtained with these instruments. Structure on a somewhat larger scale is nearly always present on images of coronal mass ejections (CME's), which consist of dense, magnetized coronal plasma ejected from the Sun. On the average they occur once per day, typically the mass ejected is $\sim 10^{16}$ g, and the energy contained in the event is $\sim 10^{32}$ ergs. They are often associated with intense type II and IV radio bursts. Fig. 1 shows the visible light image of a CME recorded by the Coronagraph/Polarimeter of the Solar Maximum Mission. The bright inner loop is an eruptive prominence, the outer loop consists of coronal material. Decameter radio emission is often associated with various parts of the coronal loop: the legs, the top of the loop, or the material just behind the bright rim. The thickness of the loop shown ranges from $\sim 1\overset{'}{.}5$ to $2\overset{'}{.}5$, and structure on a smaller scale can be seen inside it. The answer to our first question is therefore that structure on a scale size ~ 0.5 arcmin is seen at coronal heights where 75 MHz emission is expected.

2) At decameter wavelengths the emission from the quiet or background Sun is thermal in nature. Bursts observed at ~ 75 MHz include: type III bursts, type II and type IV bursts, and a variety of other bursts that occur during noise storms. Among these we mention only the S bursts.

a) At 73.8 MHz the Clark Lake radioheliograph (Kundu et al., 1983) is sensitive enough to provide an image of the quiet Sun every 0.67 seconds. The spatial resolution of the heliograph at 73.8 MHz is $4\overset{'}{.}6$; the presence of structure at or below the resolution of the telescope is often suggested by the

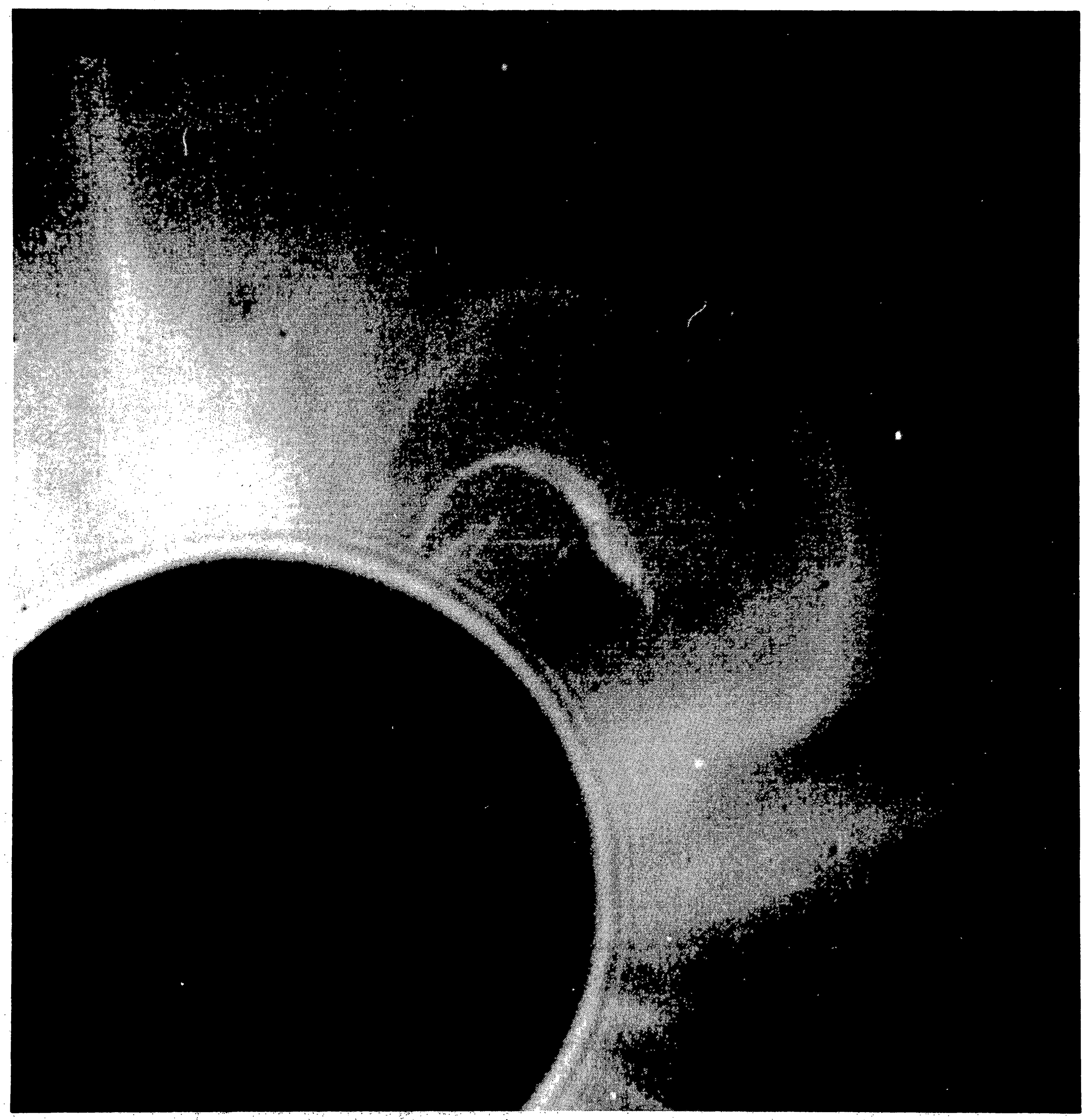

Fig.1. A coronal mass ejection recorded by the Coronagraph/Polarimeter on the Solar Maximum Mission Spacecraft on 14 April, 1980. The dark occulting disk has a radius of 2$'$.6. The white dot near the top of the outer loop is slightly larger than 20". (Courtesy of W. J. Wagner).

observations. Figs. 2a and b show images of the Sun recorded on July 25 and 26, 1984 respectively. Ten 0.67 second snapshot frames were integrated to obtain each map. A close double source is visible on the northern hemisphere on both days. Such sources are likely to mark the location of the legs of high coronal loops. The elongated source on the southern hemisphere is also likely to indicate an unresolved double source. This interpretation is borne out by the map of large scale magnetic fields present on the Sun. Fig. 2c shows the Stanford magnetogram (Solar Geophysical Data, 1984) obtained on July 27. (No magnetograms were available for July 25 or 26). Solid and dashed contours indicate positive and negative magnetic fields at 0, ± 100, 500, 1000 and 2000 microtesla levels. The location of the polarity inversion associated with features A and B are clearly seen on the magnetic map. No statistics are kept on such unresolved features, but they are frequently observed. The associated excess flux is of the order of a few hundred Janskys. High resolution studies of such sources are certainly desirable and might contribute significantly to our understanding of coronal loops.

b) Type III, II and IV bursts.

Type III bursts occur frequently at decameter wavelengths. During times of intense solar activity tens or even hundreds per hour may be observed. They may or may not be associated with flares, CME's or other surface activity. At decameter wavelengths they drift from high to low frequencies at a rate of ~ 0.1 MHz s^{-1}, their duration is a few seconds. Type II's are believed to be the radio signature of shock waves moving outwards in the corona. They also drift from the high to the low frequencies, although at a lower rate of ~ 0.04 MHz s^{-1}. They are associated with flares or CME's, and last ~ 10 minutes. Moving type IV bursts also are associated with flares or CME's. They last a few tens of minutes and are usually broadband ($\Delta f/f \sim 1$). Type III, II and moving IV sources have

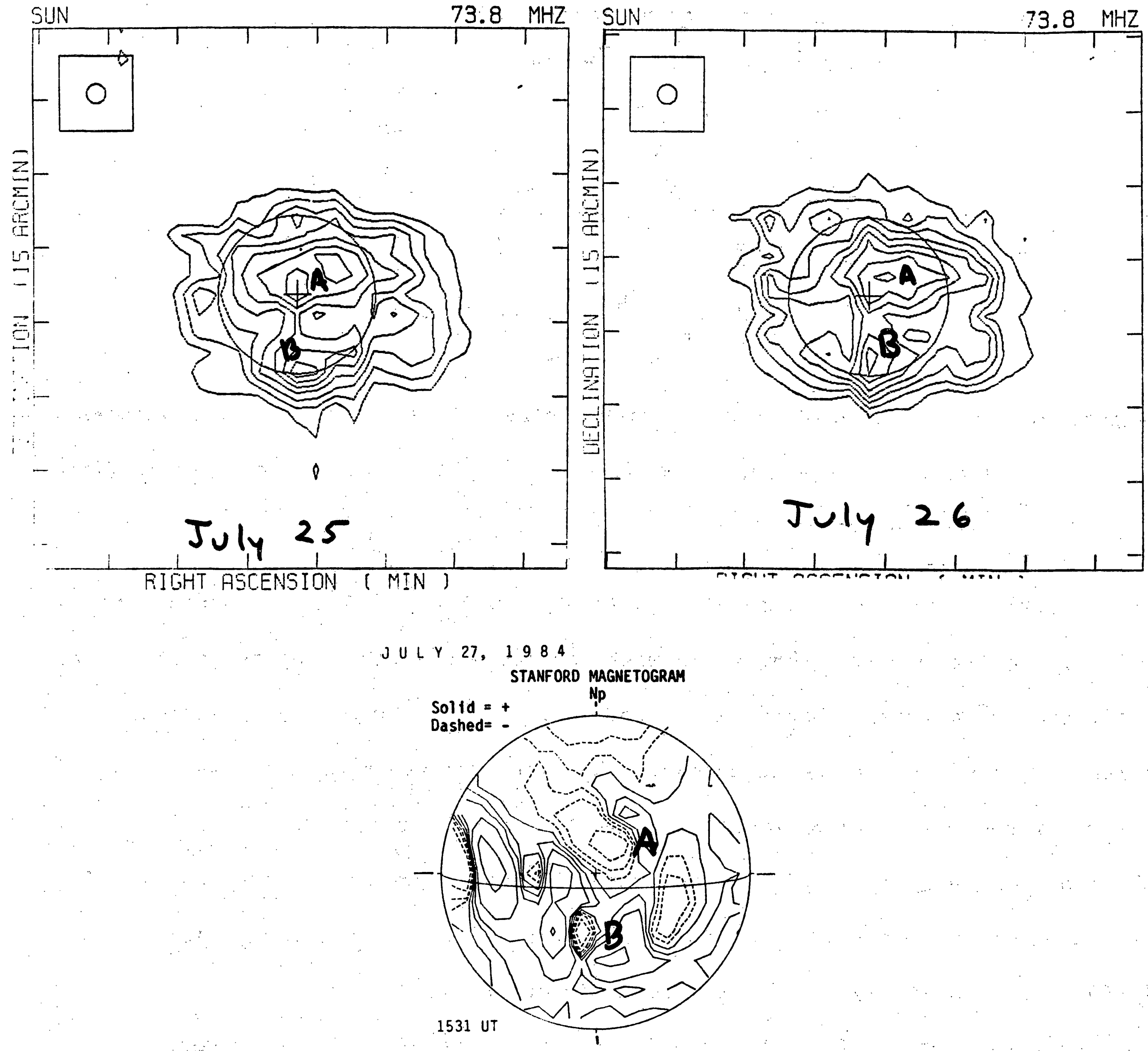

Fig. 2. 73.8 MHz snapshot images of the "quiet" Sun (τ = 0.67 s) obtained with the CLRO radioheliograph, on July 25 and 26, 1984. Also shown is the Stanford magnetogram corresponding to July 27.

been observed with the Clark Lake Teepee Tee and with the Culgoora radioheliograph at ~ 80 MHz. The distribution of the source sizes of type III's observed at Culgoora was given by Dulk and Suzuki (1980), Nelson and Robinson (1975) discussed source sizes of some type II bursts. Fig. 3 shows the type III

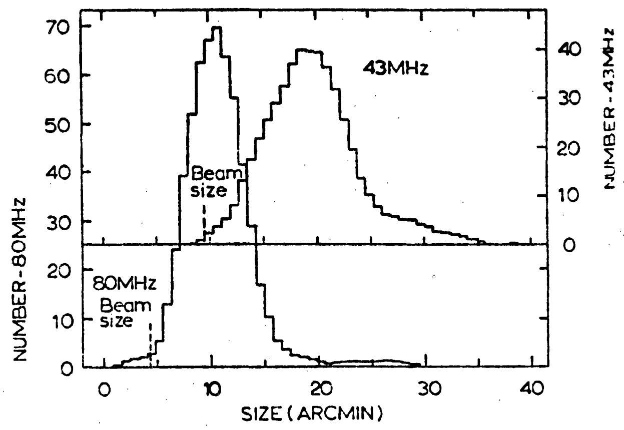

Figure 3. Distribution of type III source sizes (full width at 1/e brightness derived from measurements obtained with the Culgoora heliograph (from Dulk and Suzuki, 1980).

source size distribution obtained by Dulk and Suzuki at 80 MHz, the mean size is ~ 11ʹ.0. The figure shows that while most sources are larger than the beam, quite a few are unresolved. About half of the type III's at 80 MHz have sizes only 1-2 times the beamwidth of the telescope. The time resolution of the observations was a few seconds (1 to 3 seconds). High time resolution (0.02 seconds) observations obtained at 169 MHz indicate that many type III bursts consist of the superposition of several components of smaller size (Raoult and Pick, 1980). This is likely to be the case at lower frequencies also.

As a rule, type II sources are larger than type III's at any given frequency. Nelson and Robinson (1975) found a mean size of 10ʹ at 80 MHz, considering both harmonic and fundamental sources. They included only a few sources in their study, however. They noted that most 80 MHz fundamental sources remained unresolved by the Culgoora telescope, while harmonic sources were well resolved.

Robinson (1979) carried out a study of 23 moving type IV sources observed at Culgoora, and compiled the size of 19 of the bursts.
Fig. 4 shows this data, in the form of a histogram. We converted Robinson's 2D

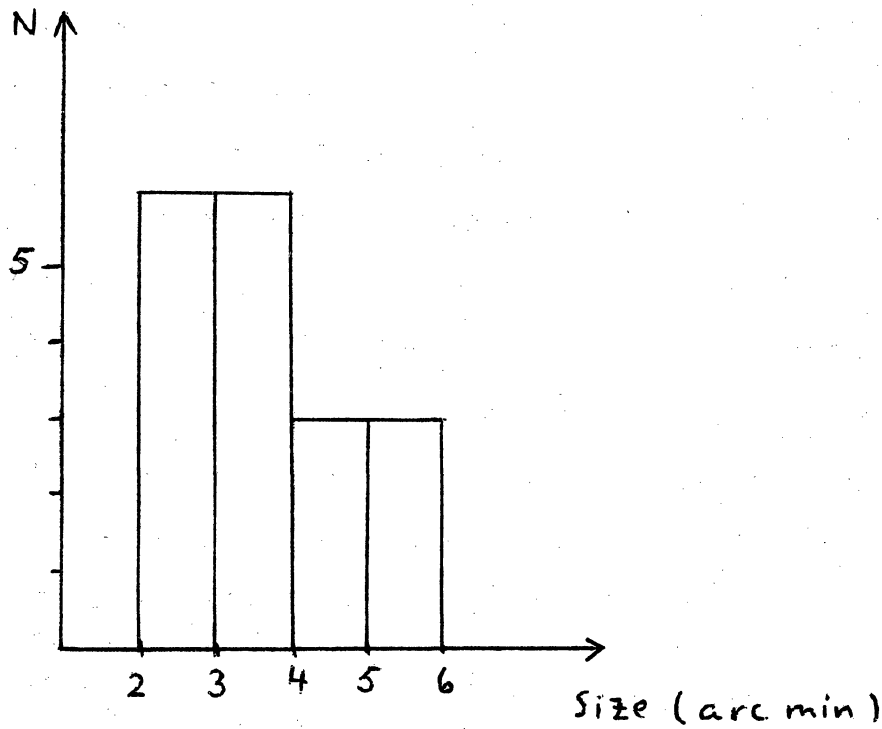

Figure 4. Distribution of the minimum sizes of moving type IV sources at 80 MHz (data from Robinson, 1979).

sizes assuming that all sources were circular in shape. In most cases the source size varied during the event. Fig. 4 is based on the minimum sizes, sources the size of which remained constant were also included. Most type IV's have minimum sizes close to or below the resolution of the telescope.

c) S bursts.

S bursts occur during noise storms. Their duration is very short (~ 5 msec) and their bandwidth is extremely narrow (~ 120 kHz). Assuming that they are generated by fundamental plasma emission, McConnell (1983) estimated the radial extension of the sources to be a few hundred kilometers, and their lateral extension to be in the 600-1800 km range. S bursts offer the most direct and convincing evidence for the presence of small scale structure in the corona.

The observation of S bursts shows clearly that transient sources in the corona exist on spatial scales an order of magnitude below the resolution of the planned telescope. Might such sources be observed? It is well known that scattering by electron density irregularities increases the apparent angular sizes of coronal sources. Many scattering models have been computed, and although they differ in details, their main features are similar. A popular one due to Riddle (1974) predicts that point sources emitting in a spherically symmetric corona at 80 MHz will be broadened to ~ 1.′5 or 1′ if the emission is due to fundamental or to second harmonic plasma emission, respectively. If the source of the burst is located on the axis of a streamer in an otherwise homogeneous corona, then sizes as small as 0.′5 would result. The above sizes refer to center of the disk sources, all models predict an increase in the size of sources at the limb.

While scattering certainly must take place in the corona, its effect on the apparent size of burst sources is uncertain. All models are strongly dependent on a number of parameters, none of which are well known. Further, all models predict an increase in size when the burst source approaches the limb. This effect has not been observed. Ocassionally, sources smaller in size than predicted by scattering theory have been observed (Kerdraon, 1979). Thus, while it should be kept in mind that scattering probably imposes limits on the observed size of some sources, this limit is not well known. Moreover, scattering affects only sources that emit at frequencies close to the corresponding plasma level. Many burst sources, such as moving type IV′s, do reach much greater heights than the plasma level corresponding to the frequency of emission and therefore should not be affected by scattering at all.

3) Finally, we ask the question: Could any of the bursts discussed above be observed on other stars? At around 80 MHz the brightest solar bursts observed to date are the moving type IV′s, which reach brightness temperatures up to $T_B \sim 10^{13}$ K. If the source region has a diameter of $\sim 10^6$ Km (1.5 $R_\odot$), and the

sensitivity limit of the telescope is $\sim$ 0.1 Jy, a stellar burst could still be observed only out to a distance less than $\sim$ 1 pc. Thus, "solar" type bursts are not likely to be observed.

References

Dulk, G.A. and Suzuki, S., 1980, Astron. Astrophys. 88, 203.

Kerdraon, A., 1979, Astron. Astrophys., 71, 266.

Kundu, M.R., Erickson, W.C., Gergely, T.E., Mahoney, M.J. and Turner, P.J., 1983, Solar Phys., 83, 385.

McConnell, D., 1983, Solar Phys., 84, 361.

Nelson, G.J. and Robinson, R.D., 1975, Proc. ASA, 2, 370.

Raoult, A. and Pick, M., 1980, Astron. Astrophys., 87, 63.

Riddle, A. C., 1974, Solar Phys., 35, 153.

Robinson, R., 1979, Solar Phys., 64, 383.

Solar Geophysical Data, 1984, U.S. Dept. of Commerce.

METER WAVELENGTH RADIO ASTRONOMY IN CHILE

J. May, F. Reyes, H. Alvarez, and J. Aparici
Observatorio Radioastronomico de Maipu
Departamento de Astronomia, Universidad de Chile
Casilla 68, Maipu, Chile

T. Carr, J. Phillips, J. Levy, and G. Lebo
University of Florida Radio Observatory
Department of Astronomy, University of Florida
Gainesville, FL 32611

Introduction

The Maipu Radioastronomical Observatory of the University of Chile is located at latitude 33°30' S, 70°51' W, 30 km southwest of Santiago. It is situated on a large plain in a valley of the Andes foothills. The first radioastronomical activity at Maipu was the construction in 1959 of a 175 MHz solar interferometer by the University of Chile with support from the Carnegie Institution. The observatory was founded in 1959 jointly by the University of Chile and the University of Florida, with support from the National Science Foundation, principally for the study of Jupiter's decametric radiation. Following the completion by the University of Chile of a 45 MHz filled rectangular array with an area of about 10,000 m^2 in 1976, activities of the observatory were extended into the meter wavelength band and beyond the solar system. To facilitate the use of this large array, the Chilean government has prohibited radio transmissions in the band from 43.7 to 47.6 MHz. A description of the array and its operation is given by May et al. (1). Current meter-wavelength research at Maipu consists largely of a galactic survey of the southern sky, a search for secondary calibration sources, pulsar studies, a search for atmospheric pulses from Saturn (SEDs), and the continuing investigation of Jovian S bursts above 30 MHz.

The 45 MHz Array.

The 45 MHz antenna is a rectangular array consisting of 528 full-wavelength dipoles oriented E-W and distributed in 48 rows of 11 colinear dipoles each. The rows are separated by a half wavelength, and the dipoles are at a height of a quarter wavelength above a reflecting plane. The dimensions of the array are 160 m in the N-S direction by 73 m E-W. The half power beamwidths are 2.4° N-S by 4.6° E-W. Four such beams, fixed to the meridian but overlapping at their N-S half-power points, are simultaneously available. The declinations of the group of beams are altered by means of phasing adjustments, coarse phasing being made manually in the field and fine phasing by remote control with the aid of a Butler matrix. Essentially interference-free night-time operation is usually possible with receiver bandwidths up to 3 MHz. Additional information on the array and its operation are given in the references (1,2).

Galactic Mapping.

The mapping of the Galaxy at 45 MHz will cover declinations from -90° to +20°, and all right ascensions. No other southern hemisphere survey of comparable resolution, sensitivity and coverage is available below 85 MHz, others at 10 and 30 MHz being limited to the vicinity of the galactic center. Fig. 1 is a preliminary map of the galactic center region prepared from a part of the 45 MHz data obtained thus far (1). The coolest region is mapped in Fig. 2. The maximum and minimum galactic brightness temperatures at 45 MHz were found to be 89,000 K and 3050 K, respectively (3). Both the galactic center and the coolest part of the Galaxy pass nearly overhead at Maipu.

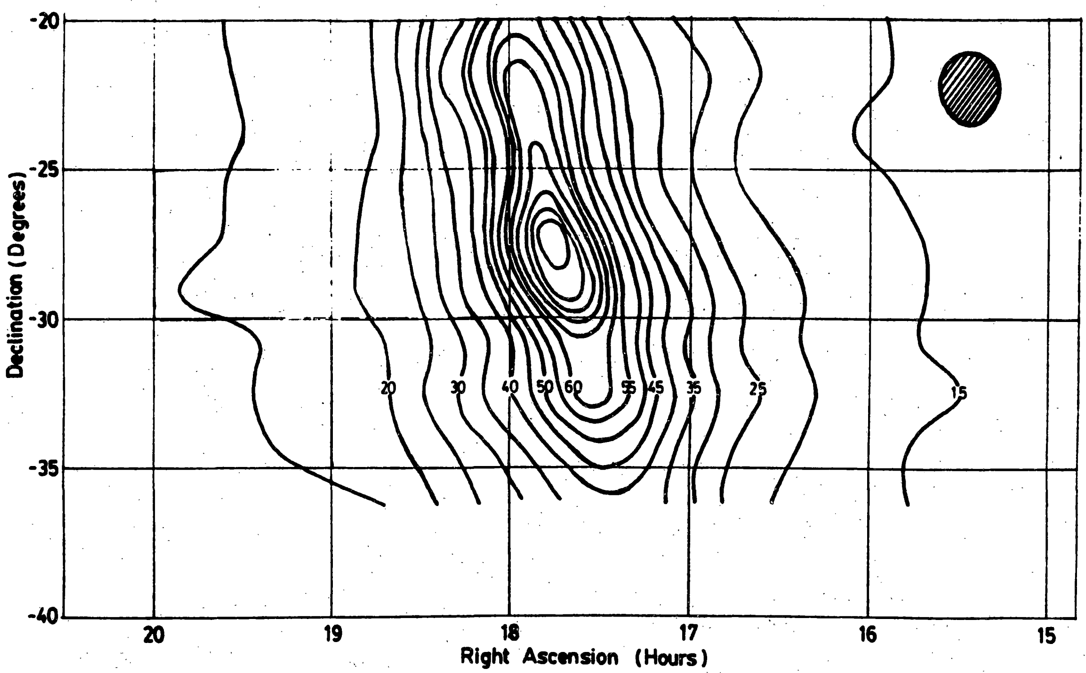

Fig. 1. Preliminary map of galactic center region at 45 MHz. Brightness temperature contours are in thousands of Kelvins. Half-power beam contour is at upper right. Map is derived from a limited number of observations. Discrete sources have not been removed, nor has correction for sidelobes been made.

The primary calibration sources for the galactic survey are Fornax A and Hydra A. A network of secondary calibrators is being built up. The flux density measurements of the 8 secondary calibrators that have been investigated so far at Maipu, by Alvarez et al. (4), are listed in Table 1 and are plotted in Fig. 3. Also plotted in Fig. 3 are the available published flux density measurements of these sources over a wide range of frequencies (5). The lowest frequency measurements that have yet been made of two of the sources, 1424-11 and 1449-12, are apparently those from Maipu.

Table 1

Flux densities at 45 MHz

Source	S(Jy)
0038-09	64
0131-36	97
0521-36	61
0806-10	46
1136-13	96
1424-11	35
1449-12	29
2032-35	33

Pulsars.

Although extensive studies of northern hemisphere pulsars at decameter and the

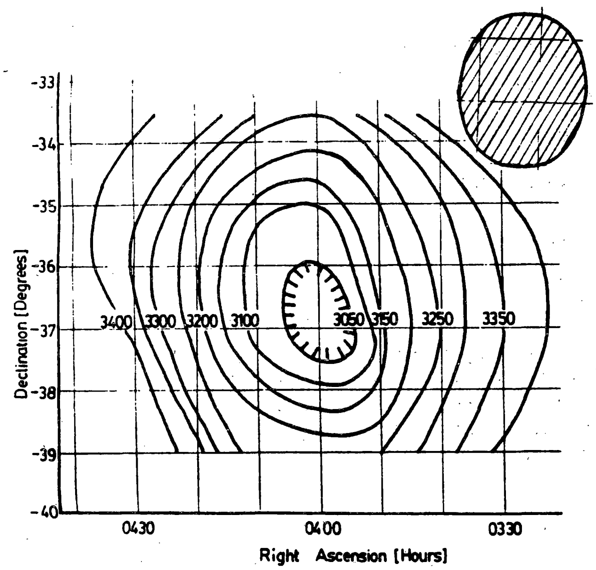

Fig. 2 (above). Region about the galactic minimum at 45 MHz. Brightness temperature contours are in Kelvins. Half-power beam contour is at upper right.

Fig. 3 (right). Spectral plots including the measured 45 MHz source flux densities (listed in Table 1) and published flux densities (5) for the same sources at other frequencies.

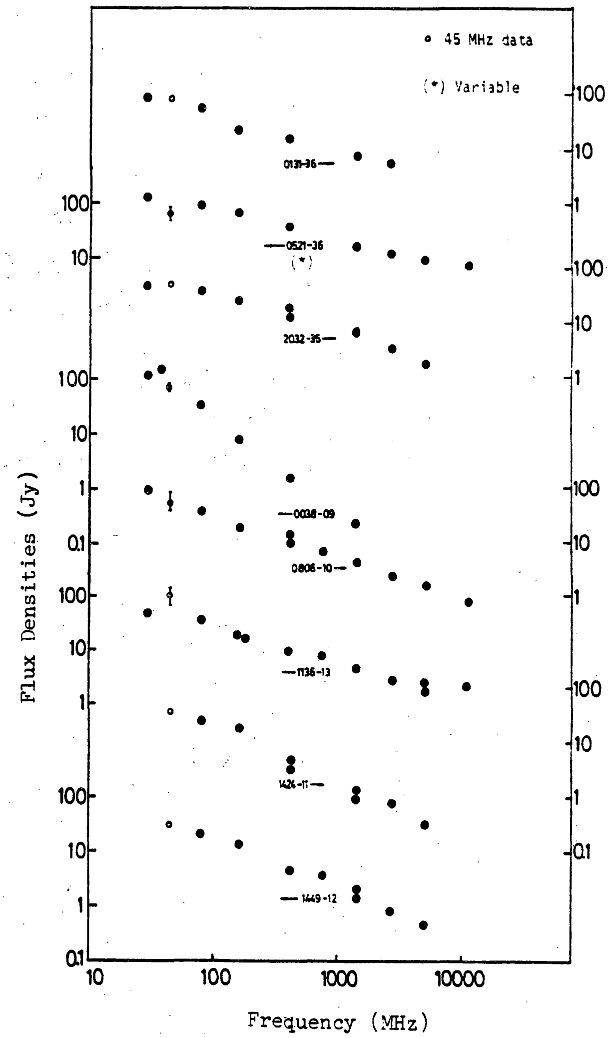

longer meter wavelengths have been made by Bruck and Ustimenko, using the large UTR-2 radio telescope of the Ukranian Academy of Sciences, very few such observations have been made in the Southern Hemisphere (6). We have therefore undertaken an investigation of known pulsars observable at 45 MHz with the Maipu array. This investigation is being supplemented by 26.3 MHz pulsar observations with the 640-dipole array of the University of Florida. Two of the seven pulsars searched for thus far at Maipu are relatively strong and are always detectable by averaging 10 to 80 pulse intervals; they are PSR 0834+06 and PSR 0628-28. Two of the others, PSR 2045-16 and MP 0031-07 are sometimes strong but are undetectable at other times. The remaining three are only marginally detectable at present. The main pulse of PSR 0834+06 is sometimes apparent with no pulse interval averaging at all, as can be seen in Fig. 4. In this photograph, the oscilloscope sweep period has been made equal to the period of the pulsar. The main pulse is discernable in 4 of the 6 successive sweeps; its failure to appear on two sweeps is probably due to interplanetary scintillation. Fig. 5 is the average of 350 periods of PSR 0834+06. The pulse peak is about 7 σ above the mean. There is definitely some interpulse activity, but the interpulse appears to be more variable than the main pulse. A 32-channel receiver is being constructed for pulsar observations. With it, correction can be made for interstellar dispersion, greatly increasing the effective bandwidth. The increased sensitivity will make possible the study of pulse structure in more detail. A further increase in the number of channels is planned in order to provide good resolution in frequency as well as time in an investigation of pulsar scintillation at this frequency.

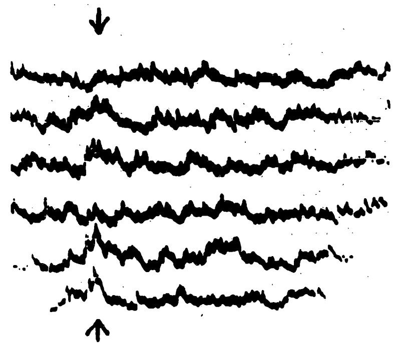

Fig. 4. Successive unaveraged oscilloscope sweeps of the receiver output indicating the presence of pulsar PSR 0834+06 at 45 MHz. The sweep period is 1.27 sec, the same as that of the pulsar. The center of the main pulse on each sweep is at the time indicated by the arrow.

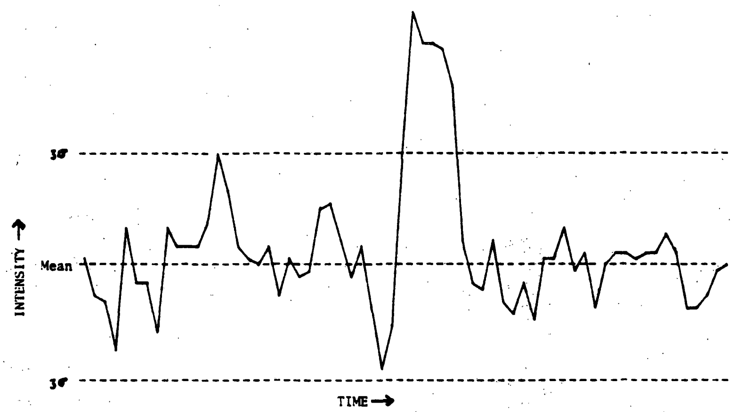

Fig. 5. Pulse profile of pulsar PSR 0834+06 at 45 MHz obtained June 11, 1983 by averaging 350 pulse periods. The period is 1.27 sec.

SEDs.

The pulses from Saturn (SEDs — Saturn Electrostatic Discharges) at meter, decameter, and hectometer wavelengths that appeared in the data from the two Voyager spacecraft when they were close to the planet (7) have never been observed from Earth. First thought to be electrostatic pulses from ring particle collisions, the idea that they instead result from lightning discharges in Saturnian thunderstorms has recently gained favor (8). The rate of occurence of SEDs underwent a pronounced maximum whenever the observing spacecraft was over a particular sector of Saturnian longitude, these episodes of activity recurring at intervals of roughly 10 hours. The SED power spectrum appeared to be relatively flat from less than 1 MHz to 40 MHz, the highest frequency observed. On the basis of data obtained during the most intense episode observed from Voyager 1, it appears that one might expect the flux density at Earth on such an occasion to exceed 50 Jy (±3db) for at least 30 msec once per minute, more or less (9). The corresponding estimate based on Voyager 2 observations would be 5 to 10 db less, probably due to source variability on time scales of days, weeks, or months.

A search for SEDs with the 45 MHz Maipu array has been initiated. The calculated SED detection sensitivity for this radio telescope is given in Table 2, together with that for the 640 dipole 26.3 MHz array at the University of Florida Radio Observatory. On the basis of the Maipu estimate, one might expect to detect an SED above the 3 σ level about once a minute during a storm of the intensity observed by Voyager 1. The Voyager 2 experience, however, suggests that there might be delays of weeks or months between the stronger storms. Occasions when the activity is even less than that observed by Voyager 2 are likely, but storms exceeding the one found by Voyager 1 in intensity are just as probable on the basis of our present knowledge. Any clear-cut information on SED detectability that can be obtained from large terrestrial meter and decameter wavelength radio telescopes, even information based on negative results, will be worth the expenditure of considerable effort.

It is apparent from Table 2 that the probability of ultimately detecting SEDs with the Maipu array at 45 MHz is good, but that the detection probability with the Florida 26.3 MHz array is less by an order of magnitude because of the higher galactic background temperature, the larger Saturn zenith angle at transit, and the narrower bandwidth. We believe, however, that the probability of detection from Florida of occasional particularly strong SEDs is large enough to justify at least one series of Florida observations, simultaneously with those of Maipu. Such simultaneous observations will be made during the approaching apparition of Saturn.

Table 2

SED Search Sensitivities

Observatory	Freq. MHz	T_G K	$A_e \cos z$ m^2	Δf MHz	τ msec	ΔS (3σ) Jy
Maipu	45	7,000	6,000	3	30	30
U. of Florida	26.3	33,000	8,000	0.5	30	280

T_G = galactic background temperature. A_e = effective area. z = Saturn zenith angle at transit. Δf = bandwidth. τ = time constant. ΔS = minimum detectable (3 σ) flux density.

Predicted SED flux density at Earth: $S \geq 50$ Jy (±3db) for at least 30 msec once per minute (more or less) during stronger episodes.

Several 20-min tape recordings of the passage of Saturn through the beam of the Maipu array were made during the previous apparition. A computer program has been developed for determining the pertinent statistical parameters of each data run, and for plotting the larger pulses. Two receivers, connected to adjacent N-S beams of the array, were used. One of the beams was centered on Saturn at transit, and the other was just off Saturn, to the south. Two of the recorded tapes have been analyzed so far. The highest pulses observed were between 3 σ and 4 σ above the mean, occuring equally often in the off-Saturn and on-Saturn beam channels (but never simultaneously on the two). The rate of occurence of pulses exceeding 3 σ was just about what would be expected for Gaussian noise fluctuations, about one per 10 sec on each channel. Examples of these largest pulses are shown in Fig. 6. The left pair of plots shows such a large pulse in the

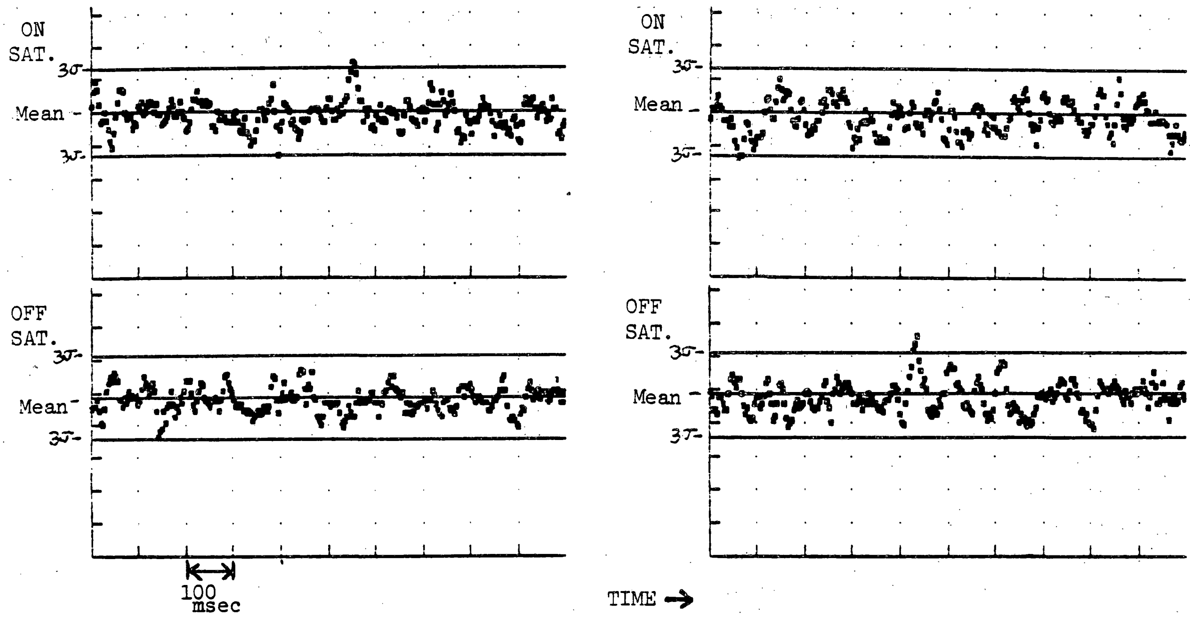

Fig. 6. Two of the largest pulses observed during a 20 min SED run at 45 MHz on April 17, 1983. Two receivers of 3 MHz bandwidth each were used, one connected to the antenna beam pointed at Saturn and the other offset from the planet. Indicated points are running 20-msec averages of the data samples.

on-Saturn channel, while the right pair shows one in the off-Saturn channel. Terrestrial interference does not seem to be a problem, despite the wide bandwidth (3 MHz). However, since the median prediction of one SED exceeding the 3 σ level per minute is only 1/6 the occurrence rate of pulses this high due to statistical fluctuations, some additional means must be provided for identifying the 3 σ SEDs. This is easily accomplished, and will be done for future measurements. Two receivers tuned to adjacent but non-overlapping frequency bands will be operated from the on-Saturn antenna beam. The SEDs, being very broad band, will always occur simultaneously in these two channels, while the 3 σ statistical fluctuations will almost never do so. Another advantage of such dual frequency channels is that they provide a means for identifying occasional pulses due to the scattering of signals from distant radio stations off meteor trails into our antenna beams. Such interference, being narrow band, will appear in only one of the two frequency bands at a time.

Jovian S Bursts.

Most of the research at Maipu on Jupiter's low frequency burst radiation has been done at decametric wavelengths. The Io-controlled components, however, often extend into the meter wavelength band (above 30 MHz), occasionally reaching the source cutoff frequency just below 40 MHz. Investigation of this radiation at Maipu is continuing at both decameter and meter wavelengths. The millisecond-burst component, S bursts, were first observed near their upper frequency limit, 32 or 33 MHz, with a small array at Maipu (10). S bursts always (or nearly always) display a negative frequency drift (i.e., to lower frequencies). This drift is consistent with the idea that the radiation is emitted near the local electron gyrofrequency by groups of electrons ascending the northern hemisphere Io-threaded magnetic flux tube, from just above its intersection with the Jovian ionosphere. It had previously been suggested that the S burst radiation arises from ascending electrons that have just mirrored. Desch, Flagg, and May (10), however, showed from the Maipu measurements that the S burst-emitting electrons possess their highest velocities at the start of their ascent from just above the ionosphere (where the gyrofrequency is highest) instead of having mirrored there. Such S burst studies jointly at Maipu and at the University of Florida Radio Observatory are continuing.

The Future.

Future meter wavelength research programs planned for the Maipu observatory are the measurement of Jupiter's synchrotron radiation at 45 MHz, searches for lightning pulses from Jupiter and Venus, measurement of the velocities of sources of Jovian S bursts with a Chile-Florida interferometer, a search for intensity variations in extragalactic sources, and the detection of absorption lines due to outer-level transitions in carbon and other atoms within clouds lying in front of the strong continuum source at the galactic center. A continuing program of array expansion in area, resolution and frequency coverage is planned. Sufficient flat land is available at the observatory for a considerable increase in array dimensions. An engineering study is in progress which is aimed toward the design of more inexpensive array elements possessing the desired frequency coverage, and the design of improved and relatively inexpensive array beam steering methods suitable for use at Maipu.

We greatfully acknowledge the support of the Departamento de Desarrollo de la Investigacion of the University of Chile, CONICYT, the European Southern Observatory, the NASA Satellite Tracking Station at Santiago, and the National Science Foundation.

References

(1) A 45-MHz array for radio astronomy. J. May, F. Reyes, J. Aparici, M. Bitran, H. Alvarez, and F. Olmos. Astron. Astrophys. 140, 377-382 (1984).

(2) Radiotelescopio en 45 MHz para fuentes extragalacticas. F. Reyes, E. E. Thesis, University of Chile, 1977.

Calibrador programable y automatico para radiofuentes en 45 MHz. J. Aparici, J. May, F. Salas, and J. Ventura. Rev. Mexicana Astron. Astrof., 6, 363-366 (1981).

Sistema computacional para la adquisicion automatica de datos en linea con un radiotelescopio de 4 haces simultaneos. Rev. Mexicana Astron. Astrof., 6, 367-372 (1981).

(3) La radiacion del fondo galactico en 45 MHz. M. Bitran. M. S. thesis, University of Chile, 1981.

Preliminary results of a galactic background survey at 45 MHz. M. Bitran, J. May, and J. Aparici. Rev. Mexicana Astron. Astrof., 6, 79-82 (1981).

Maximum and minimum galactic background radiation at 45 MHz. J. May, H. Alvarez, J. Aparici, F. Reyes, and F. Olmos. Rev. Mexicana Astron. Astrof. (in press).

(4) Preliminary flux density measurements of a few strong southern hemisphere radio sources at 45 MHz. H. Alvarez, J. May, J. Aparici, F. Reyes, and F. Olmos. Rev. Mexicana Astron. Astrof. (in press).

(5) S. Ya. Braude et al. Astrophys. Space Sci., 54, 37 (1978); 64, 73 (1979).

S. Ya. Braude et al. Ukranian Acad. Sci. Inst. Radio Phys. and Electronics, Preprint No. 147 (1980).

A. H. Bridle and C. R. Purton. Astron. J., 73, 717 (1968).

E. A. Finlay and B. B. Jones. Aust. J. Phys., 26, 389 (1973).

O. B. Slee. Aust. J. Phys. Astroph. Suppl., No. 43, 1 (1977).

O. B. Slee, B. C. Siegman, and P. S. Mulhall. Proc. ASA, 4, 278 (1982).

P. J. S. Williams, S. Kenderdine, and J. E. Baldwin. Mem. R. Astron., 70, 53 (1966).

(6) F. H. Bash, F. A. Bozyan, and G. W. Torrence. Astrophys. Letters, 7, 39 (1970).

Yu. M. Bruck and B. Yu. Ustimenko. Nature. 260, 766 (1976); Astrophys. Space Sci. 51, 349 (1977); Astron. Astrophys. 80, 170 (1979).

V. A. Izvekova et al. Aust. J. Phys. 32, 25 (1979).

O. B. Slee, et al. Proc. ASA, 4, 1 (1980).

(7) J. W. Warwick et al. Science 212, 239 (1981); 215, 582 (1982).

D. R. Evans, J. W. Warwick, J. B. Pearce, T. D. Carr, and J. J. Schauble. Nature 292, 716 (1981).

(8) J. A. Burns, M. R. Schoewalter, J. N. Cuzzi, and R. H. Durisen. Icarus 54, 280 (1983).

M. L. Kaiser, J. E. P. Connerney, and M. D. Desch. Nature 303, 50 (1983).

(9) P. Zarka and B. M. Pedersen. J. Geophys. Res. 88, 9007 (1983).

(10) M. D. Desch, R. S. Flagg, and J. May. Nature 272, 38 (1978).

FINAL DISCUSSION

The final discussion was rather short. It basically provided participants an opportunity to bring up any further points that might have been overlooked during the discussion of the 75-MHz array proposal the previous evening. The conclusions of the previous evening were re-affirmed by the group.

Therefore, the decision was made to proceed with the instrumentation of the 25-meter VLA dishes at 75 MHz as quickly as possible and to keep the initiative for free-standing antennas viable for future implementation.